UNIVERSITY OF SOUTHAMPTON

INVESTIGATION OF SCALE FORMATION IN THE BAYER PROCESS

A thesis submitted for the Degree of Doctor of Philosophy

Nicola Jane Kenyon

SCHOOL OF CHEMISTRY

FACULTY OF SCIENCE, ENGINEERING AND MATHEMATICS

SEPTEMBER 2003

UNIVERSITY OF SOUTHAMPTON

ABSTRACT

FACULTY OF SCIENCE, ENGINEERING AND MATHEMATICS

SCHOOL OF CHEMISTRY

Doctor of Philosophy

INVESTIGATION OF SCALE FORMATION IN THE BAYER PROCESS

By Nicola Jane Kenyon

Aluminosilicate 'scales' of the general formula $Na_8[AlSiO_4]6X_2.nH_2O$, X= $½CO_3$, OH that form during the Bayer process have been investigated. The 'scales' are composed of two main aluminosilicate phases, cancrinite and an intergrowth of sodalite and cancrinite, termed "intermediate".

Synthetic scales were prepared from kaolin, sodium hydroxide and sodium carbonate under hydrothermal conditions at temperatures of 150 and 220 °C. Characterisation was carried out using powder X-ray diffraction (PXD), Fourier Transformed Infrared Spectroscopy (FTIR), Scanning Electron Microscopy (SEM) and powder neutron diffraction (PND). The deuterated cancrinite structure, $Na_8Al_6Si_6O_{24}.(CO_3)_{1.06}$ $1.44D_2O$, studied using PND, crystallises in the space group $P6_3$, with lattice parameters a = 12.66624(7) Å and c = 5.16232 Å (6). The main, one-dimensional channels were found to contain two sites for carbonate ions while complete water molecule positions were located in the 11-hedral cages. The "intermediate" consists of a disordered stacking of sodalite and cancrinite structural elements. Variable temperature PND showed that the materials lose water between 100-250 °C with a contraction in unit cell dimensions as the sodium ions redistribute within the structure. At high temperatures the lattices expand with the onset of decomposition for "intermediate" being 100 °C lower (500 °C) than for ordered cancrinite (600 °C).

Addition of calcium hydroxide to systems that yielded carbonate cancrinite or "intermediate" was found to result in the formation of these two aluminosilicate phases containing a proportion of calcium replacing sodium and also, at high calcium concentrations, a sodium calcium hydrogen silicate ($NaCaHSiO_3OH$). The structure of $NaCaHSiO_3OH$ was characterised using PND, it crystallises in the $P2_1/n$ space group with lattice parameters a = 5.7075(2) Å, b = 7.0495(3) Å and c = 5.4693(2) Å, accurate hydrogen positions were determined and strong hydrogen bonds (2.534 Å) link the SiO_3OH units. Calcium doped cancrinites and "intermediate" were characterised by PXD and SEM and were shown to form over the composition range $Na_7Ca[AlSiO_4]_6.(CO_3)_{1.5}.nH_2O$ - $Na_6Ca_2[AlSiO_4]_6.(CO_3)_2.nH_2O$, with a slight contraction in unit cell dimensions.

Attempts to utilise a series of organic sulphate/sulphonate additives as potential scale modifiers/reducers resulted in the formation of the normal polycrystalline aluminosilicate phases. Seven organic polymeric additives were subsequently employed as potential scale modifiers/reducers, resulting in the formation of spherical cancrinite aggregates. The degree of spherical aggregate formation was related to temperature, reaction time and sodium hydroxide concentration and is likely to have involved decomposition of the polymeric additive.

The replacement of NaOH with KOH in synthetic sodium aluminosilicate yielding systems was studied. At low KOH levels, PXD and SEM analysis of the products revealed potassium incorporation into the cancrinite and "intermediate" structures over the composition range $Na_{7.5}K_{0.5}[AlSiO_4]_6.(CO_3)_1.nH_2O$ - $Na_6K_2[AlSiO_4]_6.(CO_3)_{1.5}.nH_2O$. At higher KOH levels the formation of $KAlSiO_4.1.5H_2O$ was observed at 135 °C, whilst at higher temperatures $KAlSiO_4$ forms.

The three systems investigated in the laboratory as possible scale reducers/modifiers were employed in large scale 25 L reactions, using a cyclic system (flow loop). $Ca(OH)_2$ addition proved the most effective, a 30 % reduction in the amount of scale formed was observed.

TABLE OF CONTENTS

ACKNOWLEDGEMENTS

I should first like to thank my supervisor Prof. Mark Weller for all of his help and support over the past four years. I would like to also say a special thank you to Prof. Weller and Dr Gill Reid for their guidance and assistance during first my month in Southampton. I must also show my appreciation to my industrial supervisor Robin Furneaux and all at Alcan International, Banbury especially John, Cheryl, Ged, Helen and John. Thank you to the members of the Weller group, with whom I have worked over the past three years, especially those who have helped me collect the data contained in this thesis during trips to the Rutherford, SOC and SEM. In alphabetical order: Doug Booth, Mariane Field, Andrew Hector, Paul Henry, Bob Hughes, Chris Knee, Craig Owens, Emmanuelle Raekelboom, Jon Reading, Lee Gerrard, Joanna Rooke and Paul Vincent.

I thank the members of the Weller and level two, who made life in Southampton more 'entertaining' – or words to that effect anyway!

Finally, but most importantly, I should like to thank all my family and friends who have always been there for me with support and encouragement. To those at Padley's who have taken an interest my work over the past year, it has been appreciated. Jamie and Raymond, thanks for being there during my time in Southampton.

ABBREVIATIONS

Common abbreviations used throughout this thesis are listed below:

XRD	X-Ray Diffraction
PXD	Powder X-ray Diffraction
PND	Powder Neutron Diffraction
SEM	Scanning Electron Microscopy
EDX	Energy Dispersive X-ray Spectroscopy
TGA	Thermogravimetric Analysis
FTIR	Fourier Transformed Infrared
e.s.d	Estimated Standard Deviation

CHEMICAL SOURCES

The chemical reagents utilised in this research and their sources are listed below:

1-Butanesulphonic acid sodium salt	Aldrich 22,151-1
Calcium hydroxide	Aldrich 49,404-6
Deuterium Oxide	Supplied by RAL
Kaolin	Aldrich 22,883-4
Methyl sulphate sodium salt	Aldrich 31,818-3
Poly(2-acrylamido-2-methyl-1-propanesulphonic acid),	Aldrich 19,197-3
Poly(anetholesulphonic acid, sodium salt),	Aldrich 44,446-4
Poly(sodium 4-styrenesulphonate),	Aldrich 24,305-1
Poly(styrenesulphonic acid-*co*-maleic acid) sodium salt	Aldrich 43,455-8
Poly(ethyleneglycol) 4-nonylphenyl 3-sulphopropyl ether, potassium salt	Aldrich 47,319-7
Poly(1,4-phenylene ether-ether sulphone)	Aldrich 44,097-3
Poly (1,4-butanediol) divinyl ether	Aldrich 41,017-9
Potassium hydroxide	Aldrich 48,401-6
Sodium carbonate	Aldrich 22,353-0
Sodium deuteroxide	Aldrich 37,207-2
Sodium hydroxide	Aldrich 36,717-6
Sodium methanesulphonate 98 %	Aldrich 30,450-6
Sodium p-toluenesulphonate 95 %	Aldrich 15,253-6

Chapter 1

Introduction

1.1 Introduction

This thesis describes an investigation into aluminosilicate scale formation within the heat exchangers of the Bayer process; the process used to refine bauxite to alumina. The formation of aluminosilicate scale is a very costly problem for aluminium producers such as Alcan International Limited who provided the funding for this work. The aim of this research was to further the understanding of the chemistry behind scale formation and to investigate methods of reducing or eliminating it.

1.2 Aluminium

Aluminium is the most abundant metal in the earth's crust (eight percent by weight). It is exceeded in abundance only by oxygen (forty six percent) and silicon (twenty six percent). Aluminium is not found in its pure state but in combination with other elements; it is a major constituent of many common igneous minerals including feldspars and micas. In most of these combinations the aluminium content is too small for economical extraction, the principal ore of commercial value is known as bauxite[1].

The mixed aluminium oxide hydroxide mineral bauxite was discovered by P. Berthier in 1821 near Les Baux in Provence[2]. Aluminium is found in bauxite as very stable hydrated oxides- gibbsite ($Al(OH)_3$), boehmite ($AlO(OH)$) and diaspore ($Al_2O_3.H_2O$). Bauxite results from the decay and weathering of aluminium bearing rocks under tropical conditions; it may form residual deposits replacing the original rock or it may be transported from its place of origin and form deposits elsewhere[3]. Deposits are known to exist in over thirty tropical and subtropical countries but only a small number of these are used in the world's production of aluminium. Bauxite deposits are normally found near the surface in layers or pockets about 1-12 metres (m) in thickness under a cover of less than 0.5 m; a condition which permits open-pit mining. The bauxite obtained is then washed and screened to remove extraneous dirt. The washed lumps may be treated locally at the place of mining or be transported to more distant locations for treatment by the Bayer process.

The largest bauxite deposits are found in Australia, North and South America, Africa and Asia. Commercial-grade bauxite contains at least 40 percent alumina (aluminium oxide, Al_2O_3) along with silica, iron, titanium and other minor trace impurities[1]. Table 1.1 displays analysis of bauxite ore used in the Bayer plant at Aughinish, Eire[4]. During the seven year period presented here the quality of the bauxite has deteriorated, in particular the iron impurities have increased by almost 100 %.

Table 1.1 Analysis of bauxite ore used in the Bayer plant at Aughinish, Eire[4]

	Al_2O_3 (%)	SiO_2 (%)	Fe_2O_3 (%)	TiO_2 (%)	LOM* (%)
1991	58.1	1.92	7.53	3.95	27.87
1998	53.4	1.92	14.0	3.27	26.93

*LOM = loss of mass on ignition, i.e. organic matter.

Twenty million tonnes of aluminium are consumed each year and this requires over one hundred million tonnes of bauxite ore; between four and six tonnes of bauxite are needed to produce two tonnes of alumina which in turn yields one tonne of aluminium.

Aluminium has unique mechanical, physical and chemical properties that make it an economical and effective material for a wide range of applications, e.g. in the transportation, packaging, electrical and building and construction sectors. It has a high strength to weight ratio, can be fabricated and cast into complex shapes, has excellent corrosion resistance, good thermal and electrical conductivity and can be recycled with virtually no deterioration of quality.

Montreal based Alcan International Ltd., financial sponsor of this research, is the second largest aluminium producer in the world with a primary production of 1,490,000 tonnes per annum. In 1998 it signed a 10-year multi-billion dollar agreement to supply aluminium to General Motors[5].

1.3 Alumina Production

1.3.1 The Bayer Process

A number of methods for refining bauxite to alumina exist but the most common is a chemical process known as the Bayer process, developed by the Austrian chemist Karl J. Bayer in 1889[1]. Although this method is over one hundred years old, process efficiency has been improved by constantly applying the latest analysis techniques and developing new ones to enable valid, accurate and precise measurements of the critical parameters involved in the process[6].

The Bayer process is summarised in Figure 1.1. It should be noticed that the process is of a cyclic nature and that there is a continuous flow of the process solution (liquor) through the plant.

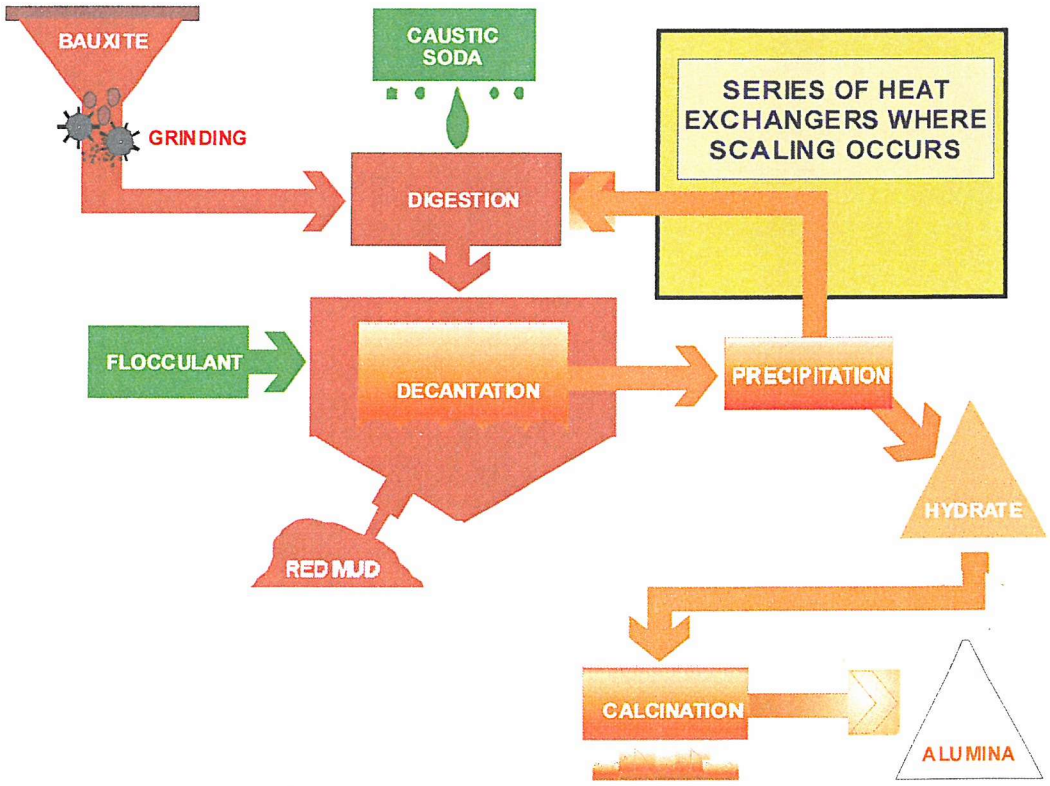

Figure 1.1 Schematic of the Bayer process.

In the first stage of the Bayer process the bauxite is crushed up into a fine powder and mixed with liquid caustic (sodium hydroxide solution). It is then pumped as slurry into the high pressure/temperature digesters. The operating conditions of these digesters are

dependent upon the form in which the aluminium oxide is present in the bauxite. The solubility of gibbsite is higher than that of boehmite and therefore the conditions for boehmite digestion must be more severe, i.e. the temperature and/or the caustic concentration must be increased[7]. An ore that is rich in boehmite requires digestion temperatures of ≈255 °C, whereas for an ore that is rich in gibbsite the temperature can be reduced considerably to ≈140 °C[8].

The aluminium oxide dissolves in the caustic to form sodium aluminate ($Na_2O.Al_2O_3$) and impurities, predominantly iron oxides, silica and titanium that remain largely undissolved, Equation 1.1.

$$2NaOH + Al_2O_3.3H_2O + \text{impurities} \rightarrow Na_2O.Al_2O_3 + 4H_2O + \text{impurities} \downarrow$$

Equation 1.1

These impurities which are red in colour due to the iron oxides are known as 'red mud'. This resulting mixture of dissolved alumina and red mud is allowed to settle in slowly stirred settling tanks. The partially clear liquid containing the dissolved alumina is then clarified by filtering under pressure, through heavy canvas in filter presses. The red mud residue is washed to remove chemicals and is then discarded in red mud deposits. Figure 1.2 shows red mud deposits with a Bayer plant nearby.

Figure 1.2 Red mud deposits, the Bayer plant can be seen at the top of the picture.

After clarification, the solution that is now a 'strong tea' colour is pumped into the precipitator tanks. The solution is known as 'green' or 'pregnant liquor', i.e. liquor from which gibbsite has not yet precipitated. Fine particles of pure alumina hydrate are added as a seed, compressed air is admitted into the tanks and agitation begins. After a period of approximately one and a half days, with gradual cooling, alumina trihydrate precipitates out of the caustic solution, Equation 1.2.

$$Na_2O.Al_2O_3 + 4H_2O \rightarrow Al_2O_3.3H_2O\downarrow + 2NaOH$$

Equation 1.2

This is the reverse of Equation 1.1.

At this stage in the process, and after washing and removal of excess liquid by vacuum filters, the alumina trihydrate is a damp, cream coloured substance. In order to remove the chemically combined water, the hydrate is fed into brick-lined rotary kilns through which it travels slowly, whilst being heated to a temperature of almost 1000 °C, Equation 1.3.

$$Al_2O_3.3H_2O \rightarrow Al_2O_3 + 3H_2O\uparrow$$

Equation 1.3

The finished product, aluminium oxide (Al_2O_3), is a white powder known as calcined alumina. The caustic solution left behind in the precipitator tanks 'spent liquor' is recycled and used again with fresh bauxite.

The calcined alumina from the Bayer process is used to produce aluminium in a factory or plant known as a smelter. The alumina is reduced to aluminium metal in electrolytical cells in a process that is similar to the one developed by Hall and Héroult in 1886[1].

1.3.2 Other Methods

Other methods for the recovery of alumina are permitted by the amphoteric nature of aluminium; allowing both acid and alkaline recovery processes[7].

For acid recovery processes the mineral which has received most attention is kaolinite ($Al_2O_3.2SiO_2.2H_2O$). This clay mineral is widely distributed, it is found in relatively pure form and in the anhydrous state contains 39 percent alumina.

Assuming kaolinite as the raw material, the first step is to roast the ore at approximately 750 °C to form meta-kaolinite from in which the alumina is more soluble. The roasted ore is then leached with a concentrated acid at or above the atmospheric boiling point. The acid may be hydrochloric acid (HCl), sulphuric acid (H_2SO_4), sulphurous acid (H_2SO_3), nitric acid (HNO_3) or, in a few cases a mixture of two of these. As a result of leaching, a solution of alumina salt is formed and the silica remains as a solid residue; the two are separated by sedimentation and filtration. Impurities in the raw material are removed by additional treatment stages. The hydrated aluminium salt is crystallised from the solution and heated in stages to 1000 °C where it decomposes to alumina, water and acid gas. The acid gas is sorbed in water and recycled to the leaching stage.

The conditions in each step of this process can be changed; temperatures and concentrations are relatively easy to vary. In some cases a basic acid salt, a mixture of the acid salt with alumina, is formed. This reduces the amount of water to be driven off in the calcination step, which in turn lowers the energy required for production.

Alkaline processes are based on the fact that sodium aluminate ($Na_2O.Al_2O_3$) is formed in a solid state reaction when sodium carbonate (Na_2CO_3) is heated with an aluminous raw material (nepheline [$(Na,K)AlSiO_4$]), at 1000 °C or higher. Unfortunately, if silica is present, sodium silicate (Na_2SiO_3) is also formed. When sodium silicate and sodium aluminate are dissolved from the sinter and the solution heated, an aluminosilicate phase is formed. In most ores the quantity of silica present is so great that there is no net recovery of alumina from a soda sinter. This is overcome by adding limestone (CaO) so that an insoluble dicalcium silicate forms. The $NaAlO_2$ is then be leached from the sinter and after the solution has been treated to remove small amounts of soluble silica,

alumina can be precipitated by neutralisation with carbon dioxide (CO_2). Sodium carbonate is regenerated at this stage and can be recycled. A modification of the sodium-calcium sinter uses only limestone as the reagent; in this case calcium aluminate ($Ca_3Al_2O_6$) and calcium silicates are formed. The calcium aluminate reacts with sodium carbonate solution to form sodium aluminate and calcium carbonate ($CaCO_3$).

Sintering processes are difficult to operate. The composition, firing temperatures and leaching conditions must be carefully controlled; if they are not, the calcium silicates will hydrate rapidly to form a product that is almost impossible to leach and wash. The economic disadvantage of the sintering process is the amount of energy required to fire the sinter and to evaporate the leach solution. Nepheline is used commercially as the raw material for the sinter process in Russia; the needs of the Russian economy make the process feasible but it is uneconomical elsewhere.

The general consensus is that except in unusual circumstances, alumina will be recovered from bauxite by the Bayer process. The costs associated with alternative processes are from 1.5 to 2.5 times higher than the Bayer process. Much of the difference is due to the higher energy requirements needed in the alternative processes and this disadvantage is likely to become greater in the future.

1.4 The Scale Problem

Unfortunately, along with the desired aluminium oxide, silica impurities in the bauxite ore are also dissolved in the caustic soda solution thus making the Bayer process not quite as perfect as described above. Once in solution the silica can react with the caustic and alumina, and precipitate as sodium aluminiosilicates, commonly known as '**scale**'. Kaolin ($Al_2O_3.2SiO_2.2H_2O$) is the major reactive silica mineral in bauxite. Quartz (SiO_2) is also found as an impurity but it is not significantly attacked in the extraction process and is removed in the red mud waste. The reaction for scale formation is generally thought to proceed via two stages. The first is the dissolution of kaolin, Equation 1.4.

$$Al_2O_3.2SiO_2.2H_2O + 6OH^- \rightarrow 2SiO_3^{2-} + 2Al(OH)_4^- + H_2O$$

Equation 1.4

This is followed by the subsequent precipitation of **'scale',** Equation 1.5:

$$6SiO_3^{2-} + 6Al(OH)_4^- + 6Na^+ + 2NaX \rightarrow \mathbf{Na_8[AlSiO_4]_6X_2.nH_2O} + (6\text{-}n)H_2O + 12OH^-$$

sodium aluminosilicate scale

where X could be $\frac{1}{2}CO_3^{2-}$, $\frac{1}{2}SO_4^{2-}$, Cl^-, OH^-, etc[9].

Equation 1.5

As equation 1.5 shows, anion impurities also present in the caustic solution play a key role in the precipitation of scale. These impurities accumulate from several different sources such as trace impurities in the ore, residual chemicals used for cleaning the pipes and the aerial oxidation of humic material to give carbon-based species such as oxalate, formate or carbonate[10]. The carbonate anion is present in the highest concentration[11] owing to the dissolution of carbon dioxide (CO_2) from the air under these highly alkaline conditions[12,13,14]. The CO_2 reaction with the hydroxide adversely affects the hydroxide concentration, Equation 1.6.

$$2OH^- + CO_2 \rightarrow H_2O + CO_3^{2-}$$

Equation 1.6

Sodium carbonate content of liquor varies from plant to plant but is typically in the region of 30-40 g/l[15].

It has been shown that silica solubility in solution increases with increasing dissolved aluminium content[7], therefore after the precipitation of gibbsite the solubility of silica in the spent liquor is also reduced. The spent liquor is recycled and reheated in a series of low and high temperature heat exchangers. The decreased silica solubility and the hot surfaces in the heat exchangers provide the ideal conditions for precipitation and it is here where the most serious scaling occurs. Figure 1.3 overleaf, presents a series of pictures that show the effect of scaling within the heat exchangers. The formation of scale presents alumina refinery plants with severe difficulties[8]. For example:

- descaling – stopping liquor flow and flushing with sulphuric acid to dissolve the scale, results in loss of production time and incurs extra costs. In severe cases the plant may be out of operation one day a week whilst descaling is carried out. This operation may also corrode the heat exchangers causing further costs and inconvenience.
- less effective heat transfer in the heat exchangers
- contamination of the final product
- loss of sodium hydroxide and alumina

The costs of dealing with the aluminosilicate scaling and with the related energy-consumption problems at the QAL refinery were estimated at 10 million dollars in 1995[16]. As stated in the aims section of this report, it is hoped that the research undertaken in this investigation may help to alleviate the scale problem and therefore lead to a reduction in production costs.

End-on pictures of 'scaled' heat exchangers

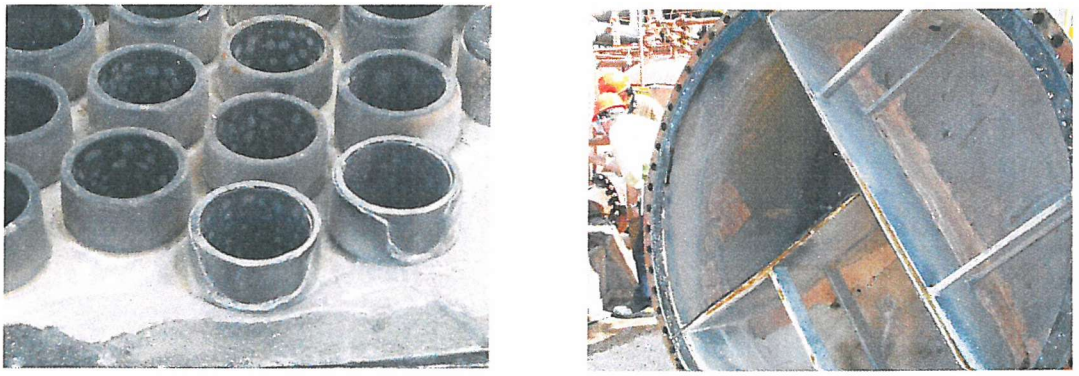

Scaling also occurs on the outside of the individual heat exchanger pipes (left) and on the 'head which cover the heat exchangers

Cross section from a severely scaled heat exchanger pipe which has been removed from a Bayer plant

Figure 1.3 Pictures showing the extent of scaling within the heat exchangers[17].

1.5 Zeolites

Zeolites form an important key class of minerals. They are widely used in ion-exchange applications, offer unique properties as sorbents and molecular sieves and they play a dominant role in hetrogeneous catalysis. Approximately 40 naturally occurring zeolites have been characterised but with the growth of academic and industrial interest in this area more than 150 synthetic structures[18] have been developed. 133 of these are currently recognised by the International Zeolite Association[19]. These structure types are each allocated a three letter code to simplify the nomenclature, for example the sodalite structure groups is referred to as SOD. The advancement of many of the solid state characterisation techniques in recent years has been crucial in providing more satisfactory zeolite structure reports thus allowing a more comprehensive understanding of zeolite chemistry[20].

The Swedish mineralogist Baron Axel Cronstedt[21] first described zeolites as a mineral class in 1756. They are a class of crystalline aluminosilicates based on rigid anionic frameworks with well-defined channels and cavities. The cavities contain exchangeable metal cations (Na^+, K^+, etc) and can also hold removable and replaceable guest molecules (such as water). It is their ability to lose water that earned them their name; Cronstedt observed that on heating with a blowpipe flame they hissed and bubbled as though they were boiling and so named them "zeolites" or "stones that boil", from the Greek "zeo" to boil, and "lithos", stone. This name describes a particular class of minerals related to the feldspars and feldspathoids.

1.5.1 General Zeolite Structure

The general formula for a zeolite is:

$$[M^{n+}]_{n/x}[AlO_4]_x[SiO_2]_{1-x}.m[H_2O]$$

where M is a cation with the charge n.

The above formula illustrates the three components of zeolites; the aluminosilicate framework, charge balancing cations and absorbate water. These three components may be altered to give rise to a wide range of characteristic properties.

The framework is comprised of the primary building units, $[SiO_4]^{4-}$ and $[AlO_4]^{5-}$ linked together by their apical oxygen atoms. Silicon-oxygen tetrahedra are electrically neutral when connected together in a three-dimensional network, as in quartz SiO_2. Replacement of the tetravalent Si^{4+} cation with the trivalent Al^{3+} in zeolite structures affects this neutrality and introduces a negative charge to the framework, Figure 1.4. Overall neutrality is preserved by entrapment of positive ions in the framework. Löwenstein's rule[22] states, 'Whenever two tetrahedra are linked by one oxygen bridge, the centre of only one of them can be occupied by aluminium; the other centre must be occupied by silicon, or another small ion of electrovalence four or more, e.g. phosphorus. Likewise, whenever two aluminium ions are neighbours to the same oxygen anion, at least one of them must have a co-ordination number larger than four, that is five or six, towards oxygen.' Thus the ratio of aluminium to silica in the zeolite framework must be less than or equal to unity.

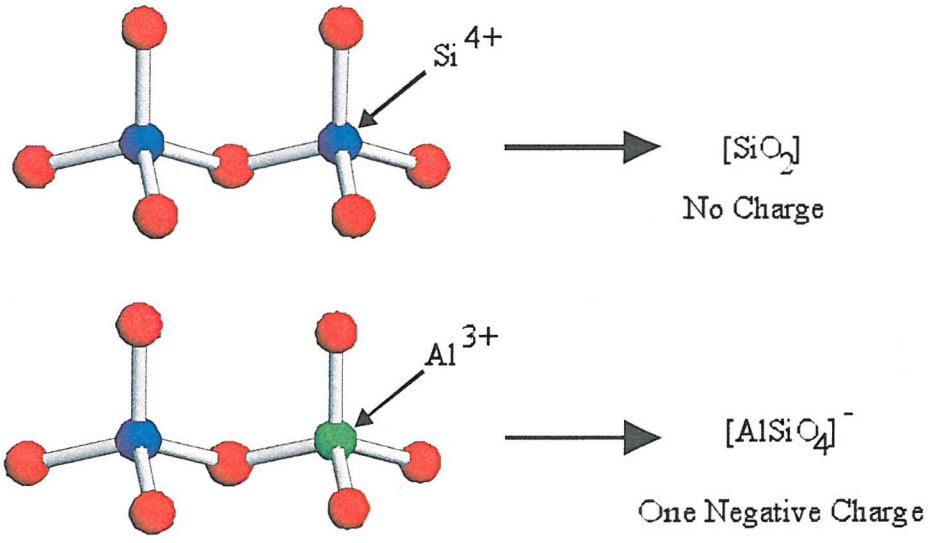

Figure 1.4 The addition of charge to zeolite frameworks by substitution of Si^{4+} with Al^{3+}.

In zeolites the $[SiO_4]^{4-}$ and $[AlO_4]^{5-}$ tetrahedra link together by sharing all four corners and can form a variety of structures. The linked tetrahedra can be illustrated by drawing a straight line to represent the oxygen bridge connecting two tetrahedral units, for example the six linked tetrahedra in Figure 1.5 are simply represented by a hexagon.

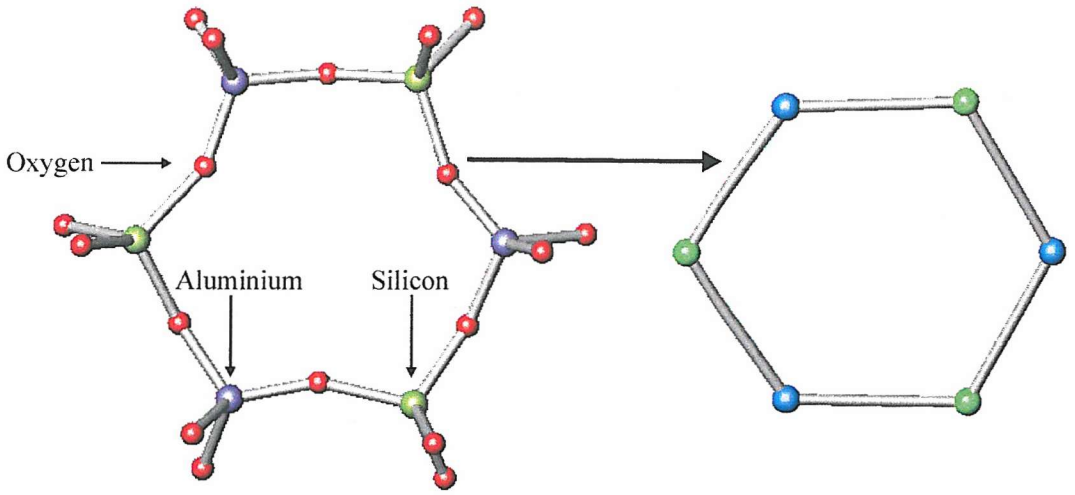

Figure 1.5 Left; 6-membered ring formed by linking 3 $[SiO_4]^{4-}$ and 3 $[AlO_4]^{5-}$ tetrahedra. Right; shorthand representation of the same ring.

This is known as a 6-membered ring and is an example of a secondary building unit (SBU). A selection of other SBUs are shown below in Figure 1.6.

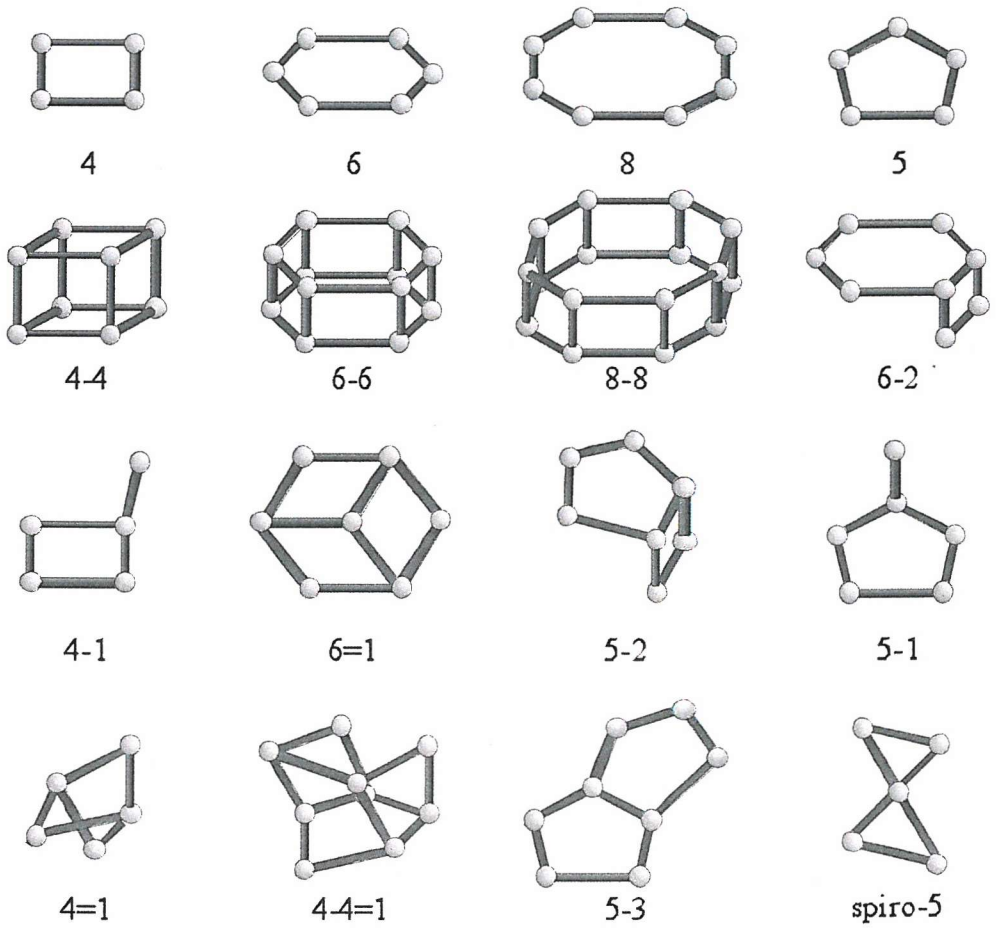

Figure 1.6 Secondary building units (SBUs).

1.5.2 Zeolite Synthesis

R.M. Barrer is regarded as the founding father of zeolite chemistry[23]. In the 1940s and 1950s he demonstrated that a series of zeolitic materials could be synthesised under hydrothermal conditions[24,25]. Such synthesis involves combining a mixture composed of an alumina component, a silica component and inorganic base(s). This mixture forms a gel or viscous liquid which is allowed to crystallise, usually under autogenous pressure, for a period of between a few hours to several weeks at temperatures between ~60 °C and ~200 °C. Temperature, time, pH and degree of agitation are all factors that can affect the final product. Barrer *et al*, report the hydrothermal synthesis of sodalites[26] and cancrinites[27] using kaolinite as the alumina and silica source. It was reported that nitrate (NO_3^-), chromate (CrO_4^{2-}) and molybdate (MoO_4^{2-}) promoted the formation of cancrinite. In the absence of these salts or in the presence of salts of chloride (Cl^-), bromide (Br^-), chlorate (ClO_3^-) and perchlorate (ClO_4^-), sodalite formed. The salts are believed to act as a template and can have a structure directing effect.

1.6 Sodalite, Cancrinite and Intermediate

Analysis of heat exchanger scale has identified three distinct aluminosilicate phases: sodalite, cancrinite and an intermediate phase[10,28]. Sodalite and cancrinite are both observed in nature and are typical feldspathoid minerals; other feldspathoid minerals include nepheline and leucite[29] ($KAlSi_2O_6$). Table 1.2 presents unit cell and crystallographic data for sodalite and cancrinite[19]. Sodalite and cancrinite both have a highly ordered three-dimensional framework, whereas the intermediate phase shows a strong one-dimensional stacking disorder.

Table 1.2 Unit cell and crystallographic data for sodalite and cancrinite.

Mineral	Unit Cell Contents	Crystallographic Data
Cancrinite	$(Na, Ca, K)_{6\text{-}8}[(AlO_2)_6(SiO_2)_6]$ $(CO_3, SO_4, Cl)_{1\text{-}2}$	Hexagonal a = 12.6 & c = 5.18 Å space group $P6_3$
Sodalite	$Na_8[(AlO_2)_6(SiO_2)_6]Cl_2$	Cubic a = 8.87 Å space group P-43n

1.6.1 Sodalite

The sodalite structure was first determined by Linus Pauling[30] in 1930 following a single crystal X-ray diffraction study of the mineral $Na_8[AlSiO_4]_6.Cl_2$. This structure was later refined in 1967 by Löns and Schulz[31]. 4- and 6-membered rings composed of alternating $[SiO_4]^{4-}$ and $[AlO_4]^{5-}$ are stacked in an ABCABC... sequence to form basket-like structures known as truncated octahedra (sodalite or β-cages). Figure 1.7 presents a sodalite or β-cage.

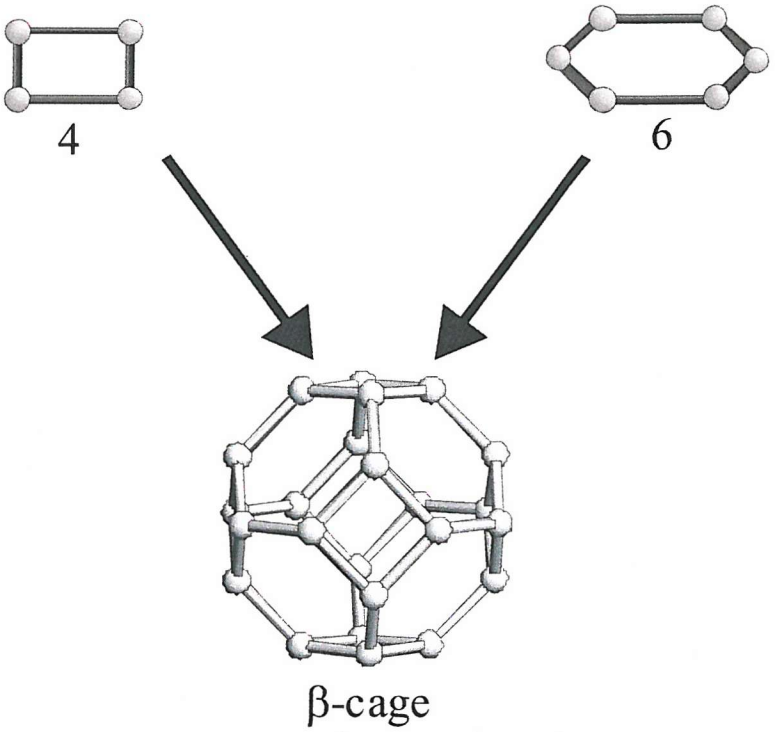

Figure 1.7 The linking together of 4- and 6-membered rings to form a β-cage.

The sodalite structure is constructed from β-cages, with each 4-membered ring shared by two β-cages in a primitive array, Figure 1.8. These sodalite cages are also used to construct other zeolite frameworks (e.g. the synthetic zeolites, A and X). In zeolite A (LTA) the sodalite units are again stacked in a primitive array, but now they are linked by oxygen bridges between the 4-membered rings, Figure 1.8. In zeolite X (FAU) the sodalite cages are linked by oxygen bridges between four of the eight 6-membered rings in a tetrahedral array, forming hexagonal prisms, Figure 1.8.

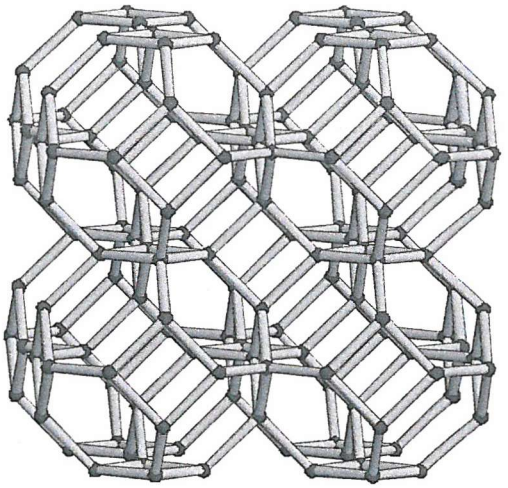

Sodalite (SOD)

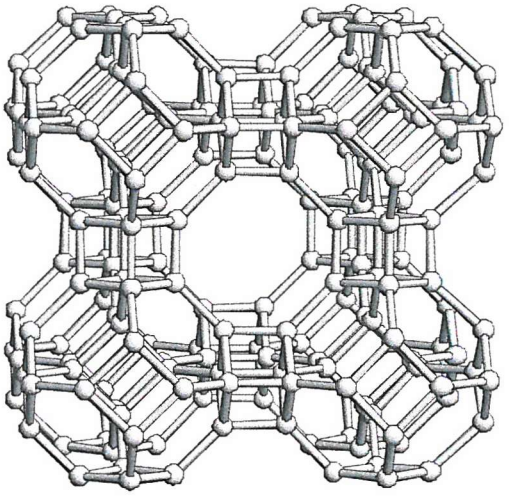

Zeolite A (LTA)

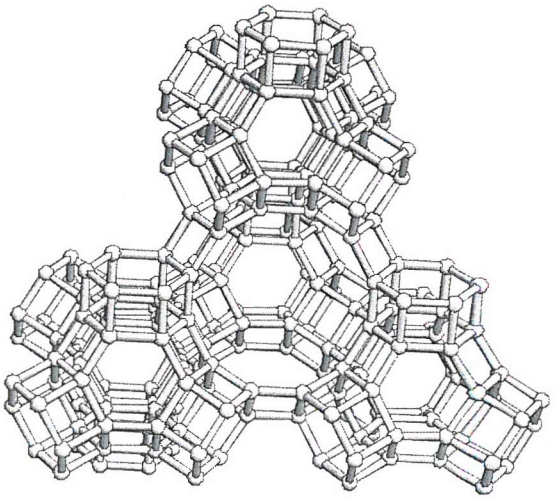

Zeolite X (FAU)

Figure 1.8 The difference in connectivity of the β-cages forming three different structures, sodalite, zeolite A and zeolite X.

The β-cages can be occupied by cations, guest molecules, such as water, and/or more complex units formed from cations, anions and water. In aluminosilicate sodalites the β-cages normally contain $[M_4X]^{3-}$ units, for example Na_4Cl^{3-} in $Na_8[SiAlO_4]_6Cl_2$ but these cages can also contain water, as in $Na_6[SiAlO_4]_6[H_2O]_2$. Figure 1.9 below presents a typical aluminosilicate sodalite structure containing both templating anions and charge balancing cations.

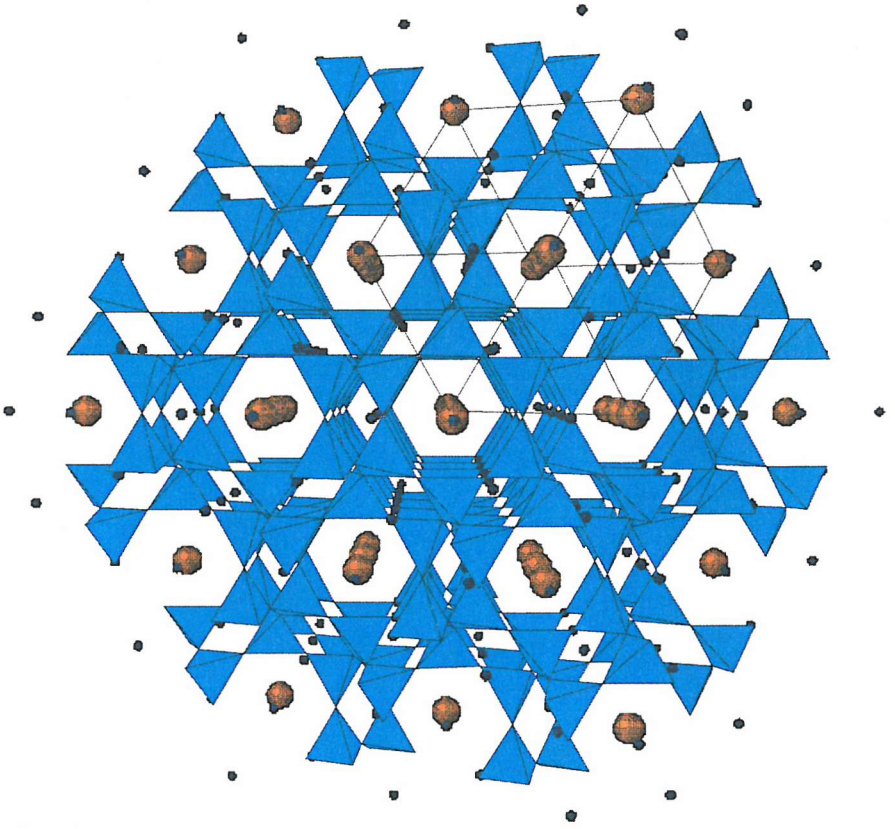

Figure 1.9 The sodalite structure. Blue polyhera represent the $[SiO_4]^{4-}$ and $[AlO_4]^{5-}$ tetrahedra, orange spheres the templating anions and blue spheres the charge balancing cations.

1.6.2 Cancrinite

The cancrinite structure was determined by Jarchow in 1965[32]. The structure possesses hexagonal symmetry which is a result of the close packing of interconnected and parallel 6-membered rings of alternating $[SiO_4]^{4-}$ and $[AlO_4]^{5-}$ tetrahedra in an ABAB… stacking sequence. A comparison of the different stacking sequences that occur in sodalite and cancrinite is made in Figure 1.10 below.

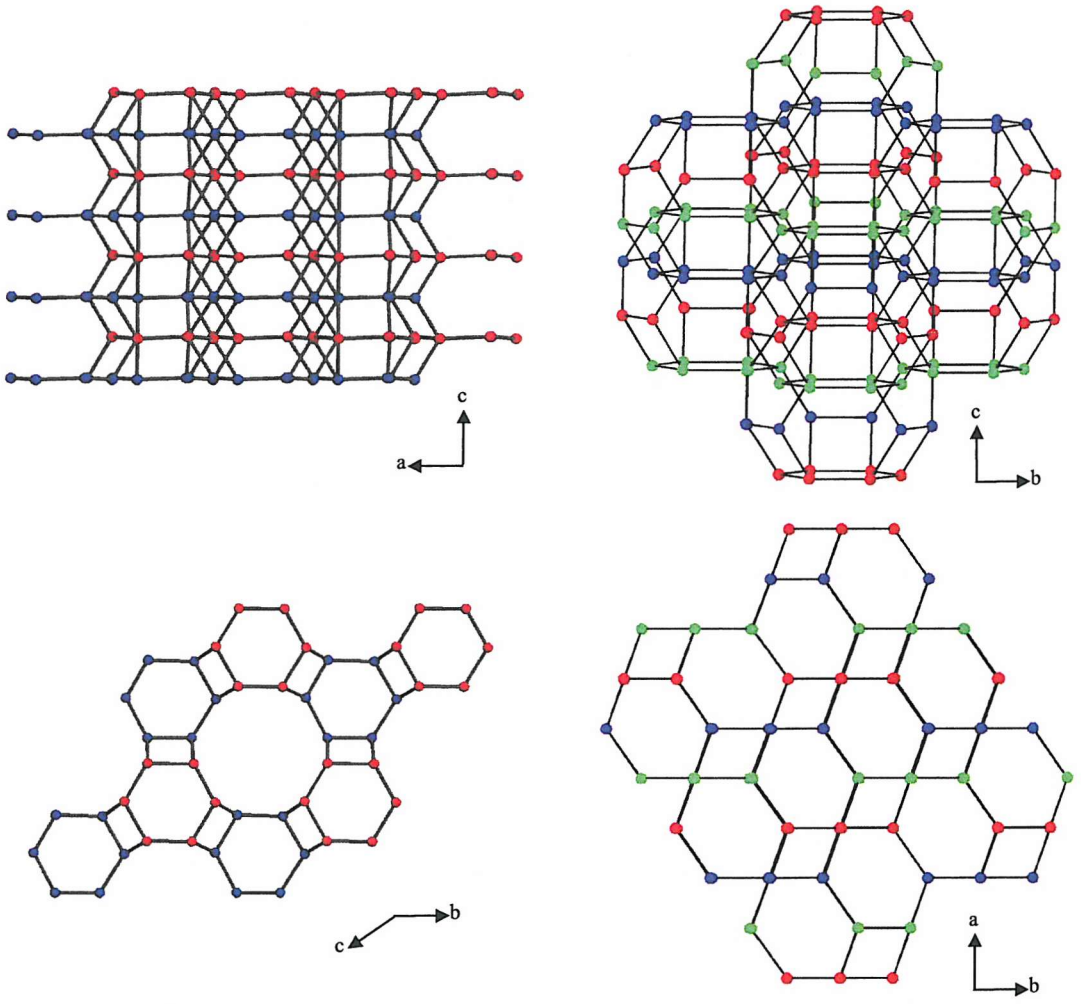

Figure 1.10 Frameworks topologies of cancrinite (left) and sodalite (right). In the left pair of diagrams the layers of tetrahedral atoms repeat positionally in the sequence ABABAB along the c direction producing the channel structure when viewed down c. In the right hand pair the repeat is ABCABCABC (the C layer is shown in pale green) producing the interlocked arrangement of sodalite cages.

The cancrinite structure has 11-hedral cavities; ∈-cages, along with a large uni-dimensional 12-ring channel that runs through the structure. These cages can be occupied by cations, guest molecules, such as water, and/or more complex units formed from cations, anions and water. The main channels may contain water molecules along with anions, such as carbonate and sulphate as well as the cations. Figure 1.11 below presents a typical aluminosilicate cancrinite structure containing both templating anions and charge balancing cations.

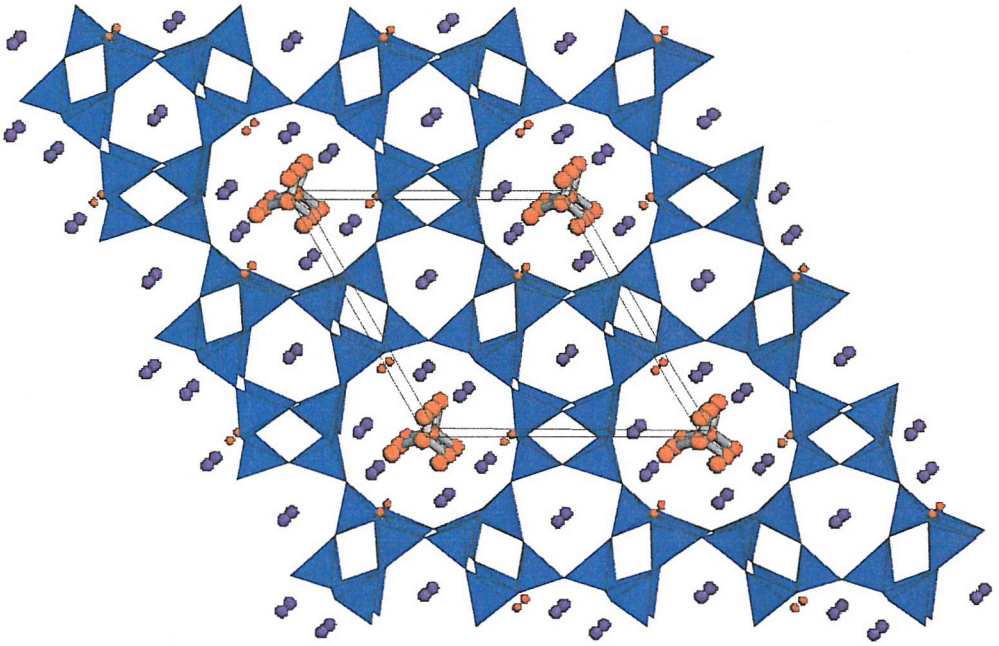

Figure 1.11 The cancrinite structure. Blue polyhera represent the $[SiO_4]^{4-}$ and $[AlO_4]^{5-}$ tetrahedra, orange spheres the templating anions and blue spheres the charge balancing cations.

1.6.3 Intermediate

When trying to crystallise carbonate cancrinite under moderate hydrothermal conditions, Hermeler *et al*[33] observed the co-crystallisation of sodalite and a product which is believed to be an 'intermediate' between the sodalite and cancrinite structures. While sodalite and cancrinite have highly ordered three-dimensional framework structures, the Intermediate shows a strong one-dimensional stacking disorder.

1.7 Literature Review of Scale Formation

Literature relating to Bayer scaling can be found dating back to the 1960s when Breuer *et al*[13] and Kraus *et al*[34] investigated the solubility of the silicate species as a function of temperature in unseeded solutions of sodium aluminate. These original findings have since been contradicted by Oku and Yamada[35] and later by Cresswell[36] and then Müller-Steinhagen[37]. A discussion of more recent literature follows.

1.7.1 The Solubility and Reaction Kinetics of Aluminosilicate Scale Formation in the Bayer Process

In 1997 Gerson and Zheng[8] characterised Bayer scale according to its location in the Bayer plant; digesters, low temperature heat exchangers and high temperature exchangers. The digester scale was found to be mainly cafetite $(Ca,Mg(Fe,Al)_2Ti_4O_{12}.4(H_2O)$ along with small amounts of haematite (Fe_2O_3). Boehmite was the major phase observed in the analysis of the low temperature heat exchanger scale. Three sodium aluminosilicate phases were identified in high temperature heat exchanger scale samples; $sodalite_1$, $sodalite_2$, and cancrinite. The relative concentration of these phases is shown to be dependent upon both temperature and *in situ* ageing. The proposed ageing mechanism[8,16] is displayed below, Equation 1.7.

$$\underset{a = 9.077(2)\text{Å}}{\text{Sodalite}_1} \rightarrow \underset{a = 8.988(1)\text{Å}}{\text{Sodalite}_2} \rightarrow \text{Cancrinite}$$

Equation 1.7

The $sodalite_1$ phase contains a high concentration of carbonate. As carbonate diffuses out of the $sodalite_1$ lattice, it shrinks to $sodalite_2$ a second distinct sodalite phase which then transforms to cancrinite. The transformation of $sodalite_2$ to cancrinite was shown to be the rate determining step in cancrinite formation. In a more recent report Barnes *et al*[38] demonstrate that the sodalite to cancrinite transformation involves a solution-mediated mechanism with sodalite dissolution being followed by the subsequent precipitation of cancrinite. At very high SiO_2 concentrations the precipitation of these phases is said to proceed by the following mechanism, Equation 1.8.

[Aluminosilicate species] → Amorphous phase → Zeolite (Linde A) → Cancrinite

Equation 1.8

The inclusion of additional stages in this mechanism is only observed at high SiO_2 levels. In the work detailed in this thesis, the formation of cancrinite via the successive transformation of a high CO_3^{2-} sodalite to a low CO_3^{2-} sodalite then to cancrinite is not observed.

The effect of sodium carbonate on sodium aluminosilicate crystallisation and solubility has been investigated by the Gerson group[12,16,39]. Stirred and unstirred stainless steel Parr autoclaves were used to perform these reactions. Again the authors describe the formation of the phases proceeding by the above mechanism. A high concentration of sodium carbonate in the synthetic liquor causes a decrease in the rate of conversion of sodalite to cancrinite. The presence of sodium carbonate in synthetic liquor causes both sodalite and cancrinite to be less soluble.

Further investigations by the Gerson group have focused on the solubility of sodalite and cancrinite, the rate of desilication and also the kinetics governing the rates of formation of the phases[40,41,42,43,44]. Sodalite is more soluble than cancrinite at all temperatures, although by raising NaOH concentration the solubility of cancrinite can be increased. The relationship between solubility and temperature is linear for both phases. When the synthetic liquor solutions are seeded with sodalite and cancrinite crystals the rate of desilication is seen to increase due to seed crystal growth; scale formation is also suppressed. These effects are more distinct when seeding with cancrinite. When seeding with a mixture of the two phases the results are more in line with those observed for cancrinite seeding.

Having discussed the formation of sodalite and cancrinite as both single and mixed phases, Barnes *et al* have since described a method for quantifying the relative concentrations of sodalite and cancrinite present in a sample[45]. The method involves measuring certain PXD peak intensities found in the two phases and using them to calculate relative cancrinite concentration; the authors describe this method as more useful than FTIR and ^{29}Si MAS NMR when quantifying these two aluminosilicates.

1.7.2 The Effect of Process Parameters on Scale Formation in the Bayer Process

Jamialahmadi and Müller-Steinhagen have investigated the effect of process parameters on scale formation from spent Bayer liquors[46,47,48]. A test rig in which the liquor flows in a closed loop consisting of a temperature controlled storage tank, pump and test sections was used to perform these experiments. Heat transfer and fouling resistances across the test section surfaces were used to measure the level of scaling when different parameters were varied. Heat flux and silica concentration were seen to be two key factors that affect the heat transfer coefficient. The heat transfer coefficient decreased with time; high heat fluxes decreased at a faster rate than low heat fluxes and increasing silica concentration also increased the rate at which the heat transfer coefficient decreased. At silica levels up to 1.2 g/l the fouling resistance is initially seen to improve at the beginning of the experiments however after this the curves show an almost linear increase in fouling resistance with time. The runs for silica levels of 1.6 g/l or higher do not conform to this linear fouling curve. The fouling rate drops off to an asymptotic value, following an initial linear period. This type of fouling curve is characteristic of particulate fouling, where considerable removal mechanisms are usually present.

Other factors considered in these investigations are the effect of flow velocity, and heat transfer mechanism. At the low silica levels scaling is independent of flow velocity as it is controlled purely by surface reaction, the scale formed was of a rippled nature and required both acid cleaning and sand papering for removal. At the higher silica levels particulate fouling occurs in the bulk flowing liquor and so scaling occurs as a result of both surface reaction and deposition of particles from the flowing solution. The deposits observed for these conditions were less rippled and less sticky and could be removed with less effort. A reduction in scaling was observed when the heat transfer mechanism was changed from convective sensible (heat transferred from one region to another by the circulation of currents) to nucleate boiling (heat transferred by a boiling effect on the surface) heat transfer.

Jamialahmadi *et al* reproduced and confirmed the results obtained on a laboratory scale (as described above) at the Alcoa of Australia refinery in Kwinana[49,50]. The authors

suggest that nucleate boiling at heat transfer surfaces and fluidised bed heat exchangers are the most promising concepts to reduce heat exchanger scaling.

In 1995 the Müller-Steinhagen group published work detailing an investigation into the desilication kinetics in spent Bayer liquor[51]. The rate of desilication of spent Bayer liquors was shown to be second order in silica supersaturation in both the presence and absence of seed; this is consistent with the work of Barnes *et al*[38]. The rate of desilication is expected to strongly dependent on the surface area and the structure of the seed being used; Barnes *et al* confirm that the structure of the seed does indeed affect the rate[40,41]. In further efforts to extend the understanding of silica solubility in Bayer liquor the authors have also attempted to utilise mathematical models to identify, manipulate and model the process variables[37].

1.7.3 Growth Mechanisms for Aluminosilicate Scale Formation in the Bayer Process

Roach identifies two basic mechanisms for scale formation; growth, and settling – cementation[52].

Growth scales form by nucleation of the supersaturated phase on surfaces such as pipe or tank walls, followed by the subsequent growth of those nuclei. The two critical factors for nucleation are the degree of supersaturation and the form of the surface; a high degree of supersaturation will increase the likelihood of nucleation and nucleation is easier on surfaces of similar crystal structure or chemistry to the supersaturated phase. When manual cleaning is employed on Bayer plant equipment, sufficient scale may remain to act as nuclei for growth. The higher the temperature the faster the growth at these nuclei; hence high temperature heat exchangers suffer from the most rapid scaling. Efforts to prevent the formation of growth scale have focused on poisoning the growth surfaces using chemical additives; Roach does not give details about specific additives.

Settled scales form in slurries, the slurry particles can settle and be cemented by the supersaturated liquor. This settling and cementation will occur preferentially in low velocity regions of the plant or during plant shutdown. The most effective way to prevent settled scale is to ensure sufficient agitation.

1.7.4 Identification of Scale Formed Throughout the Bayer Plant

Zhong-Lin and Song-Qing detail the different types of scale that form throughout the Bayer plant,[53] their findings are in agreement with Gerson and Zheng[8]. On the walls of the settler tanks, precipitators and other similar equipment, precipitation of minerals such as gibbsite, bayerite ($Al(OH)_3$), nordstrandite ($Al(OH)_3$) and boehmite occurs. In the slurry preheating, digestion and evaporating processes, the formation of sodium aluminosilicates is observed. Titanate scaling occurs in high temperature regions of the plant such as the digesters. Methods of scale removal adopted in the different areas of the plant are discussed. Chemical methods such as acid cleaning can be used in the precipitators, heat exchangers and slurry preheaters. Physical methods including the jet water cleaning method and mechanical methods are used in the slurry preheaters and settler tanks respectively. The technological method, divided heat retentiveness, is used to slow down the scaling rate in the slurry preheating process.

1.7.5 Desilication of Bayer Liquor

Whilst other authors have focused on the formation of sodalite and cancrinite as scaling products in the heat exchangers (the area of the Bayer plant under investigation in this thesis), Whittington *et al*[9] describe their formation as being a useful method for impurity removal in another area of the plant. When formed as desilication products (DSP), that is they form during pre-desilication and digestion ensuring they are discarded with red mud waste, they can incorporate NaCl, Na_2CO_3, and Na_2SO_4 impurity salts. The aim of this investigation was to establish the effect of liquor impurity concentration on the resulting DSP composition. The conditions used were designed to represent those found in the Bayer process; pre-desilication (100 °C for 15 h) then digestion (150 °C/30 min, 175 °C/30 min, 220 °C/10 min). Sodalite was the major phase formed in all cases. This result is consistent with work published by Barrer *et al*[24] and Hackbarth *et al*[54], in that carbonate cancrinite formation is only observed at higher temperatures. Less consistent is the indication that the sulphate anion preferentially forms the sodalite structure at all temperatures as divalent ions are known to template cancrinite at reasonable concentrations[55]. The results obtained by Whittington et suggest that the magnitude of anion incorporation into Bayer-sodalite under pseudo-Bayer conditions follows the trend: $OH^- << Al(OH)_4^- < Cl^- \leq CO_3^{2-} << SO_4^{2-}$.

1.7.6 Characterisation of Heat Exchanger Scale

Armstrong and Dann[10] have prepared synthetic sodium aluminosilicate Bayer refinery scale at temperatures ranging between 80 and 240 °C. The effect of anion type and anion concentration on the type of aluminosilicate phase formed was investigated; carbonate (CO_3^{2-}), sulphate (SO_4^{2-}), chloride (Cl^-) and oxalate ($C_2O_4^{2-}$) were used as these are the four trace anions present in the highest concentrations in Bayer liquor. These synthetic products were then compared with industrial scale removed from different parts of low and high temperature Bayer processing plants.

The plant scale was seen to crystallise as two different zeolitic aluminosilicate phases, depending upon on the temperature of the area of the plant from which it was removed. Comparison of high temperature scale with synthetic aluminosilicates showed that it is largely carbonate cancrinite. Low temperature plant scale was identified as being an intergrowth between sodalite and cancrinite, the disordered Intermediate phase which is formed in carbonate containing solutions at135-175 °C.

1.8 Scope of Current Work

Due to the immense costs associated with heat exchanger scaling in Bayer plants, the problem has been the subject of a considerable amount of research. Much of the research has focused on the kinetics governing the rates of formation of the scale and identifying the composition of the scale. This work aims to further characterise the observed aluminosilicate phases and then investigate possible routes to eliminate, reduce or modify such scale.

1.8.1 Characterisation of Synthetic Aluminosilicate Scale

Synthetic aluminosilicate scales were synthesised using hydrothermal routes. Subsequent analysis by powder diffraction permitted the accurate determination of structural parameters such as cell parameter, atomic positions and bond lengths and angles.

1.8.2 Effect of Additives on Synthetic Scale

A series of additives were introduced into the formulation used to produce synthetic scale. The aim of this work was to identify additives that could eliminate, reduce or modify the scale formed. A broad range of additives were investigated, from limestone, which is already used to alleviate problems elsewhere in the Bayer plant to novel organic polymeric substances.

1.8.3 Large Scale Reactions

Potential additives or modifications were then investigated using a flow loop system. This system permitted the scale up of laboratory reactions to conditions very representative of those in an actual Bayer plant.

1.9 References

1 The Aluminium Industry Worldwide, booklet produced by British Alcan Aluminium Plc., Chalfont Park, Gerrards Cross, Bucks SL9 0QB, (March 1990).

2 Chemistry of the Elements, N.N. Greenwood and A. Earnshaw, Pergamon Press plc, Oxford, (1984).

3 Chapter 2- Occurrence, F. King , Aluminium and its Alloys, edited by E. G. West, Ellis Horwood Limited, Chichester, (1987).

4 Information supplied by Alcan International.

5 The Sunday Times, 15 August 1999.

6 G. Roach, Application of Emerging Analytical Technologies to the Bayer Process, The Australian Academy of Technological Sciences and Engineering, Academy Symposium, (November 1998).

7 Chapter 3 – Alumina Production, L.K. Hudson, in Critical Reports on Applied Chemistry Volume 20- Production of Aluminium and Alumina, edited by A.R. Burkin, John Wiley & Sons, New York, (1987).

8 A.R. Gerson, K. Zheng. *Journal of Crystal Growth,* **171**, 209, (1997).

9 B.I. Whittington, B.L. Fletcher, C. Talbot, *Hydrometallurgy,* **49**, 1, (1998).

10 J.A. Armstrong, S.E. Dann, *Microporous and Mesoporous Materials,* **41**, 89, (2000).

11 B.A. Xu, D.E. Giles, I.M. Ritchie, *Hydrometallurgy,* **48**, 205, (1998).

12 A.R. Gerson, K. Zheng, *Journal of Crystal Growth,* **171**, 197, (1997).

13 R.G. Breuer, L.R. Barsotti, A.C. Kelly, Metallurgy of Aluminium, Interscience, New York, 133, (1963).

14 Y.B. Rozen, I.Z. Pevzner, D.I. Tsekhovol'skaya, *Tsvetnye Metally,* **8**, 47, (1978).

15 Information supplied by Alcan International Ltd.

16 J. Addai-Mensah, A.R. Gerson, K. Zheng. A. O'Dea, R.St.C. Smart, *Light Metals,* **23**, (1997).

17 Photographs supplied by J. Haines, Alcan International Ltd.

18 http://minerals.usgs.gov/minerals/pubs/commodity/zeolites/

19 Ch. Baerlocher, W.M. Meier, D.H. Olson, Atlas of Zeolite Framework Types, Revised Fifth Edition, Elsevier, Amsterdam (2001).

20 A.K Cheetham, P. Day , Solid state chemistry: techniques, Oxford University Press, Oxford (1987).

21 A.F. Cronstedt, *Stockholm, Akadamiens Handlingar*, **17,** 120, (1756).

22 W. Löwenstein, *American Mineralogist*, **39**, 92, (1954).

23 http://www.iza.ethz.ch/iza/RMB

24 R.M. Barrer, Hydrothermal chemistry of zeolites, Academic Press, London, (1982).

25 D.W. Breck, Zeolite molecular sieves: structure, chemistry and use, Wiley and Sons, London, (1984).

26 R.M. Barrer, J.F. Cole, *Journal of the Chemical Society,* **(A)** 1516, (1970).

27 R.M. Barrer, J.F. Cole, H. Villiger, *Journal of the Chemical Society,* **(A)**, 1523, (1970).

28 J.A. Armstrong, *M.Phil. Thesis,* Loughborough University (1999).

29 http://mineral.galleries.com/minerals/silicate/feldspat.htm

30 L. Pauling, *Zeitschrift für Kristallographie*, **74**, 213, (1930).

31 J.Löns, H. Schulz. *Acta Crystallographica,* **23**, 434, (1967).

32 O. Jarchow, *Zeitschrift für Kristallographie*, 122, 407, (1965).

33 G. Hermeler, J.Ch. Buhl, W. Hoffman, *Catalysis Today*, **8**, 415, (1991).

34 I.P. Kraus, V.A. Derevyankin, S.I. Kuznetsov, *Tsvetnye Metally*, **41**, 43, (1968).

35 T. Oku, K. Yamada, *Light Metals* **31,** 31, (1971).

36 P.J. Cresswell, Proceedings of the 12th Australasian Chemical Engineering Conference, Australia, CHEMECA, 285, (1984).

37 M. Jamialahmadi, H. Müller-Steinhagen, *Journal of the Minerals, Metals and Materials Society,* **50,** 44, (1998).

38 M.C. Barnes, J. Addai-Mensah, A.R. Gerson, *Microporous and Mesoporous Materials*, **31,** 287, (1999).

39 K. Zheng, R.St.C. Smart, J. Addai-Mensah, A.R. Gerson, *Journal of Chemical and Engineering Data,* **43,** 312, (1998).

40 M.C. Barnes, J. Addai-Mensah, A.R. Gerson, *Colloids and Surfaces*, **147,** 283, (1999).

41 M.C. Barnes, J. Addai-Mensah, A.R. Gerson, *Colloids and Surfaces*, **157,** 101, (1999).

42 M.C. Barnes , J. Addai-Mensah, A.R. Gerson, *Journal of Crystal Growth,* **200**, 251, (1999).

43 M.C. Barnes , J. Addai-Mensah, A.R. Gerson, *Light Metals,* 121, (1999).

44 M.C. Barnes , J. Addai-Mensah, A.R. Gerson, R.St.C. Smart, *Light Metals,* 131, (1999).

45 M.C. Barnes, J. Addai-Mensah, A.R. Gerson, *Microporous and Mesoporous Materials*, **31,** 303, (1999).

46 M. Jamialahmadi, H. Müller-Steinhagen, *Aluminium,* **69,** 823, (1993).

47 M. Jamialahmadi, H. Müller-Steinhagen, *Aluminium,* **69,** 920, (1993).

48 M. Jamialahmadi, H. Müller-Steinhagen, *Light Metals,* 159, (1993).

49 M. Jamialahmadi, H. Müller-Steinhagen, B. Robson, *Light Metals,* 121, (1994).

50 M. Jamialahmadi, H. Müller-Steinhagen, B. Robson, *Journal of the Minerals, Metals and Materials Society,* **46**, 36, (1994).

51 A. Duncan, H. Müller-Steinhagen, B. Verity, B. Welch, *Light Metals,* 37, (1995).

52 G.I.D. Roach, *J.B.I. Journal,* **12,** 23, (1994).

53 Y. Zhong-Lin, G. Song-Qing, *Light Metals,* 155, (1995).

54 K. Hackbarth, M. Fechtelkord, J-C. Buhl, *Reaction Kinetics and Catalysis Letters,* **65**, 33, (1998).

55 R.M. Barrer, E.A.D. White, *Journal of the Chemical Society,* 1561, (1952).

Chapter 2

Experimental Techniques

2.1 Introduction

All of the materials described in this thesis were synthesised hydrothermally; for the most part this was done on a small-scale laboratory basis, however some reactions were scaled up and carried out on a 25 L flow loop, as detailed in Chapter 7.

The materials synthesised in this work were either crystalline or polycrystalline solids. In all cases initial characterisation was carried out using a laboratory powder X-ray diffractometer. Typical data sets were collected over 30 minutes in the 2θ range 10 ° to 60 °, this allowed the product to be identified with reference to previous work and searches through the JCPDS[1] (joint committee of powder diffraction studies) data base. Phase purity and cell parameters were also examined in these initial analyses. Powder neutron diffraction (PND) data were collected on some materials of more interest. To permit the extraction of further structural information, these materials were studied in greater detail using full profile Reitveld[2,3] refinement of the PND data.

The use of Thermogravmetric analysis (TGA) allowed thermal stability and the extent of surface absorbed and entrapped water molecules to be determined. Scanning Electron Microscopy (SEM) and Energy Dispersive X-ray Spectroscopy (EDX) were used to study crystallite morphology and chemical composition. Fourier Transform Infrared (FTIR) spectroscopy was principally used in order to confirm the presence of anionic species within the cancrinite framework.

2.2 Synthetic Method

Zeolites can be prepared at low temperature and pressure using a strongly basic aqueous solution containing tetrahedral building units, such as $NaAlO_2$ and SiO_2 together with a templating ion. The shape of the templating ion directs the crystallisation of the aluminate and silicate tetrahedra and determines the structure of the zeolite product.

The crystallisation process is however, under low temperature conditions, extremely slow, hydrothermal methods speed the process up. This methodology uses a sealed vessel to heat the solution above its boiling point. During the course of this work many experiments were performed using both synthetic and Bayer liquor solutions in 23 and 125 ml hydrothermal autoclaves; this more closely replicates the conditions of Bayer plants where temperatures of above 200 °C are achieved.

The autoclave consists of a stainless steel jacket that encases a Teflon liner containing the reaction mixture. The Teflon liner is only ever filled to two thirds of its capacity for safety reasons. The stainless steel jacket is sealed around the liner and the whole autoclave is heated in an oven (with typical temperature stability of ±2 °C).

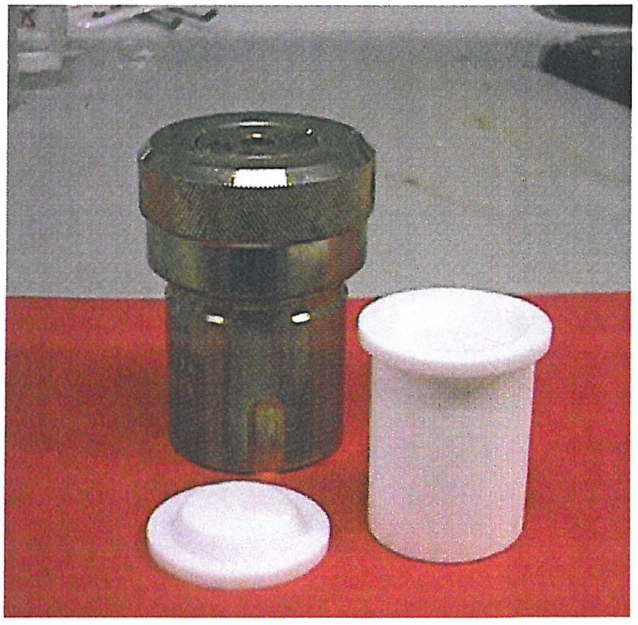

Figure 2.1 Image of a 23 ml Teflon lined stainless steel autoclave, typical of the ones used in the experimental syntheses described in this thesis.

2.3 Diffraction

A crystal can be divided up into layers by planes passing through lattice points. The planes can be described using Miller indices, hkl, which cut the crystal at a/h, b/k and c/l. Each hkl represents a set of parallel planes running through the crystal with a perpendicular spacing of d, between the planes, Figure 2.1. This is referred to as the d-spacing and can be measured using diffraction techniques.

Diffraction is conventionally explained using Bragg's Law, Equation 2.1. In a diffraction experiment the planes of atoms act as semi-transparent mirrors that run through the crystal. Some of the incident radiation is scattered whilst some passes through to be scattered by succeeding planes, interference effects between these scattered X-rays leads to diffraction Figure 2.2 shows incident radiation being diffracted by two adjacent planes.

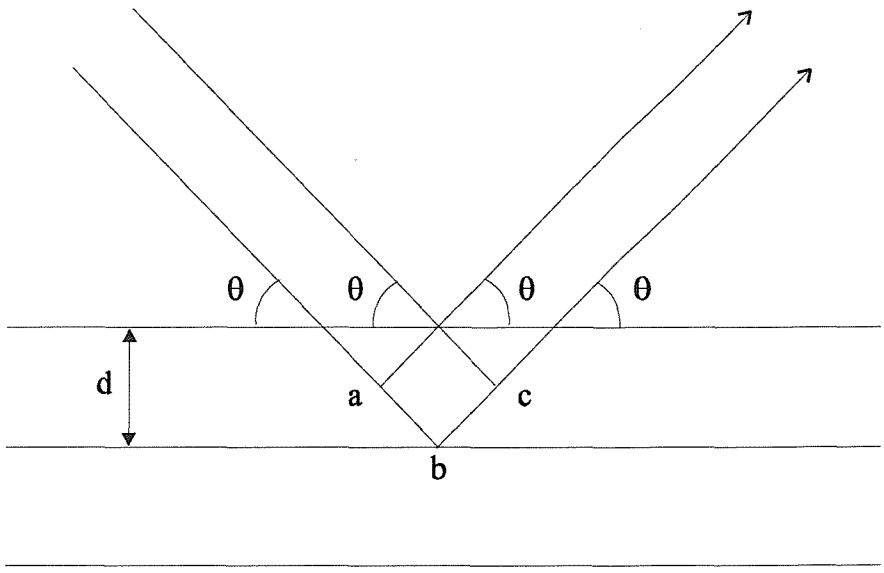

Figure 2.2 Diffraction by Bragg planes in a crystal with path difference = ab + bc.

When the path difference is equal to a whole number of wavelengths, or ab + bc = nλ, constructive interference is seen and a diffraction maxima will occur. This is summarised by the Bragg equation:

$$n\lambda = 2d \sin \theta$$

Equation 2.1

The angle of incidence, θ is known as the Bragg angle. At angles of incidence other than the Bragg angle, scattered beams are out of phase and thus destructive interference or cancellation occurs. The interplanar separations in a crystal are calculated by measuring the positions of the diffraction maxima and generally, only first order diffraction is considered. The crystal system can be derived from these d values by identification of the planes involved, Table 2.1.

Table 2.1 Expressions for d-spacings in the different crystal systems described in this thesis in terms of lattice parameters a, b and c and Miller indices h, k, and l

Crystal System	**Expression for d_{hkl}**
Cubic	$\frac{1}{d_{hkl}^2} = \frac{h^2 + k^2 + l^2}{a^2}$
Hexagonal	$\frac{1}{d_{hkl}^2} = \frac{4}{3}\left(\frac{h^2 + hk + k^2}{a^2}\right) + \frac{l^2}{c^2}$

In theory each of these planes should display diffraction, however due to the existence of reflection conditions or systematic absences, resulting from additional symmetry present in the crystal structure, this is not always the case and the resultant diffraction intensity is zero. Absences arise if the lattice type is non-primitive for example body centred (I) and face centred (F) or if elements of space symmetry such as screw axes and glide planes are present.

2.4 Powder X-ray Diffraction (PXD)

The non-destructive nature and versatility of PXD have led to it becoming the major analytical technique for the characterisation of polycrystalline, solid inorganic materials. Applications of PXD include the identification of unknowns, determination of sample purity, lattice parameters, phase diagrams, particle size and structure refinement. All of the compounds synthesised in this work were either crystalline or polycrystalline solids, thus PXD was used as a means of initial characterisation throughout.

PXD involves the study of polycrystalline samples containing an enormous number of randomly orientated crystallites in the order of $10^{-7} - 10^{-4}$ m in dimension. Ideally the crystallites, and therefore the lattice planes will adopt the whole range of possible orientations and thus the incident beam will be diffracted in all possible directions as governed by the Bragg equation, Equation 2.1. The effect of this is that each lattice spacing in the crystal will give rise to a cone of diffraction.

2.4.1 The PXD Experiment

The PXD data reported in this work, were collected on either a Siemens D5000 or Siemens D8 diffractometer. Figure 2.2 shows a schematic that is representative of the set up both diffractometers. X-rays are generated by accelerating an electron beam through 40 keV onto a copper target and monochromated to give copper $K_{\alpha 1}$ (λ=1.5406 Å) radiation. The X-rays are collimated through an aperture diaphragm and directed onto a sample, which is mounted in a recessed plastic holder. The emergent X-rays are detected by a conventional scintillation detector on both diffratometers, though in some instances a position sensitive detector (PSD) or SOLEX detector was also fitted on the D8. The SOLEX detector allows diffracted X-ray energy discrimination, removing X-ray fluorescence from the collected data. The incident beam, sample and detector are arranged according to the Bragg Brentano parfocusing geometry in which the incident beam and take off geometry is fixed at $\theta/2\theta$ relationship by rotating the sample plate at precisely half the rate of the detector through the angular range to be studied. The instrument is calibrated mechanically and this calibration checked periodically using α-SiO_2.

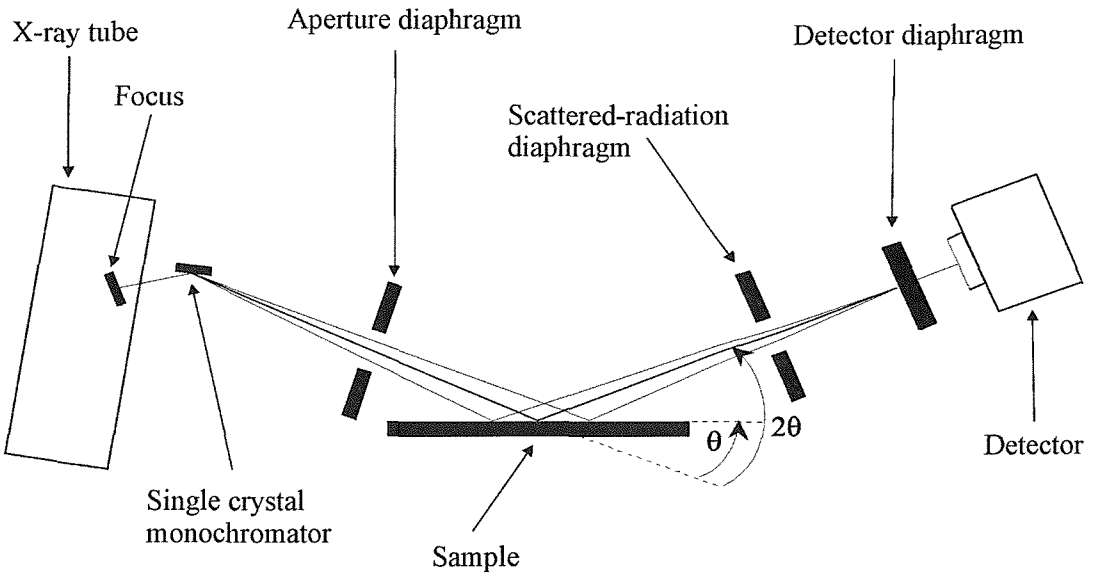

Figure 2.3 Schematic diagram of the powder X-ray diffractometers.

As data is recorded it is passed constantly to a personal computer where a real time display can be viewed. Data are collected by the SIEMENS DIFFRAC^{plus} software, upon completion the diffraction data can be analysed using the SIEMENS DIFFRAC^{plus} evaluation program (EVA). The acquired data can be compared with previous samples or diffraction patterns stored on the JCPDS database. Short run times of 20 minutes over the 2θ range 10-60 ° with a step size of 0.02 ° were typically employed to characterise the materials synthesised.

2.4.2 Analysis of PXD data

Initial analysis involved fingerprinting the observed data via JCPDS. This allowed the pattern from the target species to be compared with those from similar structures previously determined, as well as the identification of impurity phases. Lattice parameters were calculated using the CELL program which uses an iterative least squares program to minimise the equation:

$$M = \sum_n W_n (\sin^2\theta_n^{obs} - \sin^2\theta_n^{calc})^2$$

Equation 2.2

where W_n = a weighing factor

M = weighted minimised difference for observed 2θ data

The cell parameters produced, with estimated standard deviation (e.s.d's), only reflect the goodness of fit between the observed and calculated 2θ positions, and provide no indication of systematic errors or sample impurities.

2.5 Powder Neutron Diffraction (PND)

Neutrons, due to their wave particle duality, may be used for diffraction experiments in a similar way to X-rays. The wavelength of a neutron is governed by the de Broglie equation[4], Equation 2.3:

$$\lambda = \frac{h}{mv}$$

Equation 2.3

where λ = wavelength

h = Planck's constant

m = mass of a neutron

v = velocity of a neutron

The most significant difference between powder neutron diffraction (PND) and PXD experiments is the method by which the radiation is scattered. X-rays are scattered by the electrons of an atom and thus scattering power is a function of atomic number. Neutrons interact with the nucleus itself and there is no straightforward dependence of neutron scattering power on atomic number. The neutron scattering power of a nucleus is dependent upon both the potential scattering and the resonant scattering, which varies across the periodic table giving neighbouring elements and isotopes very different scattering lengths. PND can be used in circumstances where PXD is inadequate for example, to locate light atoms such as deuterium in the presence of heavy ones. As a result of differing neutron scattering lengths, it can also, in some cases be used to distinguish between atoms with similar X-ray scattering powers.

Another effect of intra atom interaction with the nucleus rather than the electrons of an atom is the absence of neutron interference effects that cause X-ray scattering to diminish with $(\sin\theta)/\lambda$ so the scatting intensity shows no angular dependence. This allows the collection of more complete data sets with reasonable intensity at small d-spacings, permitting more accurate structure determination.

Neutrons have zero charge, this allows them to penetrate the surface of materials which makes it possible investigate the bulk of a sample. It is therefore also possible to

construct equipment around a neutron diffraction sample, allowing routine experiments to be performed at low temperature in a cryostat and at high temperature in a furnace.

Some of the major difficulties encountered in the study of zeolitic materials are the similarity in the X-ray scattering lengths of silicon and aluminium, the presence of light counter cations and the inclusion of water molecules within the framework. All of these problems can be alleviated by the use of neutron diffraction, making it a very powerful technique in the structural analysis of these materials. On the downside, neutron experiments are costly and the low flux associated with neutrons leads to lengthy experiment times.

2.5.1 Time of Flight (TOF) PND

Time of flight powder neutron diffraction (TOFPND) data were collected on POLARIS (medium resolution instrument) and HRPD (high resolution powder diffractometer) at the ISIS facility located at the Rutherford Appleton Laboratory (RAL), Oxfordshire, UK. Neutrons are generated at RAL by bombarding a heavy metal target with high-energy protons. The ISIS facility employs a spallation neutron source that provides pulses of a wide range of energies (variable wavelengths). These pulses of neutron radiation are separated according to their time of flight between spallation source and detector and hence in terms of their wavelength. From the Bragg equation (Equation 2.1), for a conventional diffraction experiment, λ is fixed and d and θ are variables. However for a TOF experiment, λ and d are variables with θ fixed, the diffracted neutrons are accurately detected by fixed angle detectors according to their time of flight.

Diffractometers at pulsed neutron sources operate in a fundamentally different manner from conventional, constant wavelength detectors. Both POLARIS and HRPD measure the Bragg reflections at fixed scattering angles and monitor the time of arrival of the neutron after the initial burst produced at the source. Conventional diffractometers measure the Bragg reflections by scanning a detector over a range of angles from low to high 2θ. The relationship between TOF and d-spacing is linear and derived from de Broglie's relationship (Equation 2.3) and Bragg's law:

$$\lambda = \frac{h}{mv}$$

$$\lambda = \frac{h}{m_n v_n}$$

$$\lambda = 2d\sin\theta$$

where h is Planck's constant, m_n and v_n, are the mass and velocity of a neutron respectively, with d and sinθ as derived by Bragg's law. If the total distance travelled by a neutron (source → sample + sample → detector) is equal to L, and the corresponding time of flight is t then:

$$v_n = \frac{L}{t}$$

hence

$$\left[\frac{h}{m_n}\right].\left[\frac{t}{L}\right] = 2d\sin\theta$$

Equation 2.4

then

$$t = 2dL\left(\frac{m_n}{h}\right)\sin\theta$$

Equation 2.5

$$\therefore t \propto d$$

So for a 10 m (Polaris) and a 100m (HRPD) instrument a 1 Å d-spacing will be detected in backscattering to have a time of flight of approximately 5000 μs and 50000 μs respectively.

2.5.2 HRPD

Resolution Considerations

HRPD is the highest resolution neutron diffractometer in the world. The resolution of a diffractometer, $\Delta d/d$ is a measure of the spread in the Bragg reflection for a given d-spacing, it is crucial in determining the overall quality of a diffractometer. On a pulsed source there are three major contributions: a timing uncertainty, ΔT, an angular uncertainty, and flight path uncertainties, ΔL. Consideration of these factors in the design of HRPD has led to resolution of $\Delta d/d = 4.5 \times 10^{-4}$ in backscattering mode. The backscattering bank is comprised of a complicated array of ZnS scintillators, fixed at scattering angles of $160^\circ \leq 2\theta \leq 176^\circ$.

Samples are loaded into a vanadium sample can and placed in one of two positions, either 1 m or 2 m from the backscattering bank. Use of the 1m position enables diffraction data to be recorded simultaneously in all three detector banks; backscattering, 90°, and low angle. Scattering at low angles ($20^\circ \leq 30^\circ$) allows long d-spacings to be measured; this is crucial for cell indexing purposes.

High resolution data were collected to enable the accurate study of the cancrinite framework and the non framework species located within the system of channels and cages.

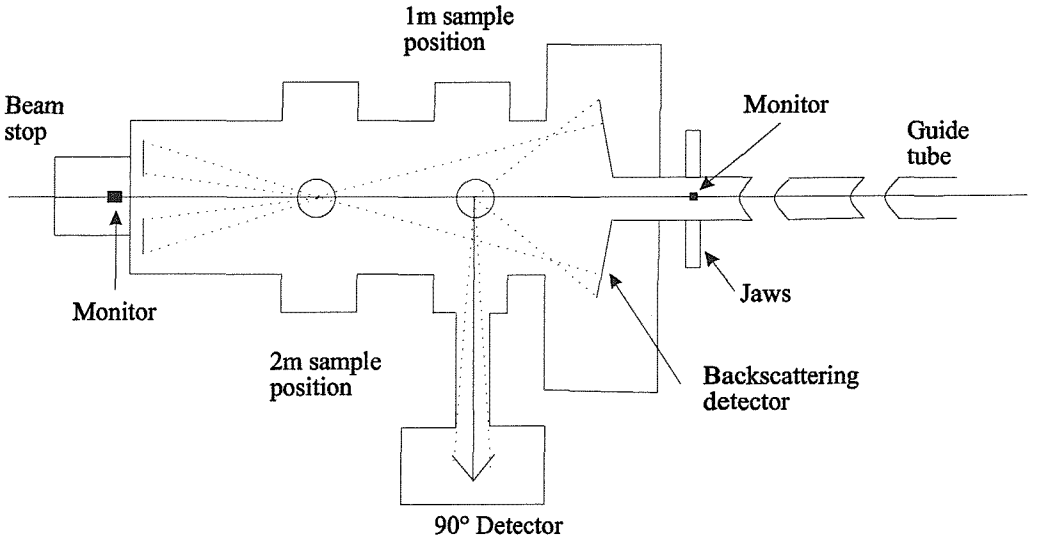

Figure 2.4 Schematic representation of the HRPD at ISIS.

2.5.3 POLARIS

POLARIS is a high intensity, medium resolution powder diffractometer. The intense neutron flux and large detector bank provide a high-count rate; allowing experiments to be performed over short counting times or with very little sample.

The instrument receives a polychromatic, 'white' beam of neutrons from the ambient temperature water moderator. The sample position on POLARIS is 12.0m from the moderator, and the incident and transmitted neutron flux is monitored by two glass scintillator detectors positioned ~4 m before the sample and ~2.5 m after it. Two motor driven collimators in the incident beamline allow the size of the beam to be reduced from the maximum dimensions of 40 mm high, 20 mm wide to match the sample size or to minimise the background from sample environment equipment.

A total of 434 ^{3}He gas and ZnS scintillator detectors are arranged into four separate banks; two at low angles, one at 2θ~90 ^{o} and one at backscattering angles. The backscattering bank of detectors yields the highest resolution the $\Delta d/d = \sim 5 \times 10^{-3}$, over the d-spacing range 0.2-3.2 Å and was used for the refinement detailed in this thesis.

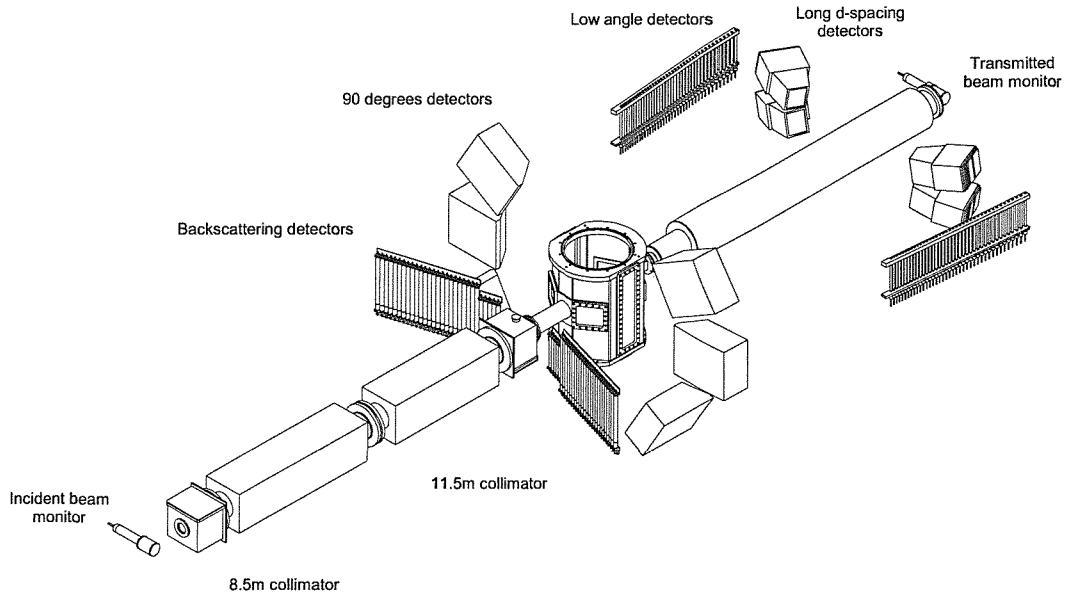

Figure 2.5 Schematic representation of the POLARIS at ISIS.

2.6 The Rietveld Method

Early attempts used in the analysis of powder diffraction data were based on those developed for the structural refinement of single crystals. These involved a least squares refinement using $|F|$ values based on structure factors extracted from the diffraction pattern. In the case of overlapping or partial coincidence of diffraction maxima the extraction of structure factors is highly problematic and so severely limited the information that could be deduced.

In 1967 H.M. Rietveld[2,3] developed a method for least squares refinement using an entire diffraction pattern, alleviating the need for structure factor extraction. Rietveld realised that although many individual reflections did overlap and thus could not be modelled as single entities, they could be fitted using simple peak shape parameters in order to determine the total intensity and peak shape of a cluster of reflections. This method took advantage of all the information contained in very complicated patterns and permitted more complex problems to be attempted. Initial work focussed on constant wavelength PND due to its intrinsic Gaussian peak shape, however the development of more complex peak shape functions has allowed the Rietveld technique to be extended to PXD and TOF PND. Today most structural refinement of powder samples is carried out so using the Rietveld method.

The refinement begins with the input of a suitable starting model. This model is obtained from a similar crystal system; a good initial model is important to the success of the Rietveld method; it greatly speeds up structure solution and helps to prevent assigning the incorrect structure to the material under investigation. The scale factors and background parameters are next introduced as refinement of these parameters involves only coefficients of ordinary orthogonal polynomials. The problem is therefore linear and should converge immediately irrespective of starting values. This is followed by the determination of the lattice parameters, zero-point correction and sample displacement which permits accurate positioning of the Bragg reflections. Atom positions can then be refined to fit peak intensities, followed by temperature factors on well-positioned atoms and peak shape parameters to allow broadening effects to be taken into account. If the data are of sufficiently high quality, anisotropic temperature factors may also be refined.

During a Rietveld refinement the 'best-fit' sought is the best least squares fit to the many of thousands of observables Y_i's, simultaneously. The quantity minimised in the least squares refinement is the residual, S_y:

$$S_y = \sum_i W_i \left[Y_i^{obs} - Y_i^{calc} \right]^2$$

Equation 2.6

where W_i = a weighting factor given by $1/Y_i^{obs}$.

Y_i^{obs} = observed intensity at the *i*th step.

Y_i^{calc} = calculated intensity at the *i*th step.

A powder diffraction pattern may be thought of as a collection of individual reflection profiles, each of which has a peak height, position, width, decay tails and an integrated area proportional to the Bragg intensity, I_K, where K represents the Miller indices h,k, and l. I_K is proportional to the square of the absolute structure factor $|F_K|^2$. In all powder patterns where the Rietveld method is employed these profiles are not all resolved, but partially overlap. A crucial feature of the Rietveld method is that no attempt is made to allocate intensity to a particular Bragg reflection or to resolve overlapping reflections in advance. Consequently a reasonably good starting model is required.

Typically, many Bragg reflections contribute to the intensity, y_i, observed at an arbitrarily chosen point, I, in the pattern. The calculated intensities y_i are determined from $|F_K|^2$ values calculated from the structural model by summing of the calculated contributions from neighbouring Bragg reflections plus the background:

$$y_{ci} = s \sum_K L_K |F_K|^2 \phi(2\theta_i - 2\theta_K) P_K A + y_{bi}$$

Equation 2.7

where *s* is the scale factor, L_K contains the Lorentz, polarisation and multiplicity factors, ϕ is the reflection profile function, P_K is the preferred orientation function, A is an absorption factor, F_K is the structure factor for the Kth Bragg reflection and y_{bi} is the background intensity at the *i*th step.

The relationship between the adjustable parameters and the intensities are non linear and thus the starting model must be close to the correct model or the least square procedure will not progress to a global minimum. Instead, the process will diverge or lead to a 'false' minimum. The use of multiple data sets or constraints allows this to be overcome. Simultaneous refinement of multiple phases and comparative analysis of the overall scale factors for the phases offers a method for quantitative phase analysis.

Background intensity, y_{bi}, at the *i*th step can be obtained a number of ways, typically it is modelled using one of a set of functions supplied with the refinement program. The type of data being refined determines the choice of background function.

The reflection profile function, ϕ, approximates the effects of instrumental and specimen features. The model should adequately describe the instrumental resolution function over a wide range of 2θ and also incorporate sample broadening effects such as particle size, strain and stacking disorder. For angle dispersive data with Gaussian peak shapes all peak shapes are corrected for breadth dependence on angle using the method of Caglioti *et al*[5]:

$$H^2 = U\tan^2\theta + V\tan\theta + W$$

Equation 2.8

where H is the full peak width at half-maximum intensity and U, V and W are the refinement parameters. This formula takes account of the peak broadening resulting from the particle size effect. For X-ray and TOF instrumentation the reflection profile is neither Gaussian or symmetric and therefore more complex expressions must be used[6].

In the Rietveld method the difference between the observed diffraction profile and that calculated for a trial structure is minimised by an iterative least squares procedure. The least squares parameters can be considered as two distinct groups. The first group defines the position and shape of the peaks and consists of the unit cell parameters, the counter zero offset and the asymmetry factor. The second group, the structural and thermal parameters, defines the content of the unit cell. These consist of the profile

scale factors the co-ordination, occupation and temperature factors of each atom. A quantitative assessment of agreement between the calculated and observed profiles is made using statistical goodness of fit functions. These reliability factors are defined as follows:

$$R_{profile} = R_p = \left[\frac{\sum_i \left| Y_i^{obs} - Y_i^{calc} \right|}{\sum_i Y_i^{obs}} \right] \times 100\ \%$$

Equation 2.9

This may be compared with the reliability index $R_{expected}$ derived purely from statistical considerations:

$$R_{expected} = R_e = \left[\frac{(N - P + C)}{\sum_i W_i (Y_i^{obs})^2} \right]^{1/2} \times 100\ \%$$

Equation 2.10

where N = number of observables, P = number of refinable parameters and C = number of constraints.

In addition, $R_{weighted\ profile}$ and $R_{integrated\ intensities}$ may be defined as:

$$R_{weighted\ profile} = R_{wp} = \left[\frac{\sum_i W_i \left| Y_i^{obs} - Y_i^{calc} \right|^2}{\sum_i W_i (Y_i^{obs})^2} \right]^{1/2}$$

Equation 2.11

$$R_{integrated\ intensities} = R_i = \left[\frac{\sum_k \left| I_k^{obs} - I_k^{calc} \right|}{\sum_k I_k^{obs}} \right]$$

Equation 2.12

Finally the chi-squared parameter may be defined as:

$$\chi^2 = \left[\frac{1}{N+P+C}\right]\sum_i W_i(Y_i^{obs} - Y_i^{calc})^2$$

$$= \left[\frac{R_{wp}}{R_e}\right]^2$$

Equation 2.13

Chi-squared is the natural measure of the fit, and is normally minimised in the refinement. Thus for a good fit, the weighted profile R-factor should approach the statistically expected R-factor value. The goodness of fit can also be measured by examining a plot of the profile fit; for a good fit, the difference line between the calculated and observed patterns should be as flat as possible.

All Rietveld refinements of powder neutron data presented in this thesis were performed using the Generalised Structure Analysis Suite (GSAS), of Larson and von Dreele[7].

2.7 Scanning Electron Microscopy (SEM)

Electron microscopy is a versatile technique that has many applications, including electron diffraction and imaging. In this study Scanning Electron Microscopy (SEM) is used to examine sample morphology and Energy Dispersive X-ray Spectroscopy (EDX) used to determine the elemental composition of individual crystallites.

In an electron microscope electrons are generated by thermionic emission and monchromated by acceleration through a potential, which alters the wavelength of the electron beam. When accelerated through a voltage V an electron acquires an energy, eV. The relationship between the wavelength and the energy of the electron beam is given by Equation 2.14 below.

$$\lambda = \left[\frac{1.5}{(V + 10^{-6} V^2)} \right]^{1/2} nm$$

Equation 2.14

2.7.1 Electron-Specimen Interactions

Upon reaching the specimen surface the electrons can interact in a number of ways, summarised in Figure 2.6.

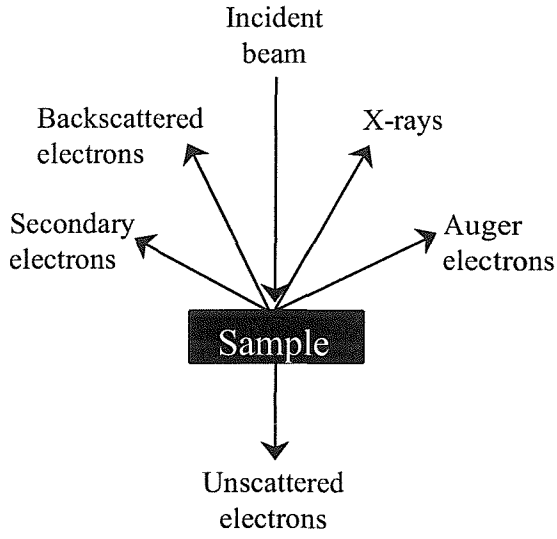

Figure 2.6 Schematic representation of the possible scattering in a SEM experiment.

There are two broad categories of electron-specimen interaction, elastic and inelastic scattering. Elastic scattering is defined as a process that changes the direction of a primary electron but not its energy. Inelastic scattering refers to any process that causes the primary electrons to lose energy (> 0.1 eV). There are a variety of inelastic scattering mechanisms.

2.7.2 Imaging

The morphology of a sample can be examined using SEM. The scanning electron microscope gives a magnified, high resolution image of the sample by illumination with an electron beam rather than light.

Single valence electron excitation gives rise to electrons which escape from the surface of the specimen with an energy below 50 eV, these are the main secondary electrons. Secondary electron detection is the most common imaging mode used in SEM.

Backscattered electrons are primary electrons that have undergone elastic collisions with the nuclei of atoms of the sample. Employment of backscattered electrons allows topographic images with improved contrast to be obtained.

2.7.3 Elemental Analysis

Upon bombardment with high energy electrons the sample also emits X-rays. X-rays are emitted when inner shell electrons are removed from the sample and outer shell electrons drop to lower energy shells to fill the holes, Figure 2.7.

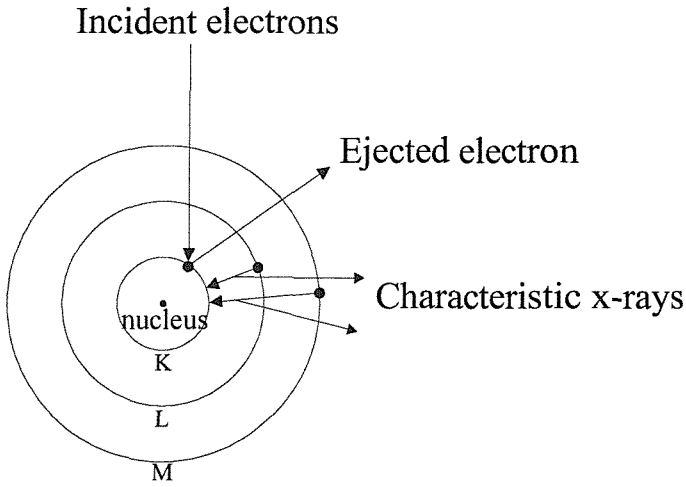

Figure 2.7 Schematic representation of the formation of X-rays in an EDX experiment.

The energies of these X-rays are characteristic of the element from which they originated. The software attached to the SEM allows quantitative collection of detected X-rays and their intensity. Care should be taken when examining these results as the errors associated with this quantitative analysis can be relatively large, especially for light elements and X-rays produced by different transitions of different elements occur at the same or similar energies.

2.7.4 Instrumentation

SEM was performed using a JEOL JSM-820 at the Banbury Laboratory, Alcan International Ltd, a JEOL JSM-6400 at the Southampton Oceanography Centre and a Philips XL30ESEM at the Southampton School of Chemistry.

A schematic diagram of the microscope is displayed in Figure 2.8. An electron gun consisting of a tungsten filament produces an electron beam using an accelerating voltage of 10-30 KeV and a probe current of 10^{-12}-10^{-15} A. The beam of electrons travels down the SEM under high vacuum and reaches the two electromagnetic condenser lenses which demagnify the emitted beam and give a minimum spot diameter of a few nm at the specimen. Below the condenser lenses there are typically four or five electromagnetic objective lenses which form the first intermediate image and diffraction pattern, one or other of which is enlarged by the subsequent projector lenses and displayed on a screen. It is these projection lenses which determine the overall magnification of the final image. The beam is then scanned across the sample using the scan coils and a detector counts the number of low energy secondary electrons or other radiation emitted from each area of the sample.

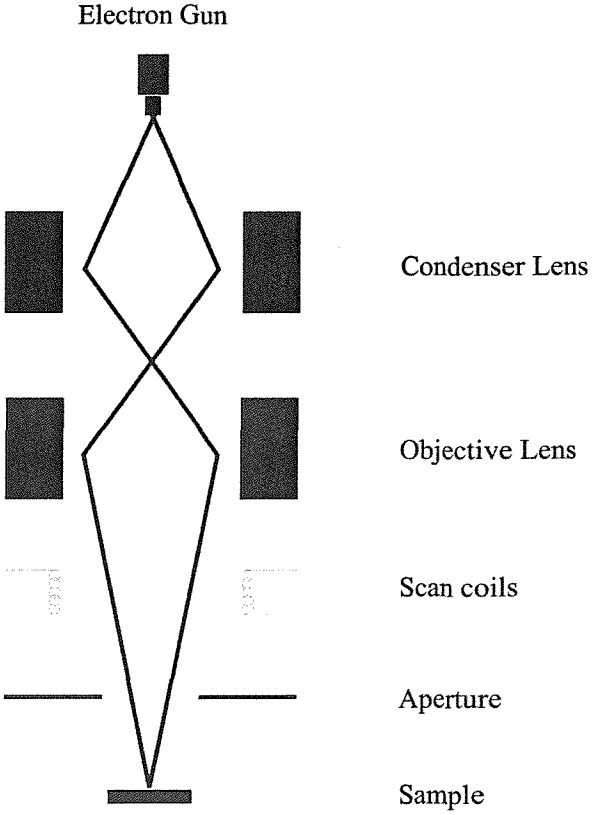

Figure 2.8 Schematic diagram of a scanning electron microscope.

2.8 Fourier Transform Infra-Red (FTIR) Spectroscopy

Infrared spectra were recorded using a Perkin Elmer FT-IR Spectrum 1 spectrometer equipped with a diffuse reflectance facility. Materials to be analysed were dried consistently to remove surface water thus leaving only imbibed zeolitic water, then intimately ground with spectroscopic KBr (1-5% w/w) and mounted in a 'macrocup' holder and spectra acquired over the range 4000 to 500 cm^{-1}, using an automatic background function as a reference. The spectra were used essentially to support PXD phase identification and to confirm the presence and nature of the species entrapped within the zeolitic frameworks.

2.9 Thermogravimetric Analysis (TGA)

Thermogravimetric analysis was performed using a water cooled Polymer Laboratories PL STA 1500 instrument. In a typical experiment 30 mg of sample was heated from room temperature to 1000 °C at a heating rate of 25 °C/minute, held for 30 minutes and cooled back to room temperature at a rate of 40 °C/minute. Data points were sampled every 4 seconds and displayed real time. The results allowed analysis of the water content, and the temperatures at which dehydration and structural collapse occur.

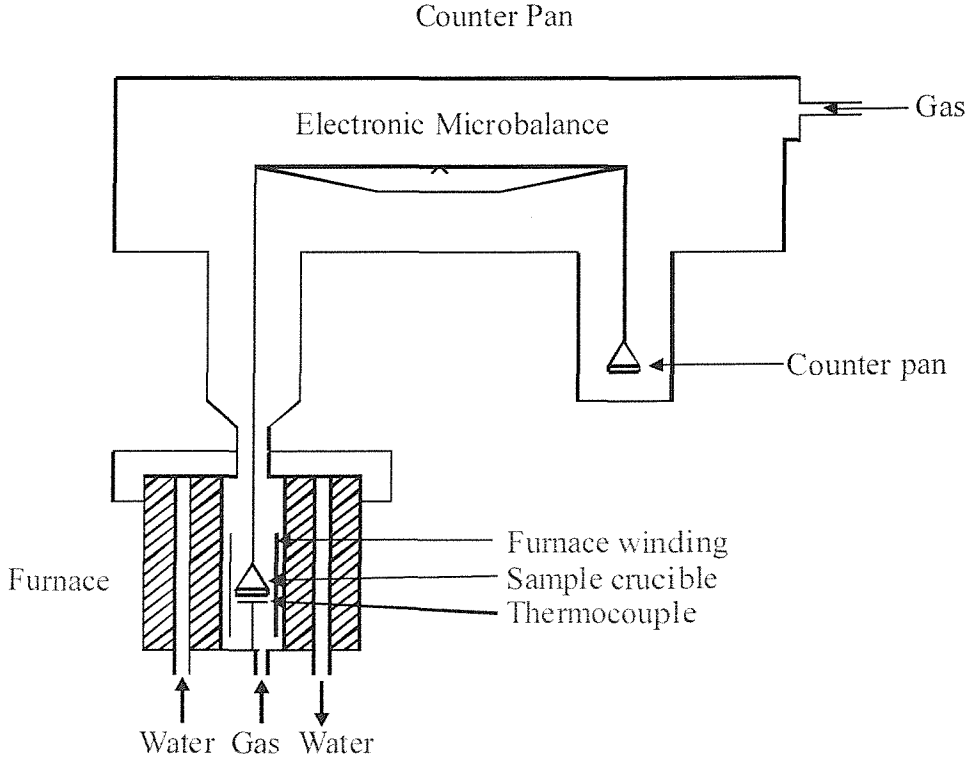

Figure 2.9 Schematic representation of the PL-STA 1500.

2.10 References

1 International Centre for Diffraction Data, 12 Campus Boulevard, Newton Square, Pennsylvania 19073-3273, USA, (1995).

2 H.M.Rietveld, Acta Crystallographia, **22**, 151, (1967).

3 H.M. Rietveld, Journal of Applied Crystallography, **2**, 65, (1969).

4 Atkins P, Physical Chemistry, 4th Edition, Oxford University Press, 298, (1992).

5 G. Calglioti, A. Paoletti and F.P. Ricci, Nuclear Instrument Methods, **35**, 223, (1958).

6 R.A. Young, The Rietveld Method, 1st Edition, Oxford University Press, 141, (1993).

7 A.C. Larson and R.B. Von Dreele, Generalized Structure Analysis System, MS-H805, Los Alamos, NM 87545, (1990).

Chapter 3

Synthesis and Characterisation of Carbonate Cancrinite and Intermediate

3.1 Introduction

Cancrinite and a sodalite-cancrinite intermediate, which for the remainder of this report shall be referred to as Intermediate, have been identified as the two major phases contributing to aluminosilicate scaling in the heat exchangers of a Bayer plants. This chapter reports studies carried out to develop the understanding of the two phases.

Cancrinite is observed in nature as a porous mineral with the composition $Na_6Ca(AlSiO_4)_6CO_z\ (H_2O)_2$[1]. Since initial crystallisation experiments by Eitel[2] cancrinites have been synthesised with a variety of anions including carbonate, sulphate, and nitrate[3,4,5,6].

The structural features of the cancrinite framework have been known since the early works of Pauling[7], Gossner and Musgnug[8] and Jarchow[9,10,11]. The framework is formed by stacking layers of 6-membered rings of SiO_4 and AlO_4 tetrahedra along the c-axis in an ABAB sequence in the space group $P6_3$. This stacking sequence results in the creation of chains of small, 11-hedral, ∈-cages and 12 ring channels (approximately 5.9 Å in diameter) along the 3-fold and 6_3 axes, respectively. The wide 12-ring channels contain cations and intracrystalline anions such as carbonate, whereas the small ∈-cages contain only cations and water molecules. In order to develop the cancrinite structure for potential industrial application, Lee *et al*[12] report the synthesis of germanium ($Na_6Cs_2Al_6Ge_6O_{24}.Ge(OH)_6$) and gallium-germanium ($Na_6Cs_2Ga_6Ge_6O_{24}.Ge(OH)_6$) cancrinite analogues.

The structures of both naturally occurring and synthetic cancrinite have been studied using X-ray diffraction methods by a number of authors. While these structure determinations show the gross structural features, significant ambiguities exist associated with light atoms (especially H) or close to isoelectronic species (e.g. Na,O,C). Further complexities result from the variations in compositions in naturally occurring and synthetic materials (e.g. calcium and water contents). In these work PND has been employed to try and resolve these structural problems.

The synthesis of carbonate cancrinite (the source of cancrinite in Bayer heat exchangers) under mild hydrothermal conditions is reported to be more difficult than for

other salt filled cancrinites[13], due to the co-crystallisation of sodalite and an intermediate between sodalite and cancrinite, termed here Intermediate. The formation of phase-pure carbonate cancrinite and Intermediate is strongly dependent on experimental conditions. The Intermediate phase, identified also by Armstrong and Dann[14] as being a major source of Bayer plant aluminosilicate scale, is believed to have a one-dimensional stacking order of the ($AlSiO_4$) layers between that of sodalite (ABC) and cancrinite (ABAB) and the entrapped species are a mixture of carbonate and water. Little else is reported in the literature about this phase.

3.2 Aims

The aims of the investigation detailed in this chapter were: to identify a reliable synthesis method for phase pure carbonate cancrinite and Intermediate, this was crucial in order to allow further investigations into additives/synthetic variations that may prevent/inhibit/modify the formation of the phases. The second aim was to assess the use of different characterisation techniques and their ability to distinguish between the two phases.

The final aim was to synthesise deuterated samples of the two phases and develop the understanding of their structural characteristics through refinement of PND data.

3.3 Cancrinite and Intermediate Synthesis and Characterisation

The most severe aluminosilicate Bayer plant scaling occurs within the heat exchangers. Heat exchanger scale removed from both high (typically 220 °C) and low (typically 150 °C) temperature Bayer plants, has been characterised by Armstrong and Dann[14] and is seen to consist largely of carbonate cancrinite and Intermediate phase respectively. Preliminary experimental investigations aimed to synthesis pure phases of carbonate cancrinite and Intermediate to assess the suitability of the characterisation techniques available to study them.

3.3.1 Experimental

Syntheses of carbonate cancrinite and Intermediate were carried out following the experimental procedures described by Armstrong[15]. A sodium carbonate concentration of 30 g/L (as per Bayer liquor) was employed initially, however this was reduced to yield to pure phase Intermediate.

Syntheses were carried out under hydrothermal conditions at temperatures of 150 °C and 220 °C under autogenous pressure in 23 ml, Teflon lined steel autoclaves under static conditions for 48 hrs.

Kaolin (0.2520 g), sodium carbonate (0.3996 g or 0.1 g) and sodium hydroxide solution (8 M, 14 ml) were added to the Teflon cup. The resultant white powders were washed with 150 ml distilled water and dried for 24 h at 80 °C.

3.3.2 Results

The resulting microcrystalline white powders were analysed using PXD, SEM, FTIR and TGA.

3.3.2.1 PXD Results

Initial phase identification was achieved by the analysis of PXD data collected over the 2θ range 10 ° to 60 ° for 30 minutes. The PXD patterns for carbonate cancrinite and Intermediate are presented overleaf in Figure 3.1. The phases yielded at the different temperatures and Na_2CO_3 concentrations are recorded below in Table 3.1.

Table 3.1 Effect of temperature and sodium carbonate concentration on phase yielded.

Temperature	Ref.	Sodium Carbonate	Phase
150 °C	**3-1**	7 g/L	Intermediate
150 °C	**3-2**	30 g/L	Intermediate/Disordered Cancrinite
220 °C	**3-3**	7 g/L	Cancrinite
220 °C	**3-4**	30 g/L	Cancrinite

Pure carbonate cancrinite is formed at both carbonate concentrations at 220 °C. At 150 °C a mixture of cancrinite and Intermediate or disordered cancrinite is observed when a carbonate concentration of 30 g/L is employed. In order to achieve a pure sample of Intermediate, a lower carbonate concentration of 7 g/L is necessary, this is consistent with the work of Armstrong and Dann[14] and Hackbarth *et al*[13]. In order to remain consistent with Bayer conditions a carbonate concentration of 30 g/L has been employed for the remainder of this work; with the exception of the preparation of phase pure deuterated samples for structural studies.

The disordered nature of the Intermediate phase results in the collection of diffraction patterns that have fewer peaks (in comparison to cancrinite patterns), noisy backgrounds and the peaks present are generally broad.

In the diffraction pattern of ideal cancrinite the (211) reflection near 27 ° 2θ exhibits maximum intensity but is absent in the powder pattern of Intermediate. The signal near 24 ° 2θ is found in both patterns but with maximum intensity for Intermediate. Thus a

diffraction pattern with the (211) reflex of a weaker intensity than the near 24 ° 2θ reflex can be the result of two different cases, a mixture of cancrinite and Intermediate or the existence of a disordered cancrinite phase alone. Disordered cancrinite is another intermediate phase but it has a much closer relationship to cancrinite, it shows typical cancrinite reflections in its PXD pattern but at much lower intensities. In addition to these differences the (101) reflection near 19 ° is characteristic of cancrinite and is absent in the case of Intermediate.

The features of the PXD described above for Intermediate are similar to those that would be observed for a sodalite pattern. In the region 50 ° < 2θ < 60 ° sodalite would produce three reflections at approximately 50 °, 52 ° and 57 °, the Intermediate however only two at 52 ° and 57 °.

Lattice Parameter Calculation

The cancrinite diffraction pattern was indexed with a hexagonal unit cell and lattice parameters calculated using the computer program 'CELL'. The limited symmetry of the disordered Intermediate phase means refinement of the lattice parameters must be performed using a reduced hexagonal unit cell, as proposed by Hermeler *at al*[16] in 1981. Calculated lattice parameters were entirely consistent with those in the literature and are displayed below in Table 3.2.

Table 3.2 Calculated lattice parameters.

Ref.	Phase	Lattice Parameters Å
3-1	Intermediate	7.305(2) 2.583(1)
3-2	Intermediate/Disordered Cancrinite	7.297(2) 2.581(1) / 12.647(2) 5.137(6)
3-3	Cancrinite	12.668(2) 5.166(2)
3-4	Cancrinite	12.679(1) 5.171(1)

During these studies Intermediate lattice parameters have also been refined using the description for cancrinite lattice parameter refinement in instances where a direct comparison of the effect of temperature or an additive was to be made. Upon synthesis of either disordered cancrinite or a mixture of cancrinite and Intermediate, lattice parameters have been refined for both cancrinite and Intermediate.

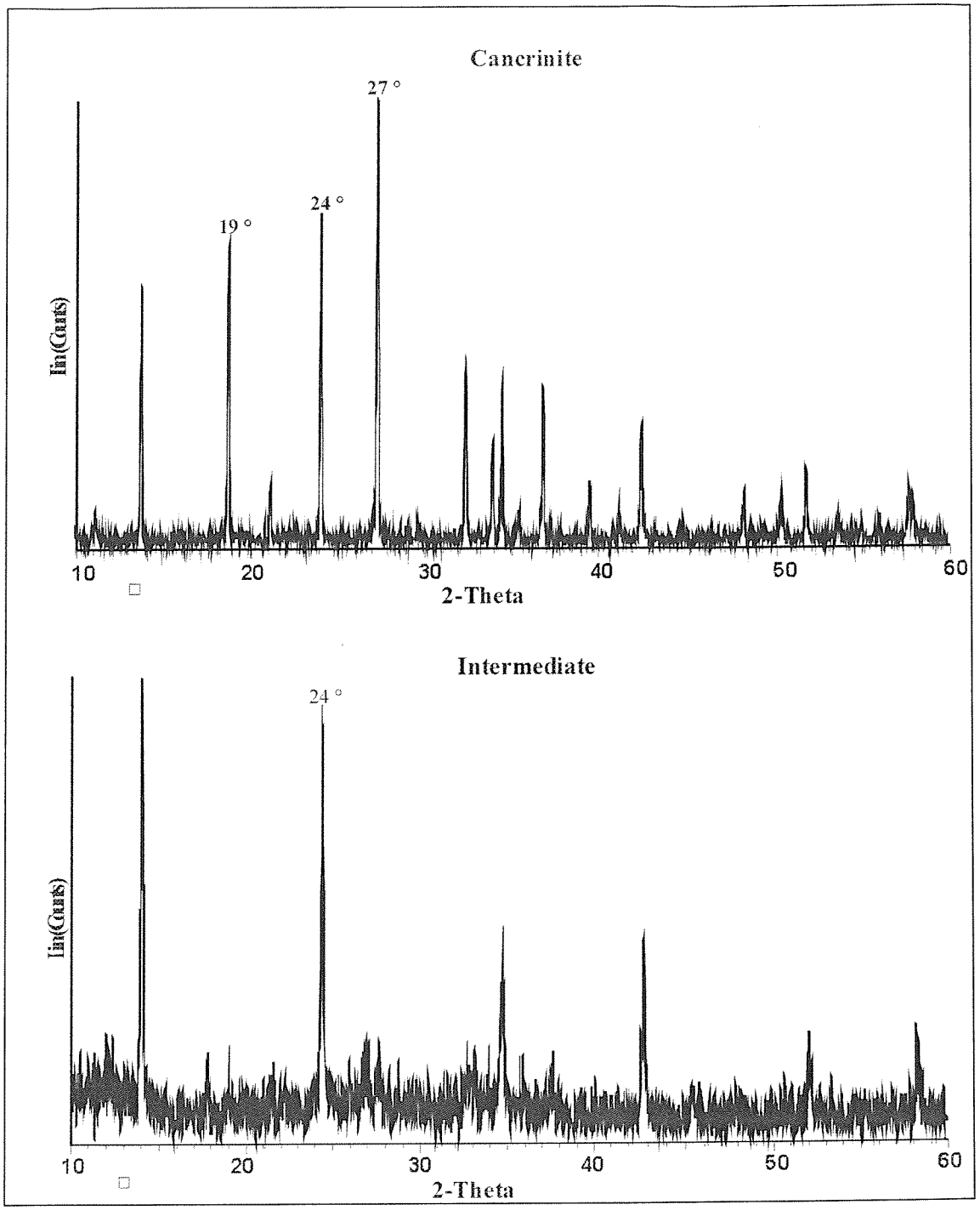

Figure 3.1 PXD patterns collected on samples of sodium carbonate cancrinite (3-4) and Intermediate (3-1).

3.3.2.2 Electron Microscopy Results

Cancrinite and Intermediate products were examined using SEM.

SEM Micrographs

SEM micrographs revealed that the two phases have very different morphologies. The cancrinite crystallites are rod-shaped and have typical dimensions of 1 x 1 x 7 μm, Figure 3.2 below. Intermediate samples are seen to consist of irregular platey fragments, with typical dimensions of approximately 2 x 10 x 25 μm, Figure 3.3 below.

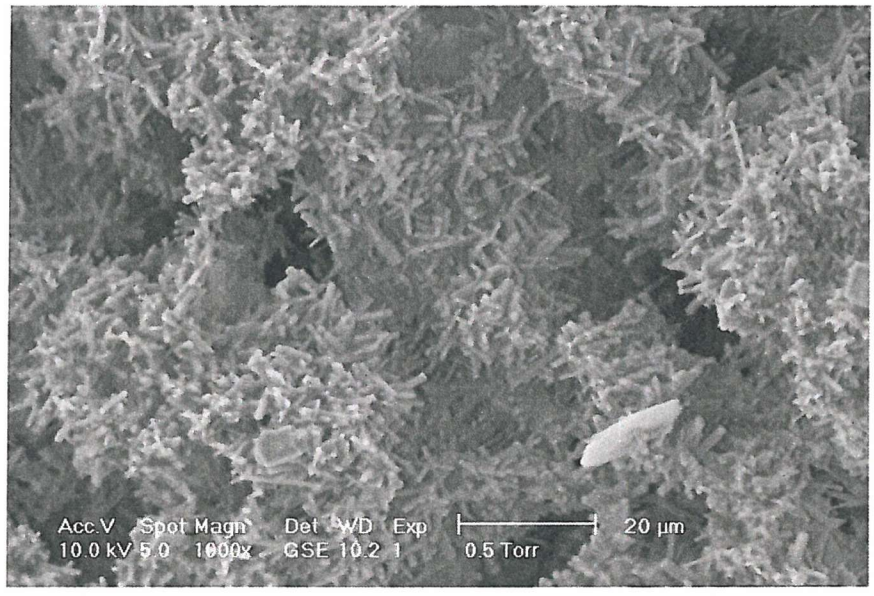

Figure 3.2 SEM micrograph of cancrinite rods (3-4).

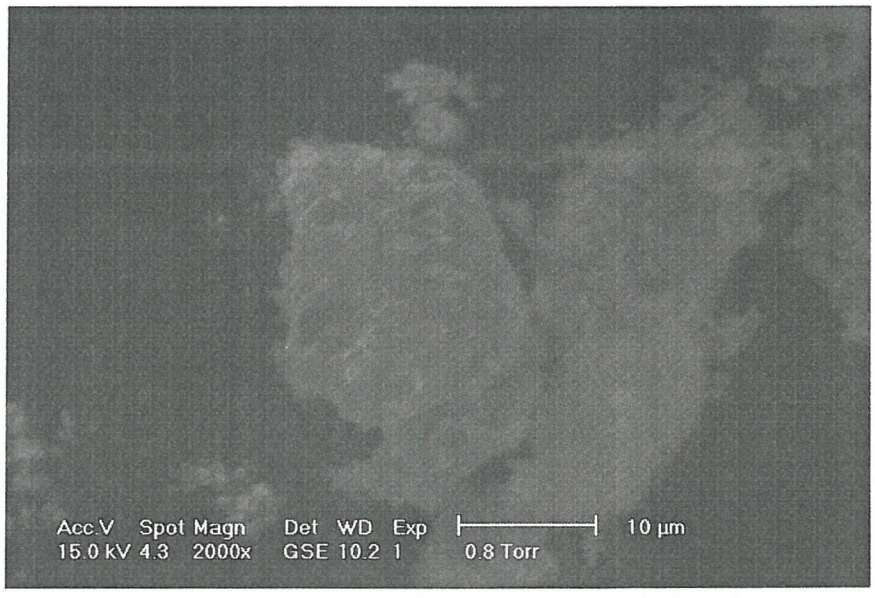

Figure 3.3 SEM micrograph of platy Intermediate crystallites (3-1).

3.3.2.3 FTIR Results

Cancrinite and Intermediate products were examined using FTIR, Figure 3.4 below.

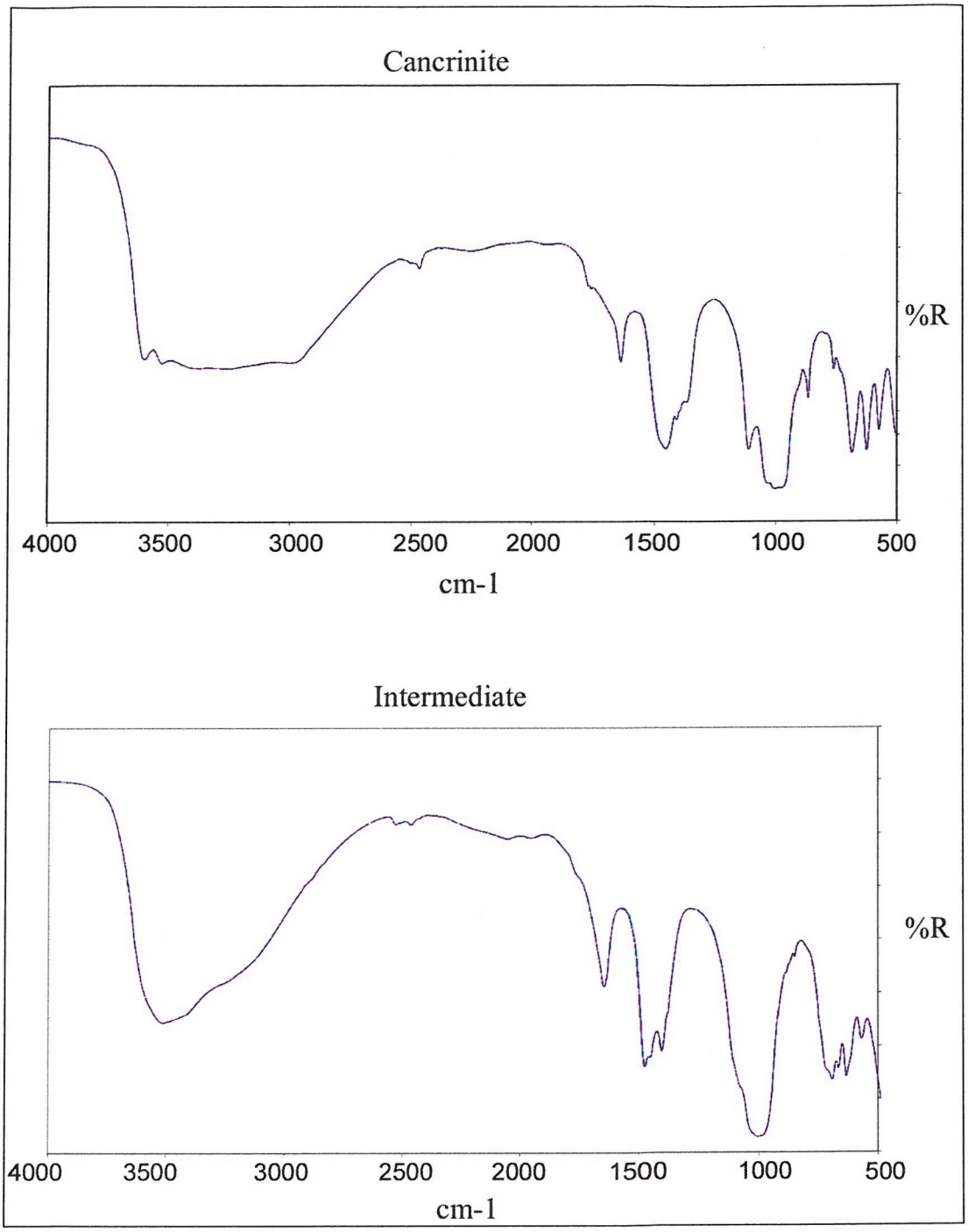

Figure 3.4 FTIR spectrum of top; cancrinite (3-4) and below; Intermediate (3-1). Measured using diffuse reflectance.

Characteristic cancrinite IR absorptions are displayed overleaf in Table 3.3.

Table 3.3 Characteristic cancrinite IR absorptions

	Asymmetric stretch of the aluminosilicate framework (cm^{-1})				Symmetric stretch of the aluminosilicate framework (cm^{-1})	
cancrinite	1095	1035	1000	965	755	600

Owing to the close relation of the framework vibrations of cancrinite with Intermediate, the two cannot be reliably separated by IR spectroscopy. The presence of other significant IR bands however, can identify the template carbonate, and water imbibed inside the frameworks. Carbonate inside the cancrinite and Intermediate frameworks creates bands at 850, 1410 and 1455 cm^{-1}. Water with its bending mode at 1650 cm^{-1} and a broad band between 3100 and 3600 cm^{-1}, is identified in all samples.

3.3.2.4 TGA Results

Thermal analysis was used to determine the amount of imbibed water and enclathrated carbonate in the framework. The TGA were collected over the temperature range room temperature to 1000 °C at a heating rate 10 °C/minute. The TGA traces of cancrinite and Intermediate are presented overleaf in Figures 3.5 and 3.6 respectively.

The carbonate and water contents of the cancrinite and Intermediate phases were calculated from the weight loss steps during the heating of the two phases to total decomposition. Thermal decomposition starts with the loss of water, completed at approximately 300 °C this is followed by the decomposition of carbonate at elevated temperatures into carbon dioxide and sodium oxide and then generation of the final nepheline products. Further examination of the structural decomposition of the two phases is detailed later, Section 3.4.4. Complete decomposition of the Intermediate phase is seen to occur at approximately 20 °C higher than that of cancrinite this is consistent with the results reported by Hackbarth *et al*[12].

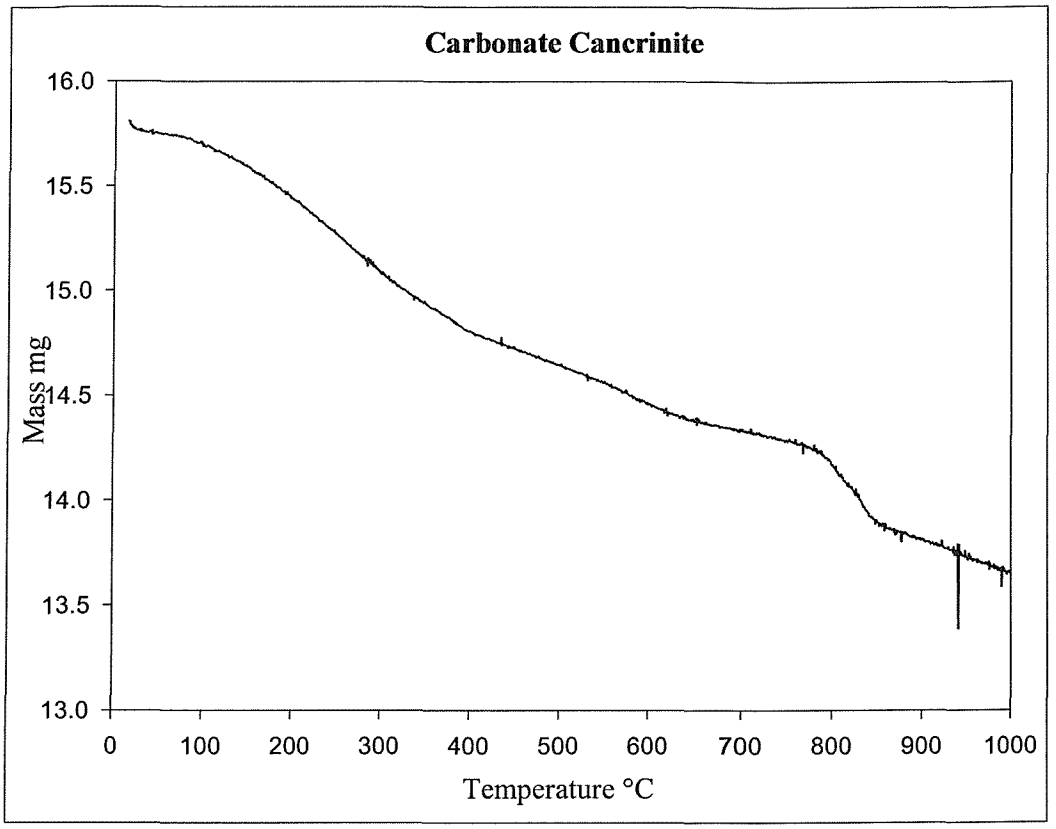

Figure 3.5 TGA trace showing the thermal properties of carbonate cancrinite (3-4).

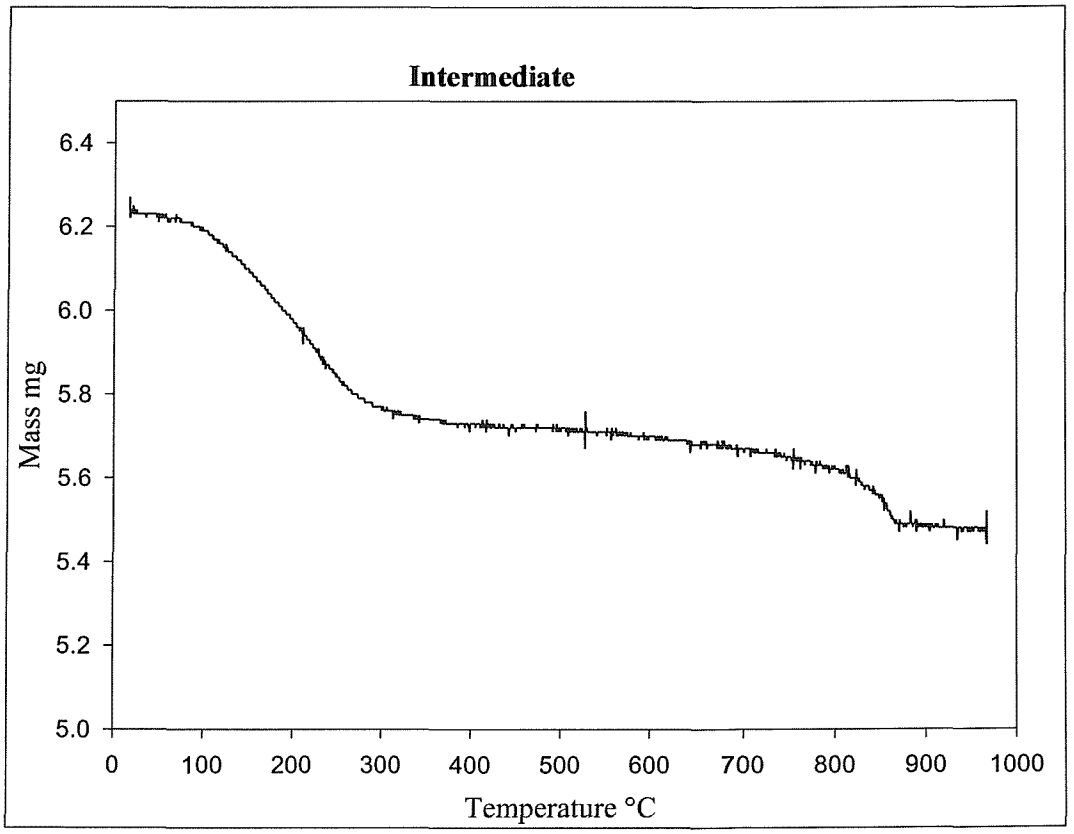

Figure 3.6 TGA trace showing the thermal properties of Intermediate (3-1).

3.3.3 Discussion

Sodium carbonate cancrinite and Intermediate have been successfully synthesised, and a reliable method of preparation identified.

Four analysis methods have been investigated for their ability to distinguish between these two phases. PXD and SEM show clear differences between the two and as such have been utilised throughout this work. FTIR can be employed to examine the nature of the anion located within the framework, whilst TGA provides an insight into the water and carbonate content of the two phases.

3.4 Structural Study of Cancrinite and Intermediate

The structure of naturally occurring cancrinite has been studied using X-ray diffraction methods by a number of authors. While these structure determinations show the gross structural features, significant ambiguities exist associated with light atoms (especially H) or close to isoelectronic species (e.g. Na,O,C); it is impossible to distinguish between isoelectronic species and hard to locate light elements using X-ray methods. Neutron diffraction, as described in Section 2.5, alleviates these problems and thus it has been utilised in these studies. Deuterated samples of cancrinite and Intermediate were therefore prepared. Hydrated samples were also prepared for use in *in situ* variable temperature PND experiments. The reactions described in Section 3.3.1 were scaled up in order to prepare larger samples of each compound for study using PND.

3.4.1 Experimental

Syntheses were carried out under hydrothermal conditions at temperatures of 150 °C and 220 °C under autogenous pressure in 125 ml, Teflon lined steel autoclaves under static conditions.

Deuterated Preparation

Dehydrated meta-kaolin (1.3696g for both cancrinite and Intermediate preparations), sodium carbonate (2.1717 g for cancrinite and 0.5435 g for Intermediate) and sodium deuteroxide solution (8 M, 83 ml) were added to the Teflon cup in a glove box flushed with nitrogen. The resultant white powders were washed with 150 ml D_2O inside the glove box and dried over P_2O_5 in a closed apparatus for 24 h at 80 °C.

Hydrated Preparation

Kaolin (1.3696g for both cancrinite and Intermediate preparations), sodium carbonate (2.1717 g for cancrinite and 0.5435 g for Intermediate) and sodium hydroxide solution (8 M, 83 ml) were added to the Teflon cup. The resultant white powders were washed with 150 ml H_2O and dried for 24 h at 80 °C.

3.4.2 Results

Small amounts of the resulting microcrystalline white powders were analysed using PXD to confirm the desired phase had been synthesised. The remaining samples were then used to collect PND data.

3.4.2.1 PXD Results

Initial phase identification was achieved by the analysis of PXD data collected over the 2θ range 10 ° to 60 ° for 30 minutes. The PXD patterns collected were consistent with those of carbonate cancrinite and Intermediate; it was therefore confirmed that pure samples of the two phases had been synthesised in preparation for PND experiments.

3.4.2.2 PND Results

Powder neutron diffraction data were initially collected from the deuterated cancrinite and Intermediate samples for 18 h at room temperature on the HRPD instrument at the Rutherford Appleton Laboratory. The hydrogenous samples were then heated *in situ* to 800 °C to monitor their decomposition, 1.5 h data sets were collected every 75 °C.

3.4.3 Structural Analysis

3.4.3.1 Cancrinite Structure Refinement

A number of descriptions of the cancrinite structure, reported in the literature were investigated as suitable starting models for the refinement. The Inorganic Chemistry Database (ICSD)[17] contains five references for the carbonate cancrinite structure starting with that of Smolin *et al* in 1981[18] and the most recent of these, Burton *et al* in 1999[19]. Of these a number are based on naturally occurring material that contains calcium and thus a higher balancing carbonate content; the others are pure sodium cation derivatives. The structures reported in the literature all use the space group $P6_3$ with unit cell parameters in the range 12.590(3) – 12.713(1) Å for *a* and 5.114(3) – 5.186(1) Å for *c*. Much of the work reported in the literature is from single crystal x-ray studies and contains no information on hydrogen positions, except for the work of Kanepit and Rider[20]. However this work distributes much of the hydrogen as OH groups in the framework rather than within water molecules; such a result does not agree with other reports.

The framework and cation positions reported in these studies, are for the most part consistent. One major difference in the reported structural models concerns the content of the main 12-ring channel with either two carbonate groups or one carbonate and one water used to model the scattering.

Clearly such differences will depend upon synthesis conditions and compound composition; the high water content cancrinite $Na_{7.86}(Al_6Si_6O_{24})(CO_3).3.3H_2O$ studied by Hackbarth *et al*[13] has a single carbonate unit in the channels plus additional water. Low water systems that occur naturally and are synthesised under high pressure $M_8(Al_6Si_6O_{24})(CO_3).1\text{-}2H_2O$ often have carbonate disordered over two sites in the main channel with water confined to the 11-hedral cages[21]. The dehydrated cancrinite, studied by Burton *et al* is also attributed two carbonate sites within the main channel. Structural studies on nitrate cancrinite by Buhl *et al*[22] describe the nitrate anions as similarly being distributed over two non-equivalent sites within the channel.

Initial structure co-ordinates for the framework atom, sodium ion and water molecule oxygen positions were taken from the very similar Kanepit and Rieder[20] and Hackbarth *et al*[13] descriptions. Initial cycles of refinement using these positions converged well using weak bond length constraints for the framework bond lengths Si-O = 1.62+/-0.01 Å and Al-O 1.73+/-0.01 Å. Modelling of the main channel species was undertaken with either two partially occupied carbonate anion units centred on (0,0,z) z ~ 0.16 and 0.40 or a carbonate unit at one of these positions and a water molecule at the other. Both carbonate and water molecules were represented as semi-rigid bodies with constrained C-O (1.28+/-0.01 Å) and O-D bond lengths (0.96+/-0.01 Å) at literature values. The model using the two carbonate ion positions was found to provide a significantly better fit to the data and this was therefore developed further. Carbonate site occupancies, positional co-ordinates and thermal displacement factors, tied to the same value for C and O, were refined.

Fourier maps were calculated to locate possible sites for deuterium on the water oxygen (OW) position reported previously. Two such atoms were introduced for possible sites identified close to 1Å from OW at approximately (0.2, 0.6, 0.1) with O-D bond length constraints of 0.96+/-0.01 Å.

Subject to the bond length constraint data mentioned above the final cycles of the refinement allowed variation of all positional, thermal and profile variables. Thermal displacement factors were tied together for similar atom types; cations, framework tetrahedral atoms, framework oxygen atoms, carbonate group atoms and water molecule atoms. Site occupancy factors were varied for each of the carbonate groups and the water molecule without constraint and yielded values close to those determined analytically. Variation of the sodium site occupancies showed no significant deviation from unity.

Final refined atomic co-ordinates are summarised in Table 3.3. Derived bond length and angle information is summarised in Tables 3.4 and 3.5; note that where no e.s.d.s are given on parameters this reflects a constraint in this part of the refinement. The final fit achieved to this data is presented overleaf in Figure 3.7.

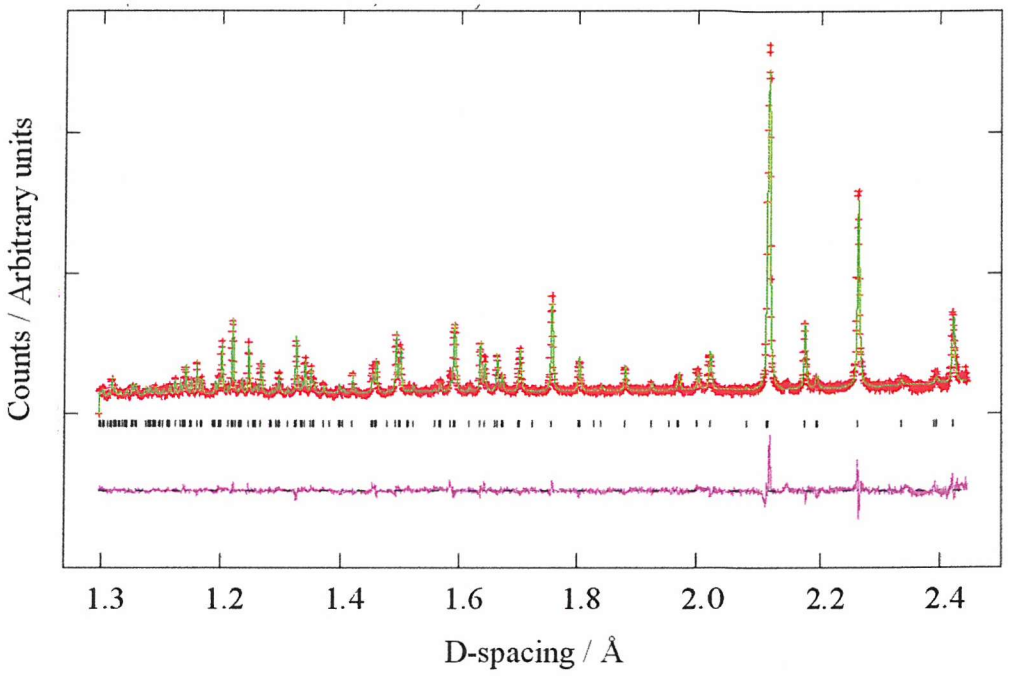

Figure 3.7 Final fit achieved to the profile for cancrinite. Red crosses are observed intensities, upper green line the calculated profile and lower magenta line the difference. Tick marks show reflection positions.

Table 3.4 Final refined atomic co-ordinates for $Na_8Al_6Si_6O_{24}.(CO_3)_{1.06}$ $1.44D_2O$ e.s.d.s are given in parentheses.

Atom	x	y	z	B_{iso} / Å^2	SOF
Na1	.3333	.6667	.6144(13)	4.3(7)	1.0
Na2	.1337(17)	.2655(6)	.2866(14)	4.3(7)	1.0
Al	.0740(6)	.4118(5)	.7535(18)	0.59(6)	1.0
Si	.3284(5)	.4117(4)	.75	0.59(6)	1.0
O1	.20159(57)	.40372(27)	.6693(11)	2.20(5)	1.0
O2	.11712(24)	.56423(48)	.7280(10)	2.20(5)	1.0
O3	.02210(39)	.34743(57)	.0588(13)	2.20(5)	1.0
O4	.32440(65)	.35951(52)	.0441(12)	2.20(5)	1.0
C1	.000000	.000000	.1518(41)	6.4(9)	.26(2)
O_C1	.11555(12)	.05985(12)	.1518(41)	6.4(9)	.26(2)
C2	.000000	.000000	.4490(30)	6.4(9)	.27(2)
O_C2	.11393(23)	.06033(24)	.4490(30)	6.4(9)	.27(2)
O_W	.3107(19)	.6350(17)	.1746(38)	9.9(14)	.24(3)
D1	.2291(22)	.6061(27)	.112(5)	9.9(14)	.24(3)
D2	.3139(22)	.5607(27)	.182(6)	9.9(14)	.24(3)

Space group $P6_3$

a=12.66624(7) Å c=5.16232(6) Å.

Cell Volume = 717.246 Å^3

R_{wp}=6.75%, R_p=5.98%, χ^2 = 2.41

Table 3.5 Selected derived bond angles for $Na_8Al_6Si_6O_{24}.(CO_3)_{1.06}$ $1.44D_2O$ e.s.d.s are given in parentheses.

Bond / Angle	**Å/°**	**Bond/Angle**	**Å/°**
Na1-O1 (x3)	2.898(3)	Na2 - O1	2.490(6)
Na1-O2 (x3)	2.444(3)	Na2 – O3	2.434(20)
Na-O_W (x3)	2.298(19)*	Na2 – O3	2.797(19)
Na-O_W (x3)	2.914(2)*	Na2- O4	2.438(19)
		Na2 – O5	2.914(20)
		Na2-O_C1 (x3)*	2.502(15) - 2.654(12)
		Na2-O_C2 (x3)*	2.410(13) - 2.711(13)
Al-O1	1.726(6)#	Si-O1	1.613(6)#
Al-O2	1.728(6)#	Si-O2	1.621(7)#
Al-O3	1.745(6)#	Si-O3	1.579(6)#
Al-O4	1.665(7)#	Si-O4	1.647(5)#
O-Al-O (x6)	105.4(4)-115.2(5)	O-Si-O (x6)	106.4(5)-112.7(4)
C1-O_C1 (x3)	1.268(1)#	O_C1-C1-O_C1	120.0 (fixed)
C2-O_C2 (x3)	1.250(3)#	O_C2-C2-O_C2	120.0 (fixed)
O_W-D1	0.963(3)	O_W-D2	0.963(3)
D1-O_W-D2	101.8(5)		

* - partially occupied site # - soft constraint used

3.4.3.2 Intermediate Structure Refinement

There are no descriptions of the Intermediate structure reported in the literature, thus a number of the cancrinite structural models were investigated in an attempt to model this data, however none proved to be completely satisfactory. The PND data collected from the Intermediate was as expected of lower quality (few broad peaks); as associated with the disorder in this material, Figure 3.8 below.

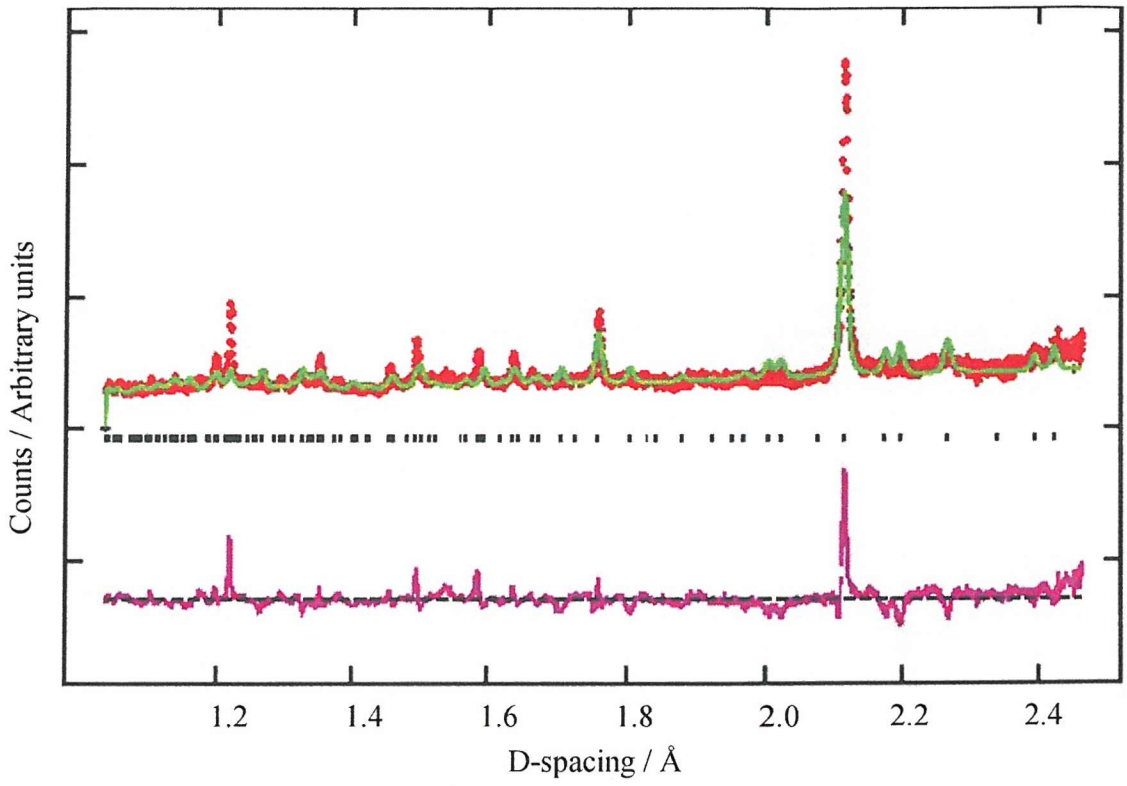

Figure 3.8 PND profile collected for Intermediate in the d-spacing range 0.8-2.3 Å and the final best fit achieved. Red crosses are observed intensities, upper green line the calculated profile and lower magenta line the difference. Tick marks show reflection positions.

3.4.4 Variable Temperature Studies

Data were collected at 75 °C intervals between room temperature and 800 °C for both cancrinite and Intermediate. Analysis of this data was undertaken in two ways. Lattice parameters were extracted through fitting of the profiles to the room temperature cancrinite structure model (without water molecules above 200 °C) and the background intensity was measured at a fixed point. The latter gives a measure of the level of hydrogen in the materials; the main contribution to the background is incoherent scattering from hydrogen. In both data sets additional reflections appeared above 500-600 °C indicating the onset of decomposition of the framework, the resulting product was identified as the condensed framework structure of nepheline.

Plots of the lattice parameters are displayed overleaf in Figures 3.9-14.

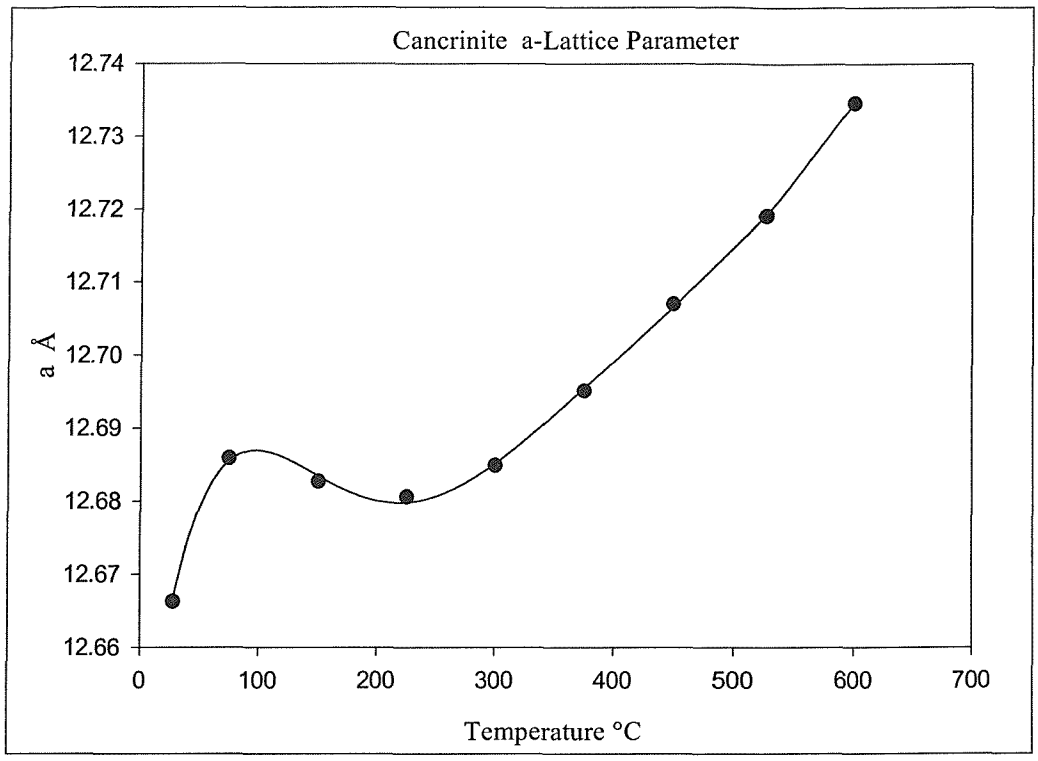

Figure 3.9 Variation of the cancrinite a-lattice parameter, obtained by fitting the PND profile at each temperature.

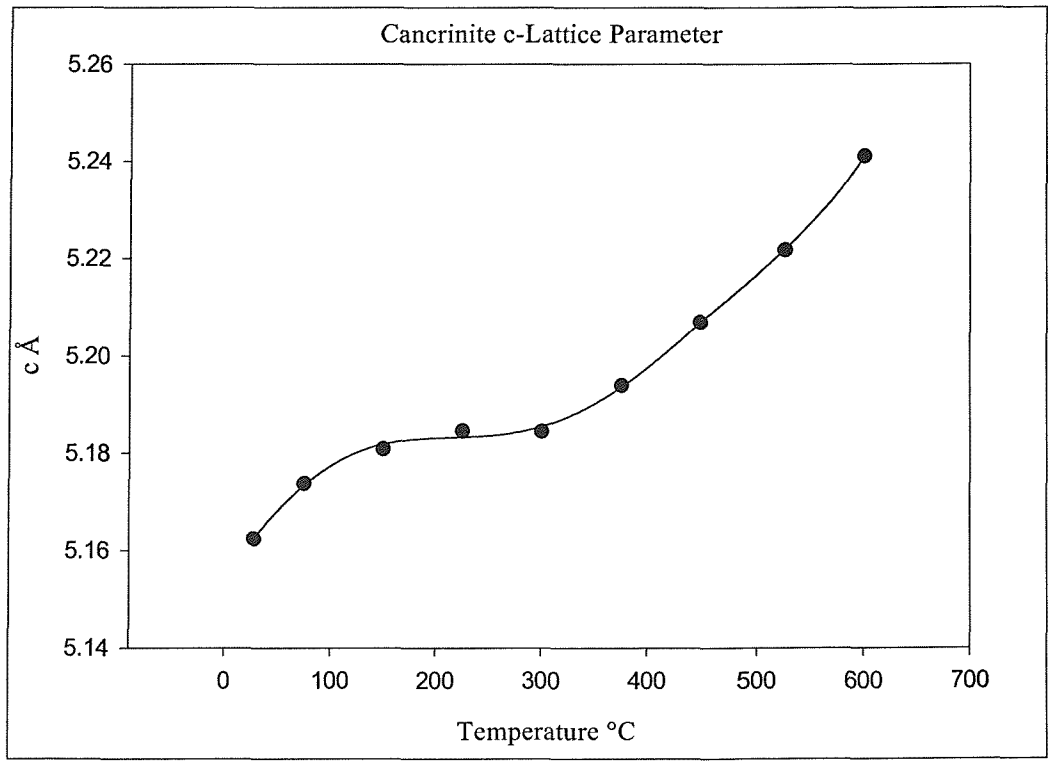

Figure 3.10 Variation of the cancrinite c-lattice parameter, obtained by fitting the PND profile at each temperature.

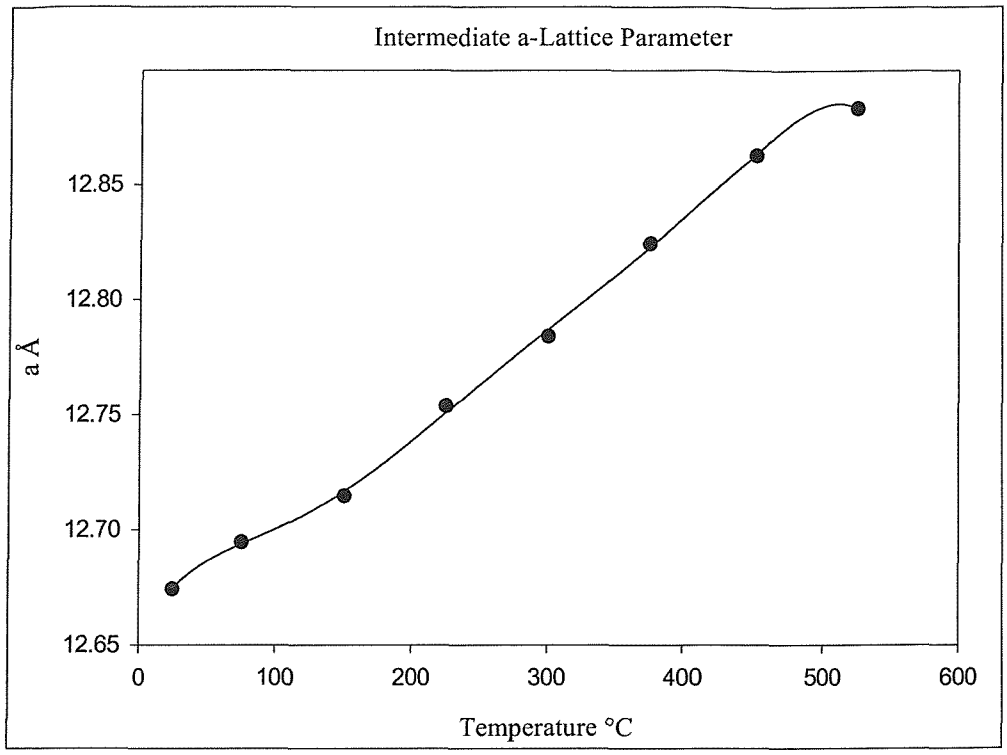

Figure 3.11 Variation of the Intermediate a-lattice parameter, obtained by fitting the PND profile at each temperature.

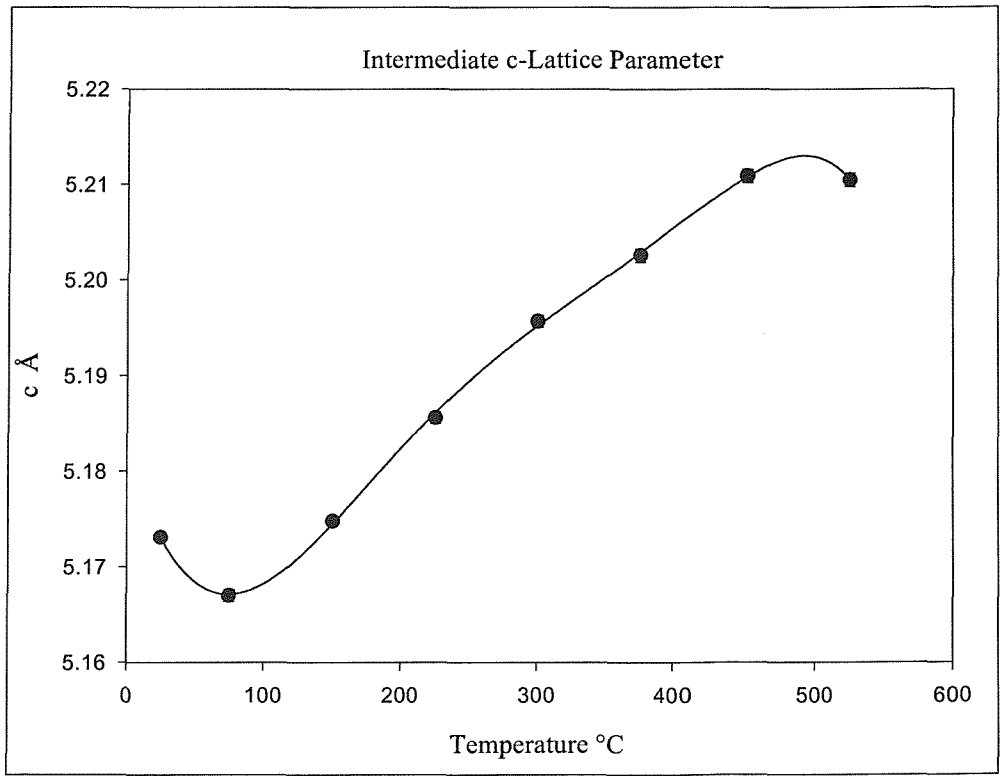

Figure 3.12 Variation of the Intermediate c-lattice parameter, obtained by fitting the PND profile at each temperature.

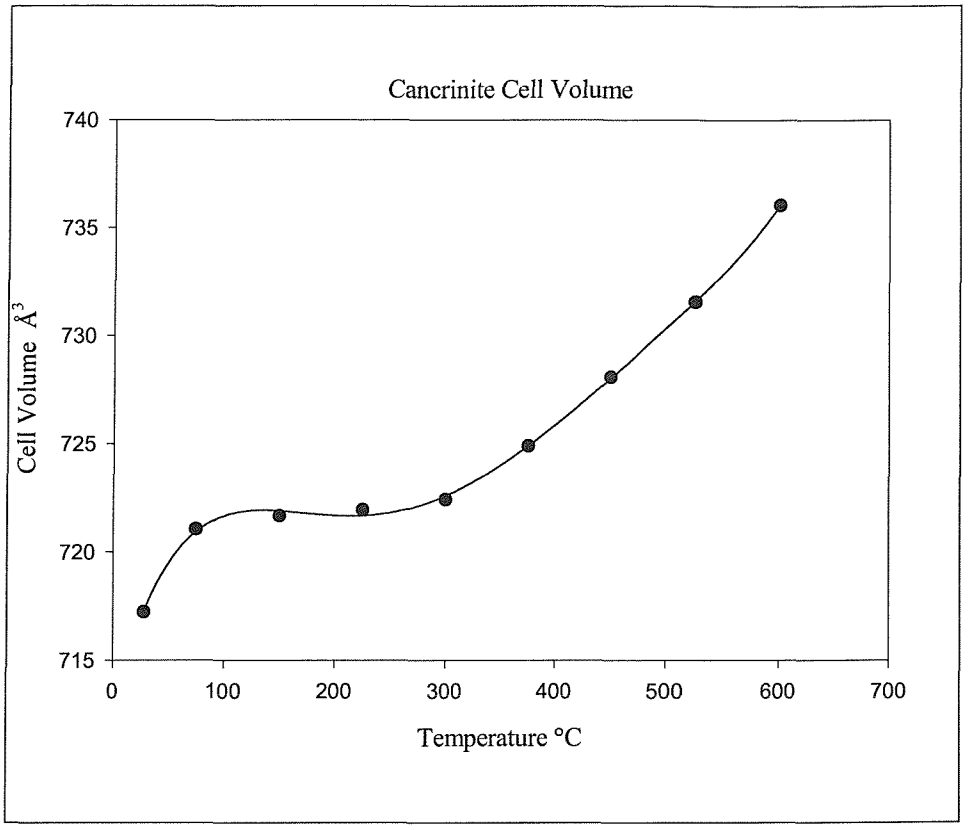

Figure 3.13 Variation of the cancrinite cell volume, obtained by fitting the PND profile at each temperature.

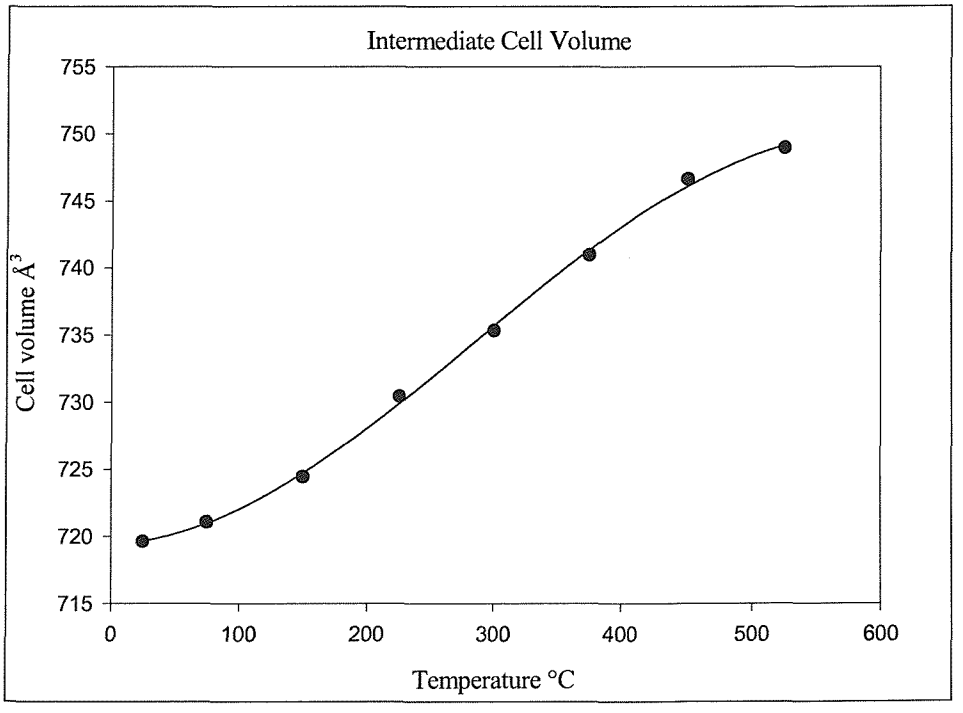

Figure 3.14 Variation of the Intermediate cell volume, obtained by fitting the PND profile at each temperature.

3.4.5 Discussion

3.4.5.1 Cancrinite Structure

The structure of $Na_8[AlSiO_4]_6.CO_3.H_2O$ consists of a 12 ring one-dimensional channel containing carbonate disordered over two positions. The relative positions of these two sites are shown in Figure 3.15. It is clear that these sites cannot both be fully occupied due to their proximity, however the refined occupancies at each site were similar. This gives rise to pairs of carbonate sites separating the portions of the channel occupied also by sodium ions. Of any pair only one site will be occupied in about 50 % of cases.

In the 11-hedral cages the sodium ion is located above the six membered ring and is shared between two such cages forming three strong interactions at 2.34 Å to the framework. The water molecule completes the co-ordination to the sodium ion and is disordered over three close sites with an average occupancy within the cage of 0.75 molecules.

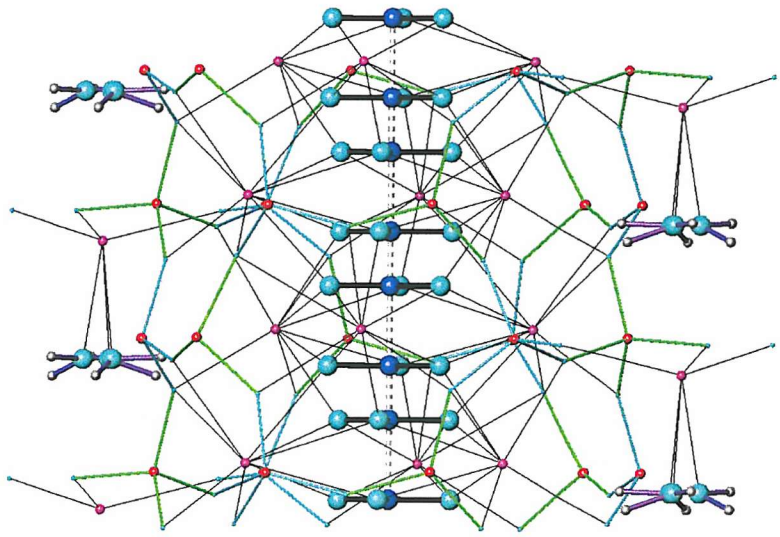

Figure 3.15 The cancrinite structure viewed perpendicular to the c direction showing the distribution of the carbonate molecules in the main channel and water molecules in the ∈-cages. The framework bonds are shown in green, silicon as small light blue spheres, aluminium as red spheres, framework oxygen are omitted. The non-framework atoms are represented as follows, carbon as large dark blue spheres, sodium as pink spheres, deuterium as grey spheres and the non-framework oxygen as large light blue spheres.

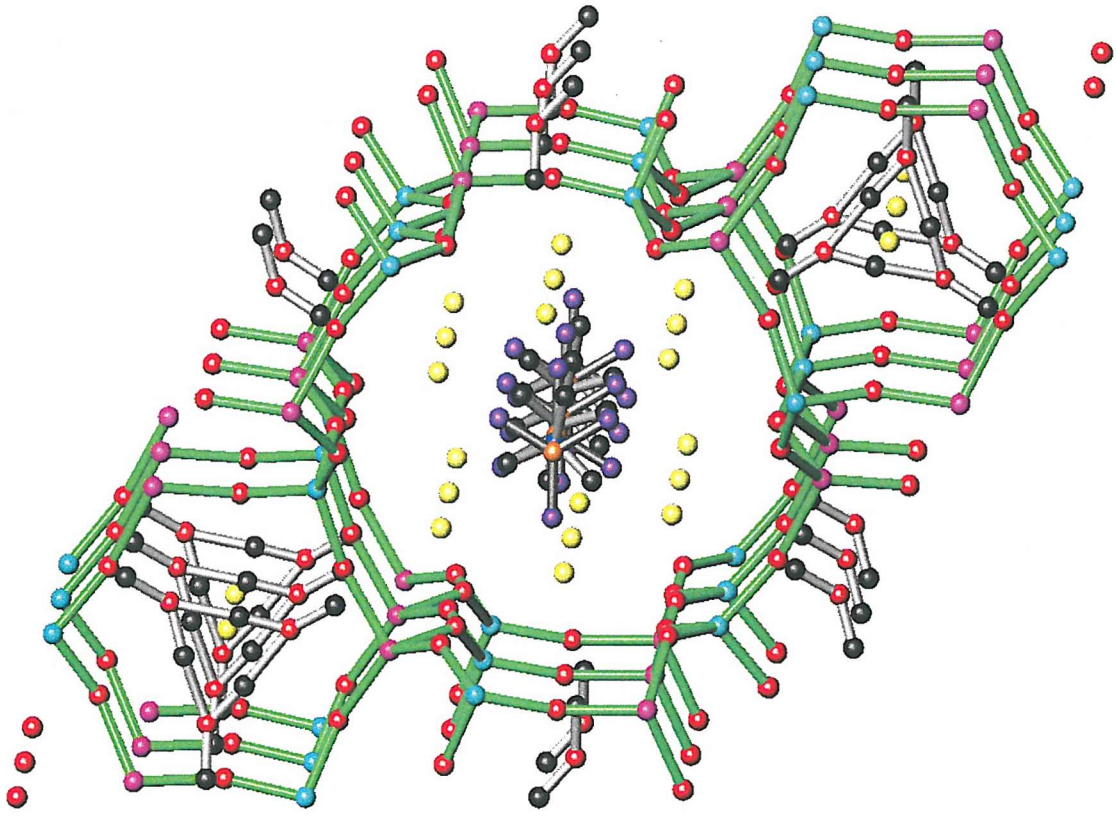

Figure 3.16 The cancrinite structure viewed close to down the c direction. The framework bonds are shown in green, silicon as light blue spheres, aluminium as pink spheres, framework oxygen as red spheres. The non-framework atoms are represented as follows, carbon as orange spheres, carbonate oxygen as purple spheres, sodium as yellow spheres, deuterium as black spheres and water oxygen as red spheres.

Refinement of the structures has thus allowed determination of all atom positions, including full water molecule descriptions, and allowed carbonate and water molecules to be distinguished.

3.4.5.2 Intermediate Structure

For the partially disordered Intermediate phase only a basic crystallographic modelling of the data could be achieved.

The Intermediate phase is believed to be an intergrowth of sodalite and cancrinite with a one-dimensional stacking disorder of the $(AlSiO_4)_n$ layers. In sodalite the $(AlSiO_4)_n$ layers are stacked in an ABCABC… sequence to form the basket-like structures known as truncated octahedra (sodalite or β-cages). The $(AlSiO_4)_n$ layers follow an ABAB… stacking sequence in cancrinite to create the channel containing structure discussed earlier. A comparison of the different stacking sequences that occur in sodalite and cancrinite is made in Figure 3.17 below.

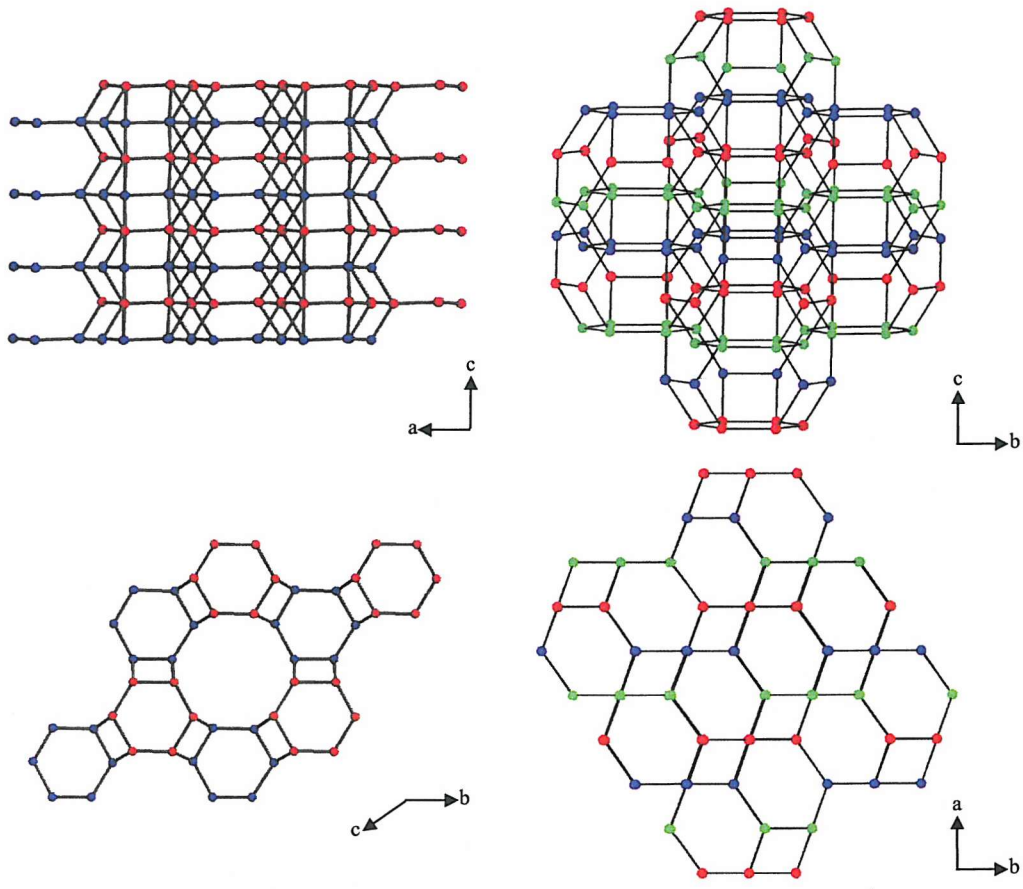

Figure 3.17 Frameworks topologies of cancrinite (left) and sodalite (right). In the left pair of diagrams the layers of tetrahedral atoms repeat positionally in the sequence ABABAB along the c direction producing the channel structure when viewed down c. In the right hand pair the repeat is ABCABCABC (the C layer is shown in pale green) producing the interlocked arrangement of sodalite cages.

The presence of this one-dimensional stacking disorder in the Intermediate destroys the system of wide channels parallel to the c-axis as seen in the cancrinite structure, instead cages of various sizes are formed. Upon refinement of the Intermediate lattice parameters using the methodology of Hermeler *et al*[16], the *c*-lattice parameter is seen to be half that of the cancrinite *c*-lattice parameter, i.e. the thickness of one aluminosilicate layer. This irregularity and disorder of this structure prevented full crystallographic modelling.

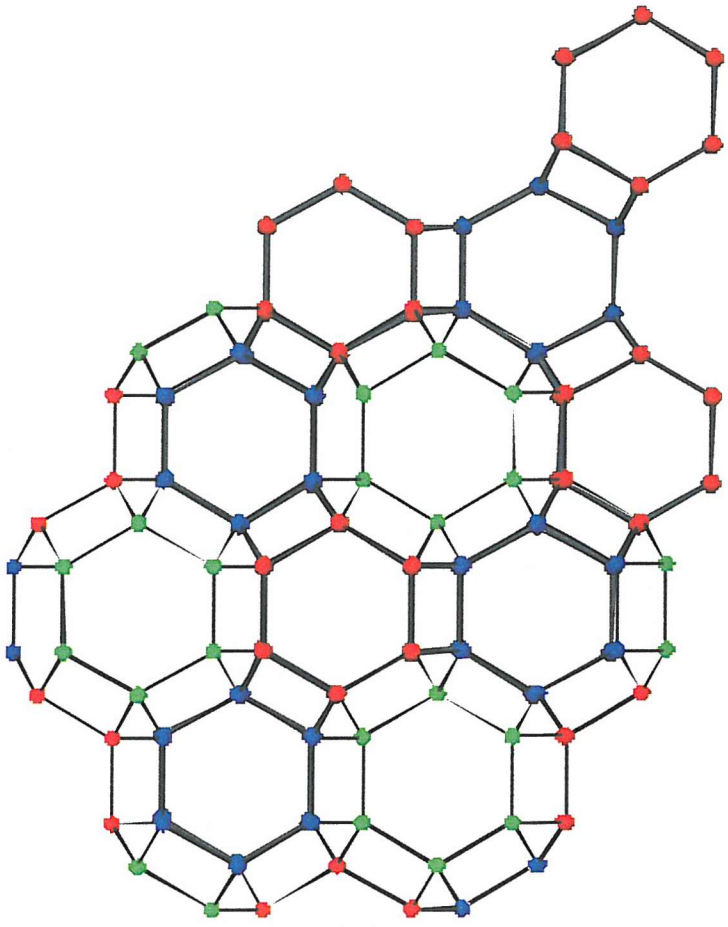

Figure 3.18 A schematic representation of the Intermediate phase. The intergrowth of the two phases is represented by superimposing cancrinite (upper right – alternating ABAB layers blue red blue red, bold lines) on the sodalite structures (bottom left – alternating ABCABC blue red green, light lines), viewed perpendicular to the layers. Note that the main cancrinite channel (12-ring) becomes blocked by the 'C' layer.

3.4.5.3 Thermal Decomposition

Upon heating to 800 °C, the cancrinite and Intermediate samples showed marked differences in their decomposition behaviour prior to the generation of the final nepheline products. Plots of the lattice parameters extracted for each temperature, are plotted for both phases in Figures 3.8-14. The values for the disordered phases were calculated using the ordered cancrinite unit cell to allow direct comparison between the two data sets. For the ordered phase significant decomposition occurred above 600 °C making extraction of lattice parameters above this temperature impossible for this structure type; for the disordered phase the maximum temperature data set that could be employed was 500 °C.

The cancrinite data displays non-linear behaviour over the temperature range room temperature to 600 °C. An initial increase in lattice parameters is seen, followed by a slight decrease before the smooth regular increase, typical of thermal expansion, sets in above 300 °C. This behaviour follows that of the overall background intensity which drops markedly between 100 and 250 °C and also the behaviour of these materials seen in TGA which both indicate that water is lost over the temperature range 100-300 °C. This water loss is associated with a contraction of the unit cell dimensions, particularly *a*, and a decrease in the level of incoherent scattering from hydrogen. The decrease in unit cell size is likely to be associated with a redistribution of the Na1 sodium ion positions and changes in framework bond angles in order to allow more effective co-ordination between the framework oxygen and sodium once the attached water molecule is removed. This behaviour generally results in the decrease of framework angles and thus overall lattice contraction. Once this redistribution is complete the framework expands normally until near 600 °C where the decomposition of the carbonate ion occurs and the framework collapses at the same time.

For the disordered phase a similar behaviour is observed though it is less marked. Only the *c* lattice parameter seems to decrease though the *a* lattice parameter and cell volume show inflections in their behaviours around 150°C. This behaviour is paralleled in the level of incoherent scattering which also decreases most markedly near 150 °C. Such weaker trends in unit cell size, fit with the less ordered structure.

3.5 Conclusions

A reliable synthesis method for the production of sodium carbonate cancrinite and Intermediate has been identified. Four analysis methods have been investigated for their ability to distinguish between these two phases. PXD and SEM displaying the most prominent differences.

The structure of ordered cancrinite, $[Na_8(CO_3).(H_2O)_n]\,[AlSiO_4]_6$, synthesised at 220 °C, consists of the previously described framework with ordered silicon and aluminium forming 12-ring one dimensional channels along the *c* direction and 11-hedral ∈ cages. The ∈ cages contain one sodium ion type, accounting for three-quarters of the sodium present on the structure, co-ordinated to the framework oxygen (3 strong and 3 weak interactions) and to water molecules (3 strong interactions to a partially occupied site). The main channel contains two possible sites for carbonate ions which are both partially occupied and a second type of sodium ion which is co-ordinated to the framework and oxygen atoms of the carbonate molecules. The structure of the Intermediate phase could not be determined from powder neutron diffraction data alone.

The thermal decomposition behaviour of cancrinite and Intermediate as studied through variable temperature powder neutron diffraction shows that the materials lose water between 100-250 °C with a contraction in unit cell dimensions as the sodium ions redistribute within the structure. At high temperatures the lattices expand with the onset of decomposition for Intermediate being 100 °C lower (500 °C) than for ordered cancrinite (600 °C).

3.6 References

1 H. Strunz, Mineralogische Tabellen, 7. Auflage. Akademische Verlagsgesellschaft Geest und Portig H.G., Leizig, (1978).

2 W. Eitel, *Neues Jahrbuch für Mineralogie,* II, 45, (1922).

3 R.M. Barrer, Hydrothermal chemistry of zeolites, Academic press, London, (1982).

4 F. Hund, *Zeitschrift für Anorganische und Allgemeine Chemie,* **509**, 153, (1984).

5 R.M. Barrer, J.F. Cole, H. Villiger, *Journal of the Chemical Society,* (A) 1523, (1970).

6 R.M. Barrer, J.F. Cole, *Journal of the Chemical Society*, (A) 1516, (1970).

7 L. Pauling, *Proceeding National Academy of Sciences,* **16** 453 (1930).

8 G. Gossner, F. Mussgnug, *Zeitschrift für Kristallographie,* **73**, 52, (1930).

9 O. Jarchow, *Fortschritte der Mineralogie,* **40**, 55, (1962).

10 O. Jarchow, *Acta Crystallographica*, 2.4 Rome Abstract, (1963).

11 O. Jarchow, *Zeitschrift für Kristallographie*, **122**, 407, (1965).

12 Y. Lee, J.B. Parise, A. Tripathi, S.J. Kim, T. Vogt, *Microporous and Mesoporous Materials*, **39**, 445, (2000).

13 K. Hackbarth, Th.M. Gesing, M. Fechtelkord, F. Stief, J.-Ch Buhl, *Microporous and Mesoporous* Materials, **30**, 347, (1999).

14 J.A. Armstrong, S.E. Dann, *Microporous and Mesoporous Materials*, **41**, 89, (2000).

15 J.A. Armstrong, *M.Phil. Thesis,* Loughborough University (1999).

16 G. Hermeler, J.-Ch Buhl, W. Hoffmann, *Catalysis Today*, **8**, 415, (1991).

17 http//cds.dl.ac.uk

18 Y.I. Smolin, Y.F. Shepelev, I.K. Butikova, I.B. Kobyakov, *Kristallografia*, **26**, 63, (1981).

19 A. Burton, M. Feuerstein, R.F. Lobo, J.C.C. Chan, *Microporous and Mesoporous Materials*, **30**, 293, (1999).

20 V.N. Kanepit, E.É. Rieder, *Journal of Structural Chemistry*, **36**, 694, (1995).

21 H.D. Grundy, I. Hassan, *Canadian Mineralogist*, **20**, 239, (1982).

22 J.-Ch Buhl, F. Stief, M. Fechtelkord, Th.M. Gesing, U. Taphorn, C. Taake, *Journal of Alloys and Compounds*, **305**, 93, (2000).

Chapter 4

Calcium Hydroxide

The work detailed in this chapter was published by the author and M.T. Weller in Microporous and Mesoporous Materials **59**, 185, (2003).

4.1 Introduction

Lime (calcium oxide, CaO), is used extensively in the Bayer process to alleviate a wide range of problems in the plant. Generally CaO is produced in a Bayer plant by the calcination of calcium carbonate ($CaCO_3$). The CaO is slaked in water to form a calcium hydroxide ($Ca(OH)_2$) suspension, 'milk of lime', which can be added to the Bayer liquor at a number of points in the refinery. The functions that CaO and $Ca(OH)_2$ perform are summarised below[1]:

Enhancement of Alumina Extraction

Enhancement of diaspore dissolution

Due to its low equilibrium solubility in sodium aluminate liquors, extraction of diaspore from bauxite ore requires high digestion temperatures (>250°C) and high caustic concentrations. By adding CaO to the bauxite slurry the dissolution of diaspore can be enhanced, thus allowing a reduction in digestion temperature. Mal'ts *et al*[2] suggest that this improvement is a consequence of the initial formation of a calcium aluminate which subsequently decomposes in the alkaline liquor, Equation 4.1.

$$Ca(OH)_2 + AlOOH \leftrightarrow CaO.Al(OH)_3 \xleftrightarrow{H_2O,OH^-} Ca(OH)_2 + Al(OH)_4^-$$

Equation 4.1.

Enhancement of aluminogoethite to hematite transformation

The conversion of aluminogoethite ($Fe_{(1-x)}Al_xOOH$ (x=0-0.33)) to hematite (Fe_2O_3) in sodium aluminate liquors makes the extraction of goethitic alumina possible. The addition of CaO at 140 °C improves this process, however this improvement is more pronounced at higher temperatures. The conversion of goethite to hematite is believed to proceed via an iron hydrogarnet intermediate.

Minimising the inhibiting effect of sodium titanates on alumina extraction

Reaction of NaOH and titanate impurities in bauxite ore can lead to the formation of sodium titanates. Formation of sodium titanates is undesirable as they form a gelatinous film over the aluminium compounds found in bauxite; it is suggested that this lowers the aluminium extraction efficiency[2]. The direct reaction of CaO with titanium dioxide

(TiO_2) to form calcium titanates may eliminate the formation of sodium titanates and the associated problems.

The Control of Carbonate, Silica and Phosphorous Impurities

Causticisation

Carbonate ions can enter Bayer liquor by either the breakdown of humic substances present in the bauxite ore, or by the absorption of carbon dioxide from the air, Equation 4.2.

$$2OH^- + CO_2 \rightarrow H_2O + CO_3^{2-}$$

Equation 4.2

The hydroxide concentration (causticity) of Bayer liquor decreases with time as a result of carbonate formation. CaO is added to the liquor to restore the hydroxide concentration (causticisation), Equation 4.3.

$$CaO\ (s) + H_2O + CO_3^{2-} \rightarrow CaCO_3\ (s) + 2OH^-$$

Equation 4.3

Xu *et al*[3] have studied the reaction between CaO and carbonate containing sodium hydroxide solutions. Having investigated the formation of sodium carbonate, the authors propose that formation proceeds by the following series of reactions, Equations 4.4a, b and c.

Initially the CaO reacts with water to give $Ca(OH)_2$.

$$CaO\ (s) + H_2O \rightarrow Ca(OH)_2\ (s)$$ Equation 4.4a

The $Ca(OH)_2$ then either reacts directly with carbonate ions to give $CaCO_3$

$$Ca(OH)_2\ (s) + CO_3^{2-} \rightarrow CaCO_3\ (s) + 2OH^-$$ Equation 4.4b

or it dissolves to give calcium ions which combine with the carbonate ions to precipitate $CaCO_3$.

$$Ca^{2+} + CO_3^{2-} \rightarrow CaCO_3\ (s)$$ Equation 4.4c

Desilication

Desilication, the process used to remove insoluble silica impurities with the red mud can be enhanced by the addition of CaO[4,5]. When CaO has been added, desilication is thought to proceed via the formation of a calcium aluminate hydrate, possibly $Ca_3Al_2(OH)_{12}$ and the subsequent incorporation of silica into the structure to give hydrogarnet, $Ca_3Al_2(SiO_4)_n(OH)_{(12-4n)}$, where n gives an indication of the amount of silica incorporated within the hydrogarnet structure.

Phosphorus Control

The dissolution of crandallite, $(CaAl_3(PO_4)_2(OH)_5.H_2O)$ is reported as being the major source of Bayer liquor phosphorus contamination for refineries using Jamaican bauxite. Lime is used to control the phosphorus concentration in the liquor through the formation of an insoluble calcium apatite $(Ca_5(PO_4)_3(OH)$.

Liquor Polishing (Filter Aid)

The filtration of pregnant liquor reduces liquor impurity levels and thereby increases the purity of the resultant gibbsite. The addition of CaO as a filter aid assists with this impurity removal and also enhances the filtration rate. The CaO used as filter aid can be recycled and have subsequent use during causticisation or desilication.

Minimisation of Soda Losses

Hydroxysodalite is one of the desilication products discarded with the red mud, upon the addition of CaO the formation of alternative products occur; hydrogarnet and calcium-containing cancrinite. Both have Na_2O/SiO_2 values lower than hydroxysodalite thus minimising the soda lost in the red mud.

4.2 Aims

This chapter describes the results obtained upon the addition of $Ca(OH)_2$ to systems that yield cancrinite and Intermediate phase products. The aim of this investigation was to see what effect $Ca(OH)_2$ has upon these systems and to assess its suitability as an additive to reduce aluminosilicate heat exchanger scaling.

4.3 Effect of Calcium Hydroxide Addition to Synthetic Liquor

4.3.1 Experimental

Syntheses were carried out under hydrothermal conditions at temperatures of 220 °C and 150 °C and autogenous pressure in Parr 23 ml Teflon-lined steel autoclaves under static conditions. Kaolin (0.2520 g), sodium carbonate (0.3996 g) and sodium hydroxide solution (8 M, 14 ml) were added to the Teflon cup; calcium hydroxide was subsequently added in varying amounts to produce calcium concentrations in the range 0.0127-0.278 mol/L. For each calcium concentration a series of experiments was performed with reaction times of 24, 48, 72 and 96 h. The resultant white powders were washed with 150 ml distilled water and dried for 24 h at 80 °C.

4.3.2 Results

The resulting microcrystalline white powders were analysed using PXD, SEM, FTIR and PND.

4.3.2.1 PXD Results

Initial phase identification was achieved by the analysis of PXD data collected over the 2θ range 10 ° to 60 ° for 30 minutes. The reaction parameters and results, in terms of the phase formed, are summarised in Tables 4.1 and 4.2.

Tables 4.1 Phase identification for experiments performed at 150 °C.

	Phase Identification for Reactions at 150 °C			
$Ca(OH)_2$ (moles)	**24 h**	**48 h**	**72 h**	**96 h**
2.78×10^{-3}	Ca I **R**	Ca I **R**	Ca I **R**	Ca I **R**
2.28×10^{-3}	Ca I **R**	Ca I **R**	Ca I **R**	Ca I **R**
1.78×10^{-3}	Ca I **R**	**Ca** I	Ca I **R**	Ca I **R**
1.24×10^{-3}	**I** R	**Ca** I	**Ca** I	**Ca** I R
8.9×10^{-4}	Ca **I** R	**Ca** I	**Ca** I	**Ca** I R
5.3×10^{-4}	Ca **I**	Ca **I**	**Ca** I	Ca **I** R
1.78×10^{-4}	**I**	**I**	Ca **I**	Ca **I**
0	**I**	**I**	I	**I**

Ca: - sodium calcium hydrogen silicate, $NaCaHSiO_3OH$ (JCPDS 25-1319)

I: - Intermediate & cancrinite or disordered cancrinite

R: - unreacted starting material ($Ca(OH)_2$)

Tables 4.2 Phase identification for experiments performed at 220 °C.

	Phase Identification for Reactions at 220 °C			
$Ca(OH)_2$ (moles)	**24 h**	**48 h**	**72 h**	**96 h**
3.89×10^{-3}	Ca C **R**	**Ca** C R	**Ca** C	**Ca**
2.78×10^{-3}	Ca C **R**	**Ca** C R	**Ca** C	**Ca**
2.28×10^{-3}	**Ca** C R	**Ca** C	**Ca** C	**Ca**
1.78×10^{-3}	**Ca** C R	**Ca** C	**Ca** C	**Ca**
1.24×10^{-3}	**Ca** C R	**Ca** C	**Ca** C	**Ca** C
8.9×10^{-4}	**Ca** C R	**Ca** C	**Ca** C	**Ca** C
0	**C**	**C**	**C**	**C**

Ca: - sodium calcium hydrogen silicate, $NaCaHSiO_3OH$ (JCPDS 25-1319)

C: - Cancrinite

R: - unreacted starting material ($Ca(OH)_2$)

The aluminosilicate phase formation is broadly in line with literature reported for systems containing no calcium[6]. That is at 150°C the main phase observed is Intermediate while at the higher temperature, 220°C, the ordered cancrinite structure is the only aluminium containing product formed.

Determination of the lattice parameters and unit cell volumes of the cancrinite phase present in the products formed at 220°C was carried out and the results for the cell volumes are summarised in Figure 4.1. Once calcium is present in the reaction medium a marked decrease is seen in the unit cell *c* parameter, and thus the unit cell volume; though increasing the calcium content has little effect on cell parameters thereafter.

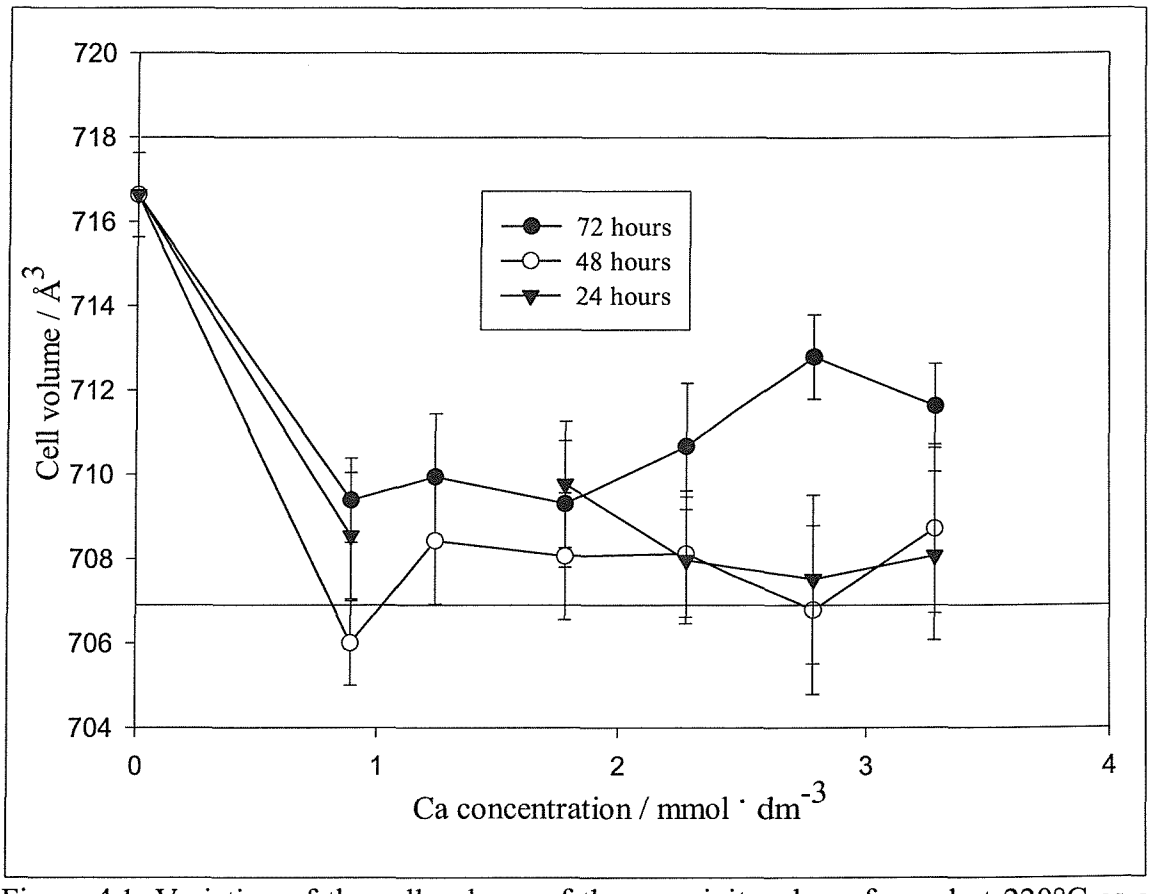

Figure 4.1. Variation of the cell volume of the cancrinite phase formed at 220°C as a function of calcium concentration in the reaction mixture at various reaction times. The horizontal lines represent typical literature values for $Na_8[AlSiO_4]_6(CO_3).nH_2O$ (upper) and $Na_6Ca_2[AlSiO_4]_6(CO_3)_2.nH_2O$ (lower).

Stoichiometric synthetic and naturally occurring cancrinite compositions can vary over the range $Na_{8-x}Ca_x[AlSiO_4]_6(CO_3)_{1+x/2}.nH_2O$ with $0 \leq x \leq 2$. The end members, $Na_8[AlSiO_4]_6(CO_3).nH_2O$ and $Na_6Ca_2[AlSiO_4]_6(CO_3)_2.nH_2O$, are reported in the literature, though the latter only from natural sources. Comparison of the determined cell volumes with those reported in the literature, shown in Figure 4.1 support the conclusion that this decrease is associated with calcium incorporation into the aluminosilicate structure. Generally replacement of sodium by calcium in zeolite structures has relatively little effect on the lattice constants due to the rigidity of the aluminosilicate framework but similar small contractions are evident in other 1:1 Al:Si frameworks (e.g. for Zeolite A sodium form a = 12.32Å , calcium form a=12.24 - 12.26Å)[7]. Hence addition of calcium into the reaction mixture leads to its incorporation into the cancrinite structure though from powder X-ray data the exact composition is impossible to define. The composition, is however likely to lie between $Na_7Ca[AlSiO_4]_6.(CO_3)_{1.5}.nH_2O$ and $Na_6Ca_2[AlSiO_4]_6.(CO_3)_2.nH_2O$. This is supported by the chemical analysis carried out using EDX in the SEM; see section 4.3.2.2.

At all the levels of calcium concentration studied and particularly the longer reaction times, further calcium is incorporated in the $NaCaSiO_3OH$ phase which readily crystallises from solutions at this higher temperature. The formation of this phase seems somewhat slower than the cancrinite phase as evidenced by the presence of unreacted calcium hydroxide in reaction products after 24 hours.

At 150 ° C the aluminosilicate phase formed is the Intermediate. The calculated lattice parameters for this phase show less marked changes as a function of calcium level or reaction time, Figure 4.2. Obviously for this material with a disordered layer structure the determined lattice parameters from the few broad reflections are accompanied by large estimated standard deviations making any trends difficult to discern. However, once again introduction of calcium into the reaction mixtures probably leads to a small reduction in the cell volume associated with incorporation of calcium into the intermediate phase structure, i.e. the formation of $Na_xCa_y[AlSiO_4]_6(CO_3)_{(x+2y-6)/2}.nH_2O$. Again this is confirmed by EDX analysis.

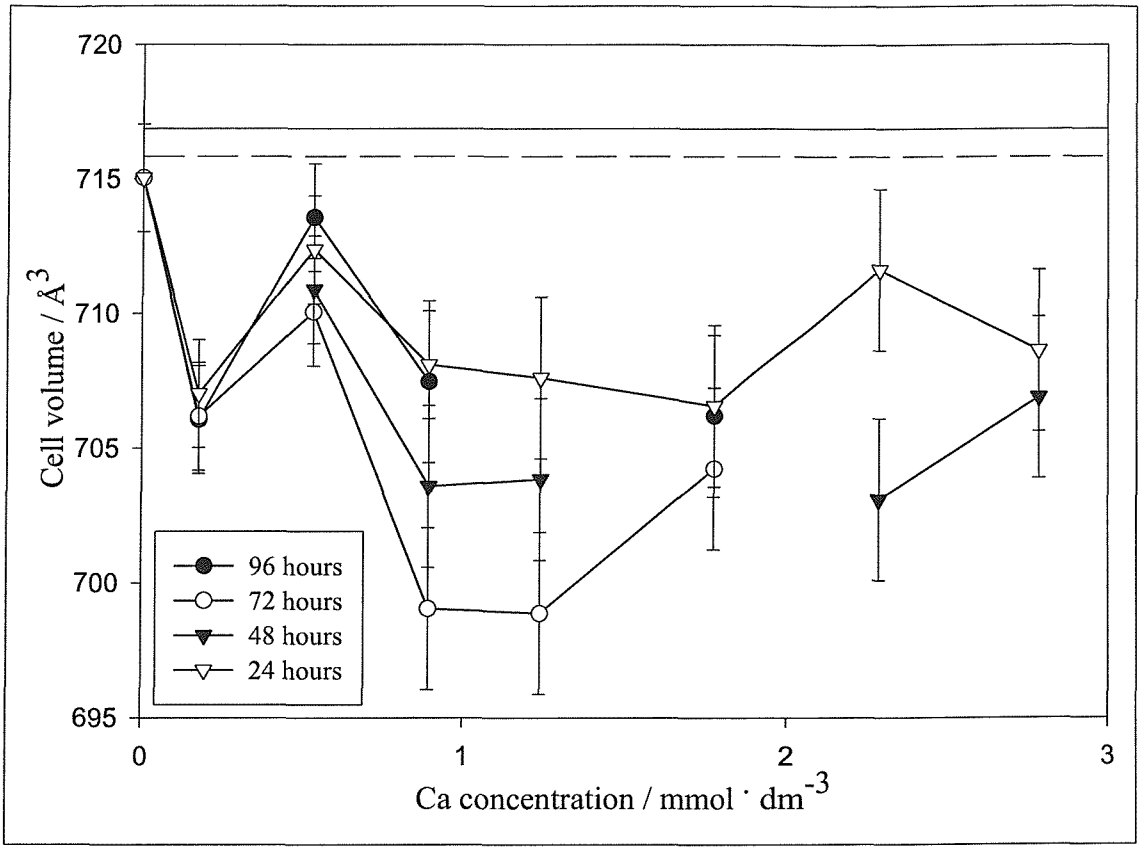

Figure 4.2. Variation of the cell volume of the intermediate phase formed at 150°C as a function of calcium concentration in the reaction mixture at various reaction times. The horizontal lines represent literature values for Intermediate (lower/dashed) $Na_{7.4}[AlSiO_4]_6(CO_3)_{0.7}.4H_2O$ (multiplied by 6 for direct comparison) and the closely related disordered cancrinite structure (upper/solid) of $Na_{7.5}[AlSiO_4]_6(CO_3)_{0.75}.4H_2O$.

4.3.2.2 Electron Microscopy Results

Products from the syntheses under the various conditions were examined using SEM.

SEM Micrographs

SEM micrographs revealed that the $NaCaSiO_3OH$ phase has a very different morphology to cancrinite and Intermediate phase. The crystallites of this phase are elongated hexagonal platelets and have typical dimensions of 100 x 30 x 30 μm, Figure 4.3.

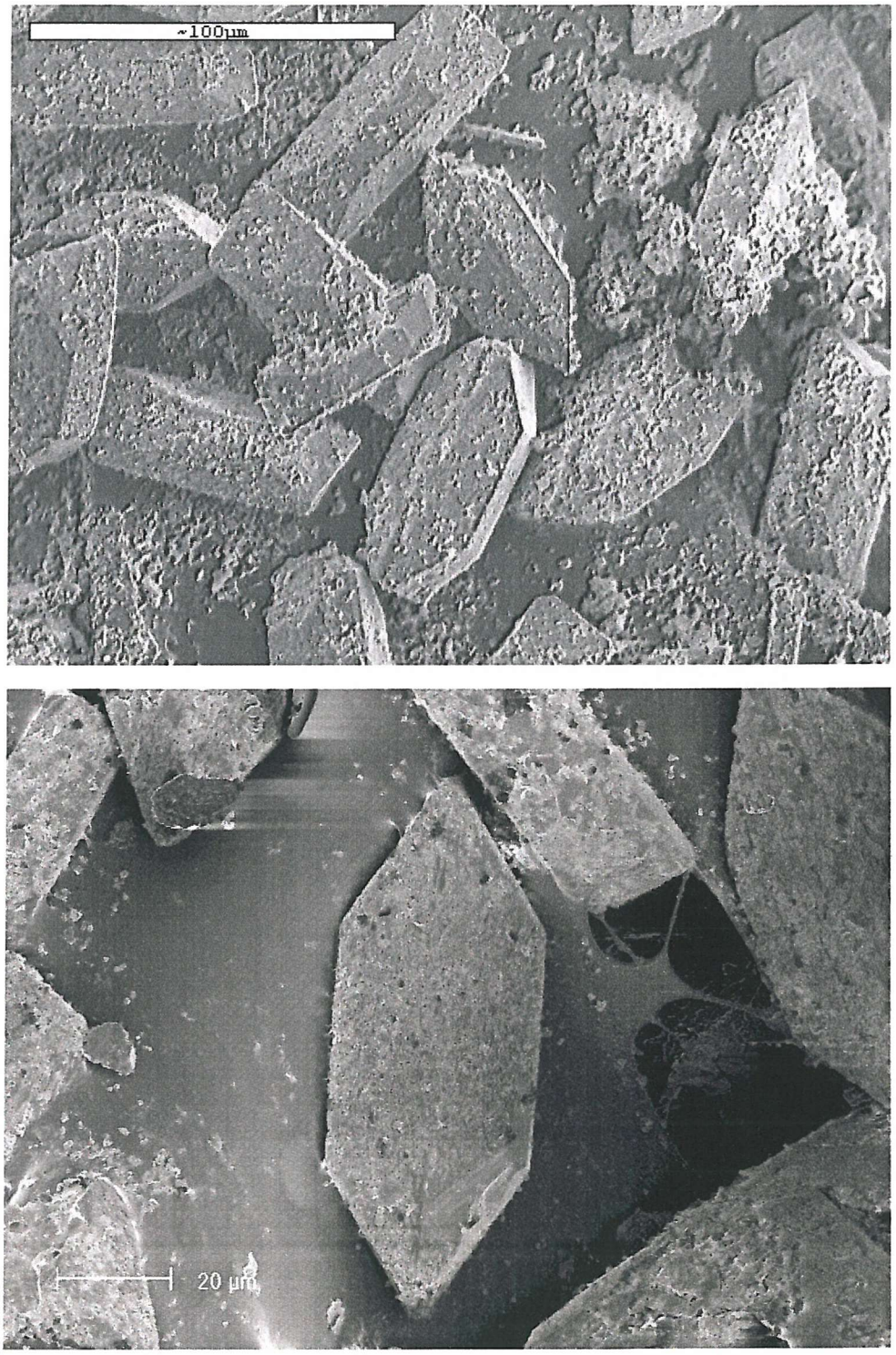

Figure 4.3 SEM micrographs of $NaCaSiO_3OH$ crystal formed at 220 °C.

EDX Analysis

Analysis of the composition of the materials formed at 220°C and 150°C was undertaken using EDX. The $NaCaSiO_3OH$ phase dominated most of the products formed at 220°C and the smaller particles of cancrinite adhered to its surface thus making analysis of the aluminosilicate phase alone impossible. Analysis of a cancrinite crystal in a mixed phase product, formed at low calcium concentrations, showed significant calcium content; though even with spot analysis it is difficult to ensure that the other phases present do not contribute to the analysis. Table 4.3 summarises the determined sodium to calcium ratio for this phase using EDX analysis. Based on this ratio a stoichiometry near $Na_{7.1}Ca_{0.9}[AlSiO_4]_6(CO_3)_{1.45}.nH_2O$ can be inferred.

Table 4.3 Sodium to calcium ratios in $NaCaHSiO_3OH$ and the aluminosilicate phase determined by EDX.

Temperature, solution calcium concentration (moles/L), reaction time, product	**Na:Ca Atomic percentage ratio determined composition of aluminosilicate phase.**
220°C, $2.28x10^{-3}$, 96 hrs $NaCaHSiO_3OH$	1.04
220°C, $8.9\ x10^{-4}$, 96 hs cancrinite	0.11, $Na_{7.1}Ca_{0.9}[AlSiO_4]_6(CO_3)_{1.45}.nH_2O$
150°C, 0.0, 96 hrs, Intermediate	0.005, $Na_8[AlSiO_4]_6(CO_3).nH_2O$
150°C, $8.9\ x10^{-4}$, 96 hrs, Intermediate	0.11, $Na_{7.1}Ca_{0.9}[AlSiO_4]_6(CO_3)_{1.45}.nH_2O$
150°C, $1.78x10^{-3}$, 96 hrs, Intermediate	0.13, $Na_{6.9}Ca_{1.1}[AlSiO_4]_6(CO_3)_{1.55}.nH_2O$
150°C, $2.28x10^{-3}$, 96 hrs, Intermediate and $Ca(OH)_2$	0.28, $Ca(OH)_2$ present in analysis
150°C, $2.7x10^{-3}$, 96 hrs, Intermediate and $Ca(OH)_2$	0.59, $Ca(OH)_2$ present in analysis

For the products formed at 150° C the interference from residual $Ca(OH)_2$ presented the most problems when determining the sodium to calcium ratio. Analysis of the Intermediate phase material formed after 96 hours with different calcium concentrations gave the compositions summarised in Table 4.3 and Figure 4.4. For products formed under high $Ca(OH)_2$ concentrations, the amount of residual $Ca(OH)_2$ was also high and the analysis of pure Intermediate crystallites proved impossible. For this reason the determined sodium calcium ratio for these products must be treated with extreme

caution. However, for materials formed at lower calcium concentrations, calcium is incorporated into the Intermediate to gives compounds with stoichiometries near $Na_7Ca_1[AlSiO_4]_6(CO_3)_{1.5}.nH_2O$.

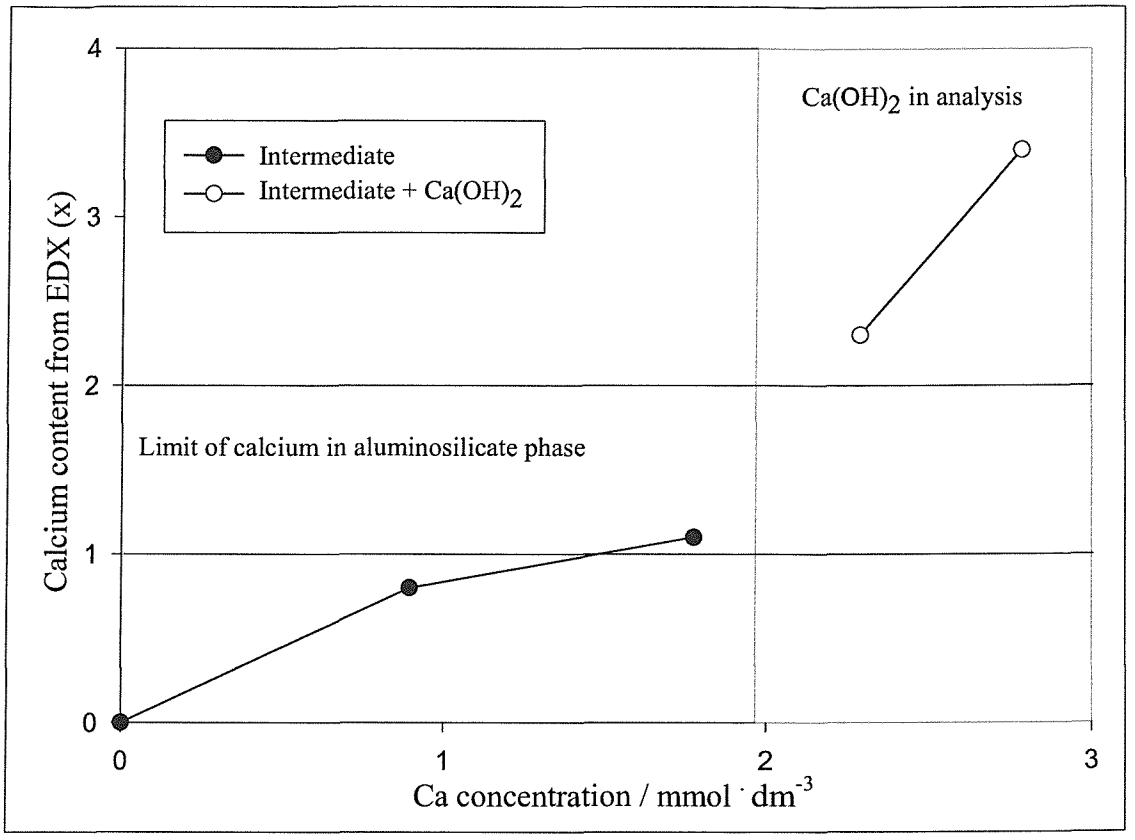

Figure 4.4 EDX determined calcium content in the reaction products formed at 150°C assuming a composition $Na_{8-x}Ca_x[AlSiO_4]_6.(CO_3)_{(1+x)/2}.nH_2O$. For the two highest calcium concentrations $Ca(OH)_2$ was also present increasing the effective calcium level. The horizontal lines represent typical calcium contents for $Na_{8-x}Ca_x[AlSiO_4]_6.(CO_3)_{(1+x)/2}.nH_2O$ with x = 1 and 2.

4.3.2.3 FTIR Results

Products from the syntheses, under the various conditions were examined using FTIR. Characteristic cancrinite and Intermediate bands confirmed the presence of these phases. An FTIR scan obtained for the solid $NaCaSiO_3OH$ phase is shown below in Figure 4.5. The presence of two broad bands in the 1900-3000 cm^{-1} region, centred on 2813 and 2417 $^{cm-1}$ separated by 300-500 cm^{-1} indicates that the structure is strongly hydrogen bonded. This characteristic is seen for other strongly hydrogen bonded materials such as alpha and beta CrOOH which have a broad background with two well-separated absorptions[8].

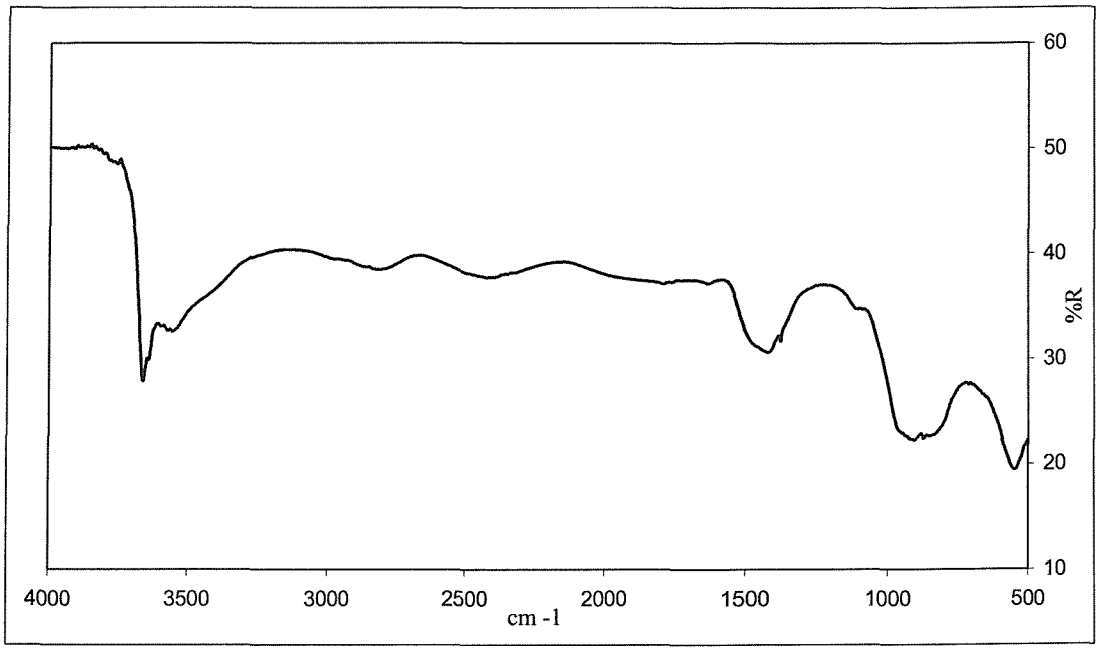

Figure 4.5 FTIR spectrum of $NaCaSiO_3OH$.

4.3.2.4 PND Results

Powder neutron diffraction data were collected from $NaCaSiO_3OH$ on the POLARIS instrument at the Rutherford Appleton Laboratory over a period of 6 hours.

$NaCaSiO_3OH$ Structure Refinement

Data collected in the back-scattering bank on POLARIS were used for the structure refinement of $NaCaSiO_3OH$. The structural model was taken from Cooksley and Taylor who originally reported a structure for $NaCaSiO_3OH$ determined using single crystal X-ray diffraction methods[9]. However, as would be expected from X-ray methods these authors had problems in distinguishing structures based on the location of the hydrogen

atom. Two possible descriptions exist: a disordered or central hydrogen atom in the space group $P2_1$ or an ordered model adopting the space group $P2_1/n$. With the sensitivity of neutron diffraction to hydrogen scattering it becomes possible to distinguish between these structures. Refinement was undertaken using both these descriptions but a significantly improved fit was obtained with the $P2_1/n$ ordered hydrogen position description. Introduction of all positional and thermal parameters led to a rapidly converging refinement. Final refined atomic co-ordinates and fit parameters are summarised in Table 4.4 and derived bond lengths and angle of interest are reported in Table 4.5. The profile fit achieved is shown in Figure 4.6.

Table 4.4 Final refined co-ordinates for $NaCaSiO_3OH$. e.s.d.s are given in parentheses.

	x	y	Z	Ui/Ue*100 / Å^2
Ca	-0.0009(21)	0.000000	-0.0069(21)	0.34(7)
Si	0.3404(6)	0.2474(25)	-0.2866(6)	0.02(7)
Na	-0.3604(10)	0.244(4)	0.3780(11)	1.74(9)
O4	0.2352(5)	0.2414(21)	-0.0643(6)	0.61(6)
O5	0.6712(5)	0.2420(24)	-0.1290(6)	0.53(6)
O6	0.2113(15)	0.0552(16)	-0.4874(15)	0.48(13)
O7	0.2074(17)	0.4296(17)	0.4929(15)	1.04(17)
H	0.0346(21)	0.4830(20)	0.5114(24)	2.52(16)

Space Group $P2_1/n$

a = 5.7075(2) Å, b = 7.0495(3) Å, c = 5.4693(2) Å, ß = 122.365(2)°

Cell volume = 185.87(2) Å^3

R_{wp} = 1.25% R_p = 2.43%

Table 4.5. Selected derived bond lengths and angles for $NaCaSiO_3OH$. E.s.ds are given in parentheses.

Atom	Co-ordinated Oxygen	Length (Å)
Si	O1	1.619(4)
Si	O2	1.602(4)
Si	O3	1.649(14)
Si	O4	1.643(14)
Na	O1	2.280(6)
Na	O2	2.873(5)
Na	O2	2.605(8)
Na	O3	2.31(2)
Na	O4	2.35(3)
Ca	O1	2.294(13)
Ca	O1	2.413(14)
Ca	O2	2.349(14)
Ca	O2	2.430(15)
Ca	O3	2.451(11)
Ca	O4	2.312(11)
O3	O4	2.534(4)
H	O3	1.432(12)
H	O4	1.110(13)

Atoms	Derived Angle / °	Atoms	Derived Angle / °
O4-Si-O5	113.54(21)	O4-Si-O6	105.4(7)
O4-Si-O7	111.1(7)	O5-Si-O6	108.4(8)
O5-Si-O7	111.2(8)	O6-Si-O7	106.69(23)
O6-H-O7	171.1(11)		

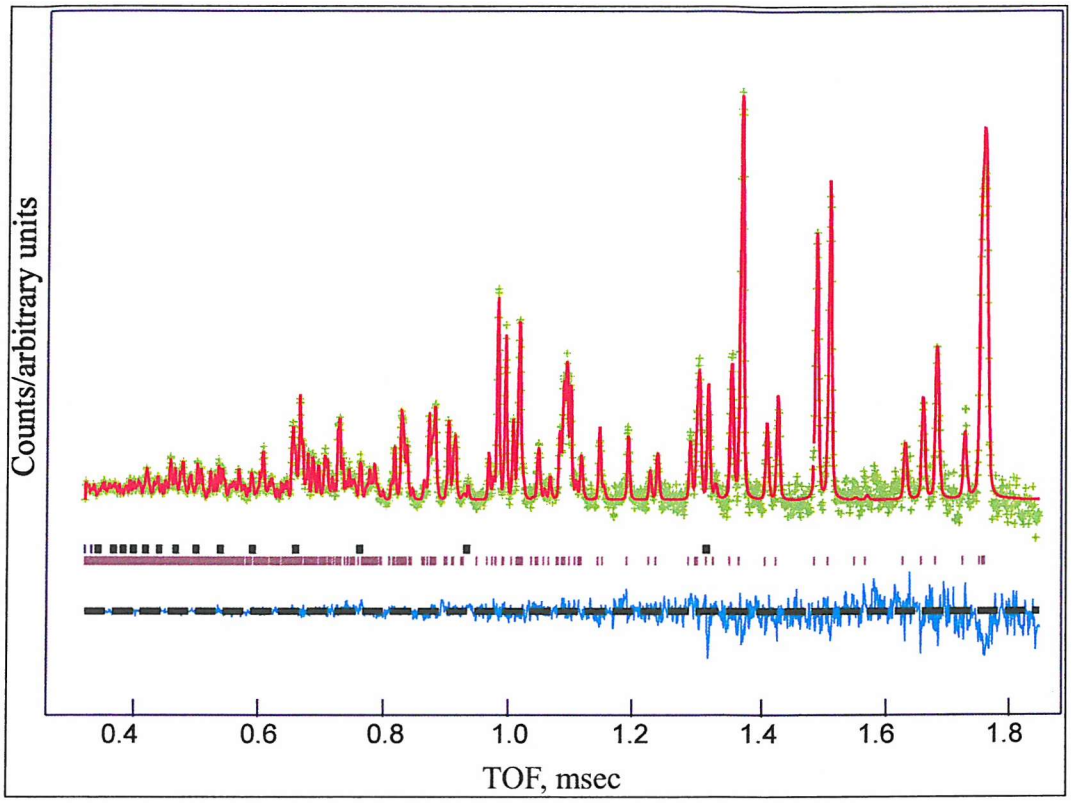

Figure 4.6 Profile fit to the powder neutron diffraction data from $NaCaSiO_3OH$. Crosses are experimental data, upper continuous line the calculated profile, lower continuous line the difference. Tick marks show reflection positions.

The $NaCaSiO_3OH$ structure consists of $Si(O_3OH)$ tetrahedra which are hydrogen bonded to form a zigzag layer of chains, Figure 4.7. The calcium co-ordination is octahedral and the sodium co-ordination is best described as a distorted trigonal bipyramid. The SiO_3OH units are reasonably regular tetrahedra with O-Si-O bond angles all in the range 105-114°. The most significant part of this structure is the hydrogen bond which has a short O(Donor) - O(Acceptor) distance of 2.534 Å that is among the shortest observed for inorganic materials with discrete anions. Similar distances are found in sodium hydrogencarbonate, 2.55 Å, and ammonium dihydrogenphosphate, 2.49 Å. The strength of this interaction is seen in the derived O-H distance of 1.10Å which is longer than the normal discrete OH distance found with neutrons for hydroxides of around 0.96Å; the O(Donor)- H-O(acceptor) angle of 171° is also consistent with the strong hydrogen bond being close to 180° [10]. This strong hydrogen bond is also compatible with the observed O-H stretching frequency obtained from the IR spectrum consisting of two bands in the 1900-3000 cm^{-1} region, separated by 300-500 cm^{-1}.

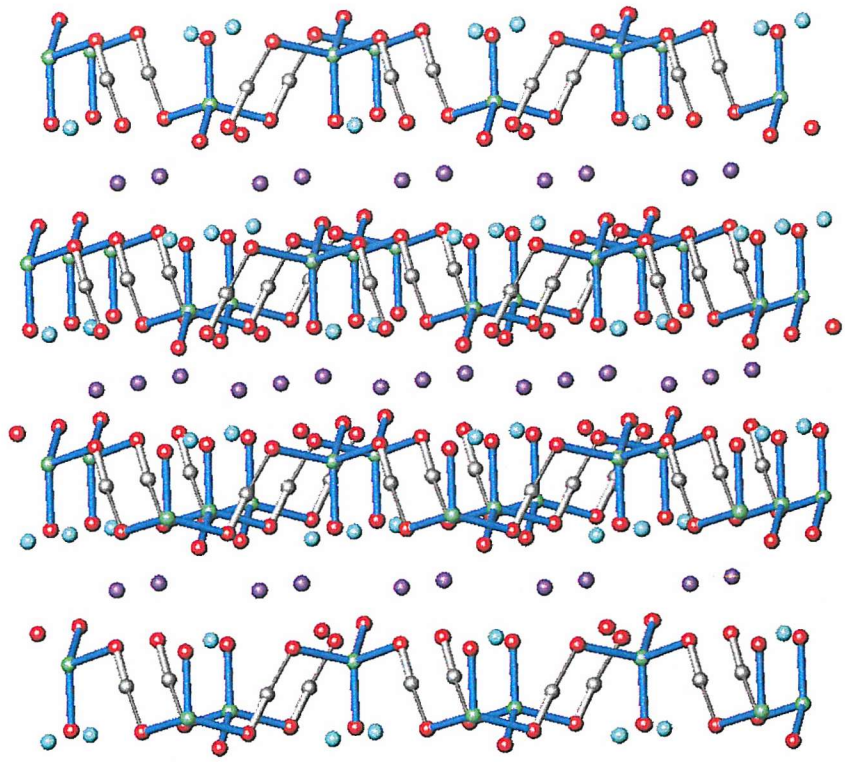

Figure 4.7 The hydrogen bonded layers in $NaCaSiO_3OH$. Blue spheres represent calcium, light blue spheres sodium, green spheres silicon, red spheres oxygen and grey spheres hydrogen.

4.3.3 Discussion

The extent to which $NaCaHSiO_3OH$ forms is dependent upon the concentration of $Ca(OH)_2$ in the system, the reaction time and temperature. When the reaction is carried out at 220 °C for 96 hrs using a high concentration of $Ca(OH)_2$, $NaCaSiO_3OH$ can be obtained as a single phase. As the $Ca(OH)_2$ concentration and reaction time decrease a mixture of this phase and cancrinite results. At 150 °C the $Ca(OH)_2$ has a lesser effect on the phase formation, much of it tends not to react and is present in the final reaction product again supporting the evidence that formation of $NaCaSiO_3OH$ from $Ca(OH)_2$ is a slower process than cancrinite/Intermediate phase formation.

4.4 Effect of Calcium Hydroxide Addition to Bayer Liquor and High Aluminium Concentration Solutions

The experiments described in section 4.3 have all used kaolin as a source of aluminium and silicon, thus giving an Al to Si ratio of 1:1. In spent Bayer liquor the alumina concentration is 102 g/L and the silica concentration is 0.5 g/L, giving an Al to Si ratio of approximately 240:1. Having observed the formation of $NaCaSiO_3OH$, an alternative phase to the Intermediate and cancrinite, the next series of experiments aimed to monitor the effect of gradually increasing the Al to Si ratio on the formation of $NaCaSiO_3OH$.

4.4.1 Experimental

Syntheses were carried out under hydrothermal conditions at a temperature of 220 °C and autogenous pressure in Parr 23 ml Teflon-lined steel autoclaves under static conditions for 48 h. Kaolin (0.2520 g), sodium carbonate (0.3996 g) and either sodium hydroxide solution (8 M, 14 ml) or Bayer liquor (14 ml) were added to the Teflon cup; calcium hydroxide was subsequently added in varying amounts to produce calcium concentrations in the range 0.0635-0.235 mol/L. In instances where sodium hydroxide was used, aluminium powder was added to produce aluminium concentrations in the range 0.285 to 5.07 mol/L. The exact combinations of reagents used are presented overleaf in Table 4.6.

The resultant white powders were washed with 150 ml distilled water and dried for 24 h at 80 °C.

Table 4.6 Reagents used in experiments performed at 200 °C for 48 h.

Quantities of Reagents Used					
Na_2CO_3 (g)	**Kaolin (g)**	**NaOH (ml)**	**Liquor (ml)**	**Al (g)**	**Al:Si**
0.3996	0.2520	14	0	0	**1:1**
0.3996	0.2520	14	0	0.108	**3:1**
0.3996	0.2520	14	0	0.189	**5:1**
0.3996	0.2520	14	0	0.27	**6:1**
0.3996	0.2520	14	0	0.675	**14:1**
0	0.2520	0	14	0	**14:1**
0.3996	0.2520	14	0	0.9558	**19:1**
0.3996	0.2520	14	0	1.917	**37:1**
0	0.025	0	14	0	**88:1**
0	0	0	14	0	**240:1**

4.4.2 Results

The resulting microcrystalline white powders were characterised using PXD and SEM.

4.4.2.1 PXD Results

Initial phase identification was achieved by the analysis of PXD data collected over the 2θ range 10 ° to 60 ° for 30 minutes. The reaction parameters and results, in terms of the phases formed, are summarised in Table 4.7.

Table 4.7 Phase identification for experiments performed at 220 °C for 48 hours. Where actual Bayer liquor has been used the results are presented in red.

$Ca(OH)_2$ (moles)	**Phase(s) Present**									
	Aluminium to Silicon Ratio (Al:Si)									
	1:1	3:1	5:1	6:1	14:1	14:1	19:1	37:1	88:1	240:1
0	**C**	**C**	**C**	**C**	**C**	**C**	**C**	**C**	**C**	**C**
8.9×10^{-4}	**Ca** C	**Ca** C	**C**	**C**	**C**	**C**	**C**	**C**	**C**	**C**
1.24×10^{-3}	**Ca** C	**Ca** C	**C** R	**C** R	**C** R	**C** R	**R** C	**R** C	**Al** C	**Al** C
1.78×10^{-3}	**Ca** C	**Ca** C	**R** C	**R** C	**R** C	**R** C	**R** C	**R** C	**Al** C	**Al**
2.28×10^{-3}	**Ca** C	**Ca** C	**R** C	**R** C	**R** C	**R** C	**R** C	**Al** R C	**Al** RC	**Al** R
2.78×10^{-3}	**Ca** C R	**Ca** C R	**R** C	**R** C	**R** C	**R** C	**R** C	**Al** R C	**Al** R	**Al** R
3.29×10^{-3}	**Ca** C R	**Ca** C R	**R** C	**R** C	**R** C	**R** C	**R** C	**Al** R C	**Al** R	**Al** R

Ca: - sodium calcium hydrogen silicate, $NaCaHSiO_3OH$ (JCPDS 25-1319)

C: - Cancrinite

R: - unreacted starting material ($Ca(OH)_2$)

Al: - aluminium calcium hydroxide $Al_2Ca_3(OH)_{12}$.

The results in Table 4.7 show that increasing aluminium concentration to achieve an aluminium to silicon ratio >1:1 has a significant effect on the phase formed. The formation of carbonate cancrinite is observed across the table though only as a pure phase at low $Ca(OH)_2$ concentrations. As aluminium concentration increased the level of $Ca(OH)_2$ remaining in the final product also increased, suggesting that $Ca(OH)_2$ solubility decreases with increasing aluminium concentration. The formation of $NaCaSiO_3OH$ is only observed for Al:Si ratios of 1:1 and 3:1. Once the Al:Si ratio is increased to $\geq$5:1 this phase is not obtained as a product. The most favourable phase formed at high aluminium and high calcium concentrations is calcium aluminium hydroxide $Al_2Ca_3(OH)_{12}$. Rosenberg *et al*[11] reported the formation of this phase for the reaction of $Ca(OH)_2$ aluminate solutions. They suggested that the reaction proceeds via the formation of a calcium hemicarbonate species ($[Ca_2Al(OH)_6]_2.½CO_3.OH.5½H_2O$). This species was not observed in these investigations.

4.4.2.2 Electron Microscopy Results

Products from the syntheses, under the various conditions were examined using SEM.

SEM Micrographs

SEM micrographs revealed that the $Al_2Ca_3(OH)_{12}$ phase is different in morphology from cancrinite and Intermediate phase. The crystallites of this phase are irregular shaped balls and have typical dimensions of 3 x 3 x 3 μm, Figure 4.8.

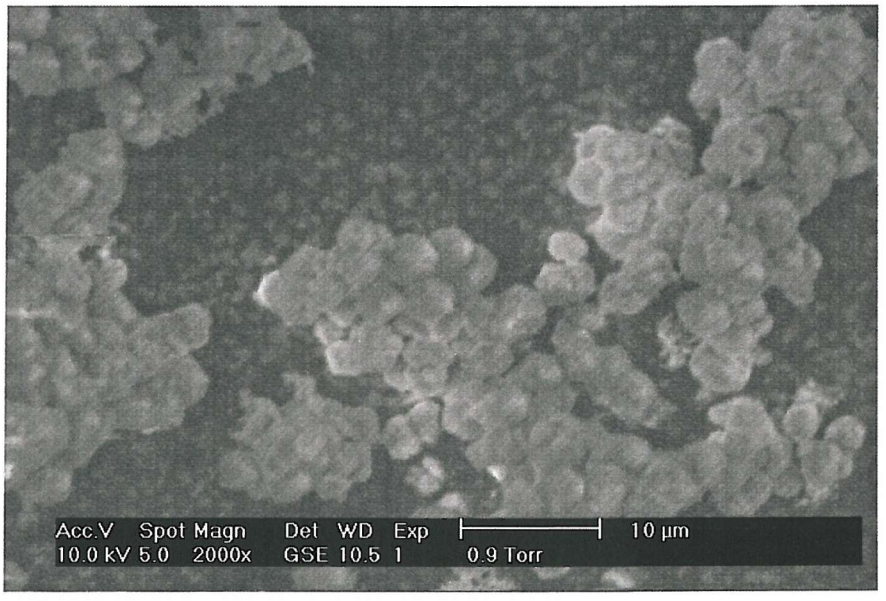

Figure 4.8 SEM micrograph of $Al_2Ca_3(OH)_{12}$ crystals formed at 220°C.

EDX Analysis

EDX analysis of cancrinite crystals revealed that calcium had been incorporated into the structure, stoichiometries of near $Na_7Ca_1[AlSiO_4]_6(CO_3)_{1.45}.nH_2O$ were observed.

4.4.3 Discussion

Reactions using actual Bayer liquor and synthetic liquor with increased aluminium concentration have shown that the formation of $NaCaHSiO_3OH$ is also dependent upon the aluminium to silicon ratio in the system. An Al to Si ratio of near 1:1 is required in order to yield $NaCaHSiO_3OH$. The solubility of $Ca(OH)_2$ is seen to decrease with increasing aluminium concentration and as a result the major phases yielded at high aluminium and high calcium levels are $Ca(OH)_2$ and $Al_2Ca_3(OH)_{12}$. At high aluminium and low/moderate $Ca(OH)_2$ levels, the phases obtained are carbonate cancrinite, $Ca(OH)_2$ and $Al_2Ca_3(OH)_{12}$. The cancrinite formed under these conditions is again sodium-calcium carbonate cancrinite.

4.5 Conclusions

The addition of $Ca(OH)_2$ to synthetic systems that yield carbonate cancrinite or Intermediate, results in the formation of these two aluminosilicate phases and also $NaCaHSiO_3OH$. The formation of $NaCaHSiO_3OH$ is dependent upon the concentration of $Ca(OH)_2$ in the system, the reaction time and temperature. When the reaction is carried out at 220 °C for 96 hrs using a high concentration of $Ca(OH)_2$, $NaCaSiO_3OH$ can be obtained as a single phase. As the $Ca(OH)_2$ concentration and reaction time decrease, a mixture of this phase and cancrinite results. At 150 °C the $Ca(OH)_2$ has a lesser effect on the phase formation; much of it tends not to react and is present in the final reaction product again supporting the evidence that formation of $NaCaSiO_3OH$ from $Ca(OH)_2$ is a slower process than cancrinite/Intermediate phase formation. The crystal morphology of $NaCaHSiO_3OH$ is very different from that of both cancrinite and Intermediate; typical dimensions of the crystallites are 100 x 30 x 30 μm. Calcium incorporation into cancrinite and Intermediate is observed at both temperatures.

As a result of these synthetic investigations it was proposed that the difference in size and morphology could make this phase a more favourable scale product; the size and shape being less likely to form such tight packing crystallites as cancrinite and Intermediate. The reaction conditions that are required to form this phase as a single product would be impossible to achieve in the heat exchangers of a Bayer plant (e.g. a reaction time of 96 h). However a mixture $NaCaHSiO_3OH$ and cancrinite/Intermediate could modify the way the scale adheres to the heat exchanger surfaces and perhaps make it easier to remove. The incorporation of calcium into the structures of both cancrinite and Intermediate may permit easier removal of these phases; further investigations into how the sodium-calcium form of these phases differs to the pure sodium forms are required; one possible difference is the acid dissolution rate.

Reactions using actual Bayer liquor however, showed that the formation of $NaCaHSiO_3OH$ is very unlikely to occur under plant conditions. Examination of the results obtained in these investigations showed that the formation of $NaCaHSiO_3OH$ is very dependent upon the aluminium to silicon ratio in the system. An Al to Si ratio of near 1:1 is required in order to yield $NaCaHSiO_3OH$. In spent Bayer liquor this ratio is close to 230:1, thus under these conditions the formation of $NaCaHSiO_3OH$ is not

observed. The solubility of $Ca(OH)_2$ is seen to decrease with increasing aluminium concentration and as a result the major products at high aluminium and high calcium levels are $Ca(OH)_2$ and $Al_2Ca_3(OH)_{12}$. At high aluminium and low/moderate $Ca(OH)_2$ levels, the resulting products are cancrinite $Ca(OH)_2$ and $Al_2Ca_3(OH)_{12}$. Further studies into the formation of sodium-calcium cancrinite/Intermediate are needed to determine the effect that these modified aluminosilicate phases may have on scale formation.

The structural model of $NaCaHSiO_3OH$ proposed by Cooksley and Taylor[9] has been confirmed and accurate hydrogen positions have been determined by refinement of neutron data.

4.6 References

1 B.I. Whittington, *Hydrometallurgy,* **43**, 13, (1996).

2 N.S. Mal'ts, V.P. Poddymov, L.S. Rudashevskii, V.E. Kiselev, *Tsvet. Metal*, **5**, 38, (1985).

3 B.-A. Xu, D.E. Giles, I.M. Ritchie, *Hydrometallurgy,* **48**, 205, (1998).

4 A. Noworyta, *Hydrometallurgy*, **7**, 99, (1981).

5 B.I. Whittington, *Hydrometallurgy*, **45**, 289, (1997).

6 J. Buhl, M. Fechtelkord, Th.M. Gesing, K. Hackbarth, *Microporous and Mesoporous Materials*, **30**, 347, (1999).

7 J.Breck, *Journal of the American Chemical Society*, **78**, 5963, (1956).

8 W.C. Hamilton, J.A.Ibers, Hydrogen Bonding in Solids, W.A.Benjamin, New York (1968)

9 B.G. Cooksley, H.F.W. Taylor, *Acta Crystallographica*, **B30**, 864, (1974).

10 S.N. Vinogradov and R.H. Linnell, Hydrogen Bonding, Van Nostrand Reinhold Company, (1971).

11 S.P. Rosenbery, D. J. Wilson, C.A. Heath, *Light Metals Conference*, 19, (2001).

Chapter 5

Polymeric Additives

5.1 Introduction

The addition of calcium hydroxide to systems that yield cancrinite and Intermediate, results in the formation of an alternative phase. Unfortunately the reaction conditions required to synthesise this phase are not viable in a Bayer plant. The aim of this investigation is to identify potential additives that may be utilised in Bayer plants to reduce/modify aluminosilicate scaling.

The use of hydroxamated organic polymers to 'alter Bayer process scale' is reported in two international patents submitted by the Cytec Technology Group[1,2]. The patents relate to the use of polymers containing hydroxamic acid or salt groups to treat Bayer liquors that contain a scale forming component. The polymers are reported to inhibit or modify the formation of scale that forms in the mixer, digester and flash tanks, sand trap cyclone and the charge or recycle stream. The examples of scale modification presented in the above mentioned patents are concerned specifically with titanate scale products.

The utilisation of chemical additives for the reduction of scale formation has also been investigated by Addai-Mensah *et al*[3]. The study focuses on the introduction of a new polymeric additive; upon addition of this polymer a significant reduction in the extent of sodalite scale formation at steel surfaces is observed. The mechanism behind the suppressant action of the polymer and the presence of certain functional groups are believed to be directly linked. The nature of the polymer is not revealed in the literature.

Cancrinite synthesis requires the presence of a templating anion, such as carbonate (CO_3^{2-}) or sulphate (SO_4^{2-}) that has three-fold symmetry. Substances containing sulphate and sulphonate functional groups were investigated as potential additives. It was anticipated that the ionic end of the additive would template the structure, leaving the organic molecule protruding out and the presence of the organic molecule thus inhibiting or preventing further growth in that direction, Figure 5.1. Initially low molecular weight organic sulphate and sulphonate sodium salts were examined. The study was then extended to high molecular weight organic polymers possessing similar/related functional groups.

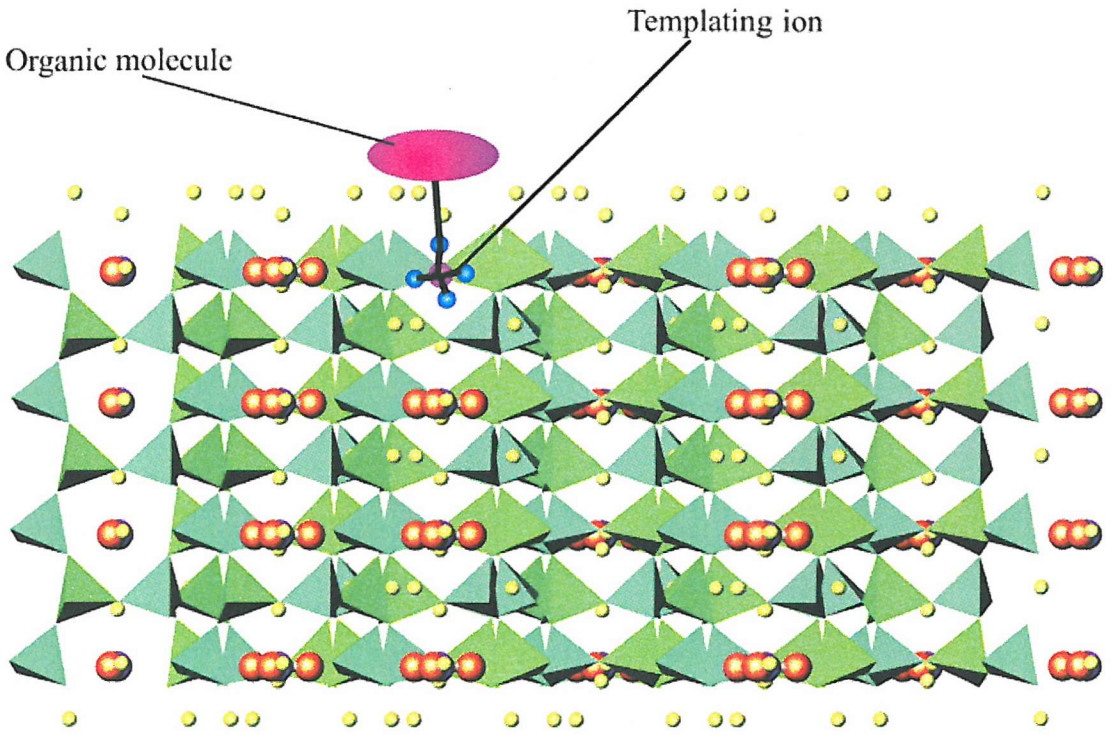

Figure 5.1 Theoretical representation of an organic molecule with an ionic group replacing a templating anion in the cancrinite structure, thus inhibiting further growth in that direction. Green polyhera represent the $[SiO_4]^{4-}$ and $[AlO_4]^{5-}$ tetrahedra, orange spheres the templating anions and yellow spheres the charge balancing cations of the cancrinite structure. The pink oval represents the organic molecule and the pink and blue spheres the ionic group.

5.2 Aims

A range of organic substances have been added to systems that yield cancrinite and Intermediate phase products. The aim of this investigation is to identify potential additives that eliminate, reduce or modify the formation of these aluminosilicate phases.

5.3 Organic Sulphate/Sulphonate Additives

5.3.1 Experimental

Syntheses were carried out under hydrothermal conditions at temperatures of 100 and 220 °C and autogenous pressure in Parr 23 ml Teflon-lined steel autoclaves under static conditions. Kaolin (0.2520 g), sodium carbonate (0.3996 g) and sodium hydroxide solution (4/8 M, 14 ml) were added to the Teflon cup; sulphate/sulphonate additives were subsequently added in varying amounts. The additives employed and the quantities in which they were used are presented in Table 5.1 below. Each reaction was performed for 48 h. The resultant white powders were washed with 150 ml distilled water and dried for 24 h at 80 °C.

Table 5.1 Sulphate or sulphonate additive and quantity used.

Sulphate or Sulphonate Salt		**Amount (moles)**
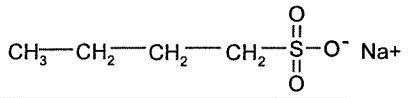	1 Butanesulphonic acid sodium salt	8.92×10^{-4} (conc. 1)
		1.78×10^{-3} (conc. 2)
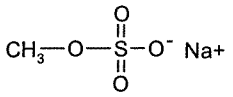	Methyl sulphate, sodium salt	8.92×10^{-4} (conc. 1)
		1.78×10^{-3} (conc. 2)
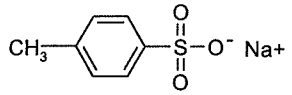	Sodium p-toluensulphonate	8.92×10^{-4} (conc. 1)
		1.78×10^{-3} (conc. 2)
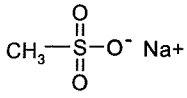	Sodium methanesulphonate	8.92×10^{-4} (conc. 1)
		1.78×10^{-3} (conc. 2)

5.3.2 Results

The resulting microcrystalline white powders were analysed using PXD, SEM, FTIR.

5.3.2.1 PXD Results

Initial phase identification was achieved by the analysis of PXD data collected over the 2θ range 10 ° to 60 ° for 30 minutes. The reaction parameters and results, in terms of the phases formed and corresponding lattice parameters, are summarised in Tables 5.2, 5.3 and 5.4.

Table 5.2 Phase identification and calculated lattice parameters for experiments performed at 100 °C for 48 hours using 4 M NaOH solution (e.s.d.s. in parentheses).

Phase Identification and Lattice Parameters for Reactions at 100 °C (4.7M)		
Additive (concentration 1/2)	**Phase Formed**	**Lattice Parameters (Å)**
1-Butanesulphonic acid sodium salt (1)[a]	I	7.304(3) 2.584(2)
1-Butanesulphonic acid sodium salt (2)[b]	I	7.288(2) 2.580(1)
Methyl sulphate sodium salt (1)[a]	I	insufficient data
Methyl sulphate sodium salt (2)[b]	I	7.30(5) 2.59(1)
Sodium p-toluenesulphonate 95 % (1)[a]	I	7.297(1) 2.582(1)
Sodium p-toluenesulphonate 95 % (2)[b]	I	7.296(3) 2.581(2)
Sodium methanesulphonate 98 % (1)[a]	I	7.31(5) 2.59(1)
Sodium methanesulphonate 98 % (2)[b]	I	insufficient data
Blank	I	7.301(4) 2.587(6)

I: - Intermediate

a: - concentration 1 (8.92×10^{-4} moles)

b: - concentration 2 (1.78×10^{-3} moles)

Where 'insufficient data' is recorded and the phase present assigned as being Intermediate, too few diffraction peaks were present in the PXD pattern to allow lattice parameter calculations to be performed. Those peaks that were present were at the same 2θ as major peaks indicative of Intermediate. Other Intermediate peaks may have been present at a lower intensity but it was impossible to distinguish between those and the noisy background.

Table 5.3 Phase identification and calculated lattice parameters for experiments performed at 100 °C for 48 hours using 8 M NaOH solution, (e.s.d.s. in parentheses).

Phase Identification and Lattice Parameters for Reactions at 100 °C (8M)		
Additive (concentration 1/2)	**Phase Formed**	**Lattice Parameters (Å)**
1-Butanesulphonic acid sodium salt (1)[a]	I	7.303(1) 2.582(1)
1-Butanesulphonic acid sodium salt (2)[b]	I	7.308(4) 2.587(2)
Methyl sulphate sodium salt (1)[a]	I	7.326(4) 2.586(2)
Methyl sulphate sodium salt (2)[b]	I	7.324(4) 2.586(1)
Sodium p-toluenesulphonate 95 % (1)[a]	I	7.317(4) 2.582(1)
Sodium p-toluenesulphonate 95 % (2)[b]	I	7.305(2) 2.582(1)
Sodium methanesulphonate 98 % (1)[a]	I	7.312(3) 2.586(2)
Sodium methanesulphonate 98 % (2)[b]	I	7.319(4) 2.585(3)
Blank	I	7.313(2) 2.588(4)

I: - Intermediate

a: - concentration 1 (8.92×10^{-4} moles)

b: - concentration 2 (1.78×10^{-3} moles)

Table 5.4 Phase identification and calculated lattice parameters for experiments performed at 220 °C for 48 hours using 8 M NaOH solution, (e.s.d.s. in parentheses).

Phase Identification and Lattice Parameters for Reactions at 220 °C (8M)		
Additive (concentration 1/2)	**Phase Formed**	**Lattice Parameters (Å)**
1-Butanesulphonic acid sodium salt (1)[a]	C	12.640(5) 5.13(4)
1-Butanesulphonic acid sodium salt (2)[b]	C	12.650(2) 5.159 (2)
Methyl sulphate sodium salt (1)[a]	C	12.638(2) 5.156(1)
Methyl sulphate sodium salt (2)[b]	C	12.641(2) 5.158(2)
Sodium p-toluenesulphonate 95 % (1)[a]	C	12.640(3) 5.166(3)
Sodium p-toluenesulphonate 95 % (2)[b]	C	12.630(3) 5.153(3)
Sodium methanesulphonate 98 % (1)[a]	C	12.634(9) 5.156(9)
Sodium methanesulphonate 98 % (2)[b]	C	12.634(2) 5.153(2)
Blank	C	12.650(1) 5.159(2)

I: - Intermediate

a: - concentration 1 (8.92×10^{-4} moles)

b: - concentration 2 (1.78×10^{-3} moles)

The aluminosilicate phase formation is consistent with that reported in the literature for systems containing no additives[4]. That is at 100 °C the phase observed is Intermediate whilst at the higher temperature 220 °C, the ordered sodium carbonate cancrinite is the only product yielded. The calculated lattice parameters are consistent throughout the investigation; no change occurred as a result of introducing the additives. No alternative or secondary phases were observed in these investigations.

5.3.2.2 Electron Microscopy Results

Products from the syntheses, under the various conditions were examined using SEM.

SEM Micrographs

SEM imaging revealed that no change in product morphology had occurred. Regular shaped rods 2 – 7 μs long were observed for the products formed at 220 °C, Figure 5.2. Irregularly shaped plate-like crystallites were seen for the products yielded at 100 °C, characteristic of Intermediate.

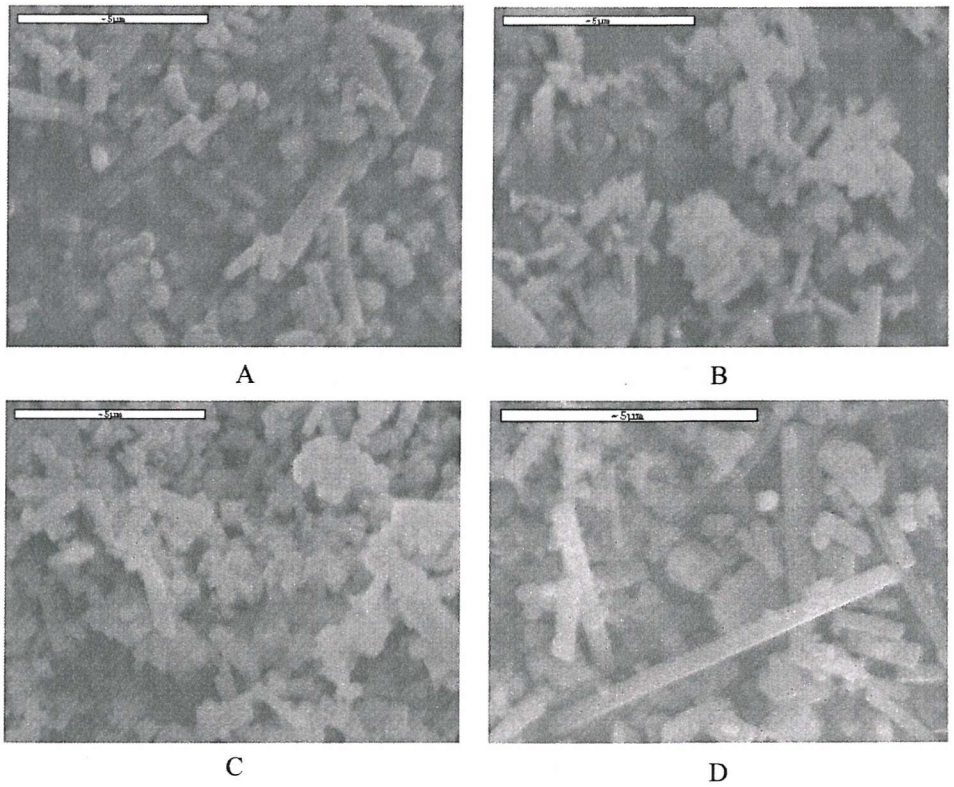

Figure 5.2 SEM images of the products obtained from reactions at 220 °C using:
A: - 1-Butanesulphonic acid sodium salt, B: - Methyl sulphate sodium salt, C: - Sodium p-toluenesulphonate and D: - Sodium methanesulphonate.

EDX Analysis

EDX analysis revealed that no sulphur had been incorporated into the structures.

5.3.2.3 FTIR Results

Products from the syntheses, under the various conditions were examined using FTIR. Characteristic cancrinite and Intermediate absorptions confirmed the presence of these phases. Presented below in Figure 5.3 are the FTIR scans measured on the products formed upon the addition of each additive during the 220 °C, 48 h, 8 M reactions. The scans were not measured quantitatively and so a comparison of intensities cannot be made, however the bands present in each scan are identical and are indicative of carbonate cancrinite.

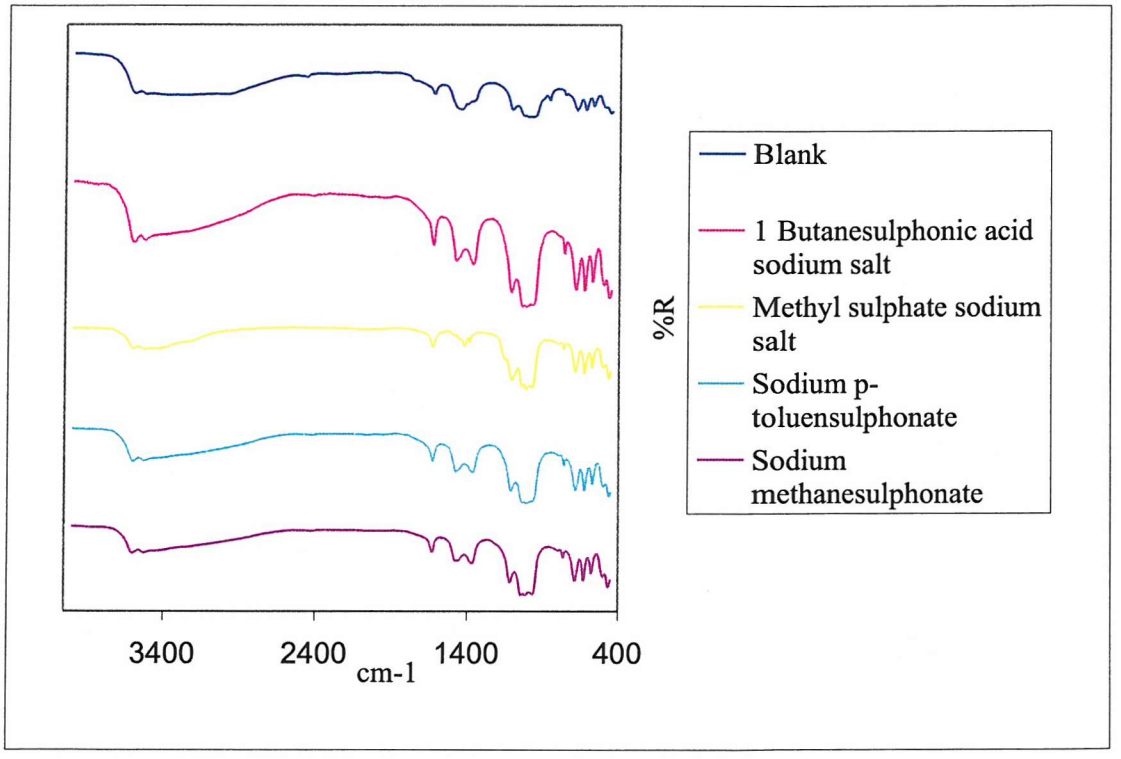

Figure 5.3 IR spectra recorded on the products formed upon the addition of sulphate/sulphonate additives.

5.3.3 Discussion

The inclusion of organic sulphate/sulphonate additives does not affect *the phase* formed under standard cancrinite/Intermediate reaction conditions. That is at 100 °C, Intermediate formation is observed and at 220 °C cancrinite is the phase yielded. No changes in the lattice parameters or morphology of the products obtained were detected.

5.4 Polymeric Additives

5.4.1 Experimental

Syntheses were carried out under hydrothermal conditions at temperatures of 135, 150 and 220 °C and autogenous pressure in Parr 23 ml Teflon-lined steel autoclaves under static conditions. Kaolin (0.2520 g), sodium carbonate (0.3996 g) and sodium hydroxide solution (8 M, 14 ml) were added to the Teflon cup; polymeric additives were subsequently added (0.014 g). The polymers used and the abbreviation given to each one are listed below in Table 5.5. The resultant products were washed with 150 ml distilled water and dried for 24 h at 80 °C.

Table 5.5 Polymeric additives employed in the investigation and corresponding abbreviation.

Polymer	Abbreviation	Structure
Poly(2-acrylamido-2-methyl-1-propanesulphonic acid) M_w *ca.* 2,000,000	Polymer 1	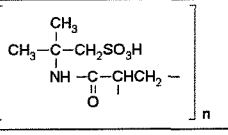
Poly(anetholesulphonic acid, sodium salt)	Polymer 2	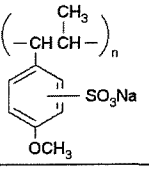
Poly(sodium 4-styrenesulphonate) M_w *ca.* 70,000	Polymer 3	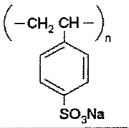
Poly(styrenesulphonic acid-*co*-maleic acid) sodium salt M_w *ca.* 20,000	Polymer 4	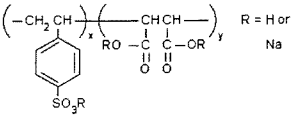
Poly(ethyleneglycol) 4-nonylphenyl 3-sulphopropyl ether, potassium salt	Polymer 5	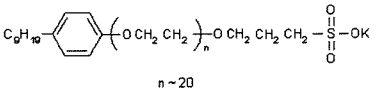
Poly(1,4-phenylene ether-ether sulphone)	Polymer 6	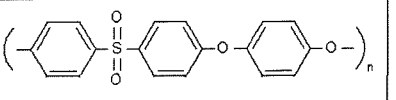
Poly (1,4-butanediol) divinyl ether M_n *ca.* 290	Polymer 7	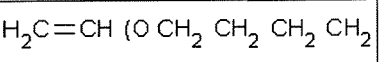

Polymers were chosen according to their functional groups and current applications; including suspension aid for particulates, mineral scale removers and anticoagulants.

The reaction parameters investigated were temperature, time, additive concentration, sodium carbonate concentration and sodium hydroxide concentration. The results are presented below in Tables 5.6 - 5.9.

For the variable temperature experiment each reaction was performed twice, hence two results for each polymer in Tables 5.6a-c.

5.4.2 Results

The resulting products were found to be white microcrystalline powders, hollow white beads/balls or a combination of powder and beads. The terms beads and balls are used to describe the products as both complete hollow spheres (balls) and hollow spheres with sections missing at each end (beads) are present. For the remainder of this chapter the two will be generally termed as spheres. The spheres are relatively robust and maintain their shape upon filtering. The spheres range from 0.5 – 4 mm in diameter. Figure 5.4 presents images for the spheres formed in a reaction using Polymer 5 at 220 °C. Both the powders and beads were analysed using PXD, SEM and FTIR.

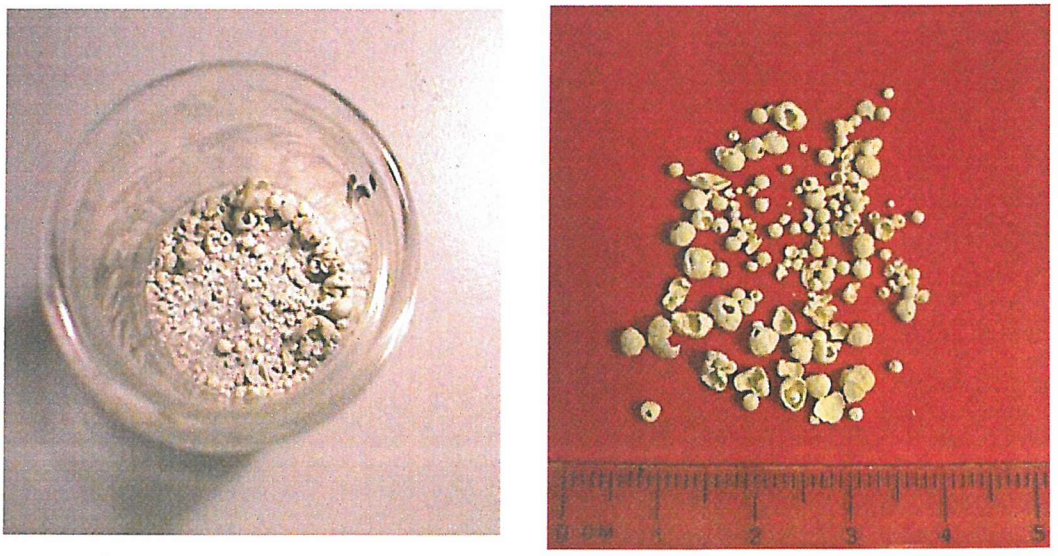

Figure 5.4 Images showing typical beads/balls formed in these investigations.

5.4.2.1 PXD Results

Initial phase identification was achieved by the analysis of PXD data collected over the 2θ range 10 ° to 60 ° for 30 minutes. The reaction parameters and results, in terms of the phases formed, the nature of the product (powder or spheres) and corresponding lattice parameters, are summarised in Tables 5.6 – 5.9.

Effect of Reaction Temperature

Table 5.6a Phase identification, nature of product formed and lattice parameters for experiments performed at 135 °C for 48 hours, (e.s.d.s. in parentheses).

Polymeric Additives 135 °C				
Polymer	**Phase**	**Form**	**Lattice Parameters Å (Intermediate)**	**Lattice Parameters Å (Cancrinite)**
1	I	P	7.300(2) 2.583(1)	12.61(2) 5.132(6)
1	I	P	7.306(3) 2.583(2)	12.64(2) 5.141(8)
2	I	P	7.303(2) 2.584(2)	12.61(2) 5.133(8)
2	I	P	7.305(2) 2.583(1)	12.62(2) 5.132(7)
3	I	P	7.302(4) 2.583(1)	insufficient data
3	I	P	7.297(2) 2.581(1)	12.647(2) 5.137(6)
4	I	P	7.293(3) 2.581(2)	12.63(2) 5.138(9)
4	I	P	7.302(2) 2.584(1)	12.649(3) 5.128(2)
5	I	P	7.300(1) 2.582(1)	12.490(4) 5.159(4)
5	I	P	7.304(1) 2.582(1)	12.648(2) 5.166(3)
6	I	P	7.297(1) 2.581(1)	12.664(5) 5.173(5)
6	I	P	7.299(1) 2.585(1)	12.674(5) 5.159(4)
7	I	P	7.303(2) 2.582(1)	12.671(6) 5.182(7)
7	I	P	7.304(1) 2.580(1)	12.669(6) 5.183(4)
Blank	I	P	7.3039(2) 2.582(1)	12.64(2) 5.143(8)

I: - Intermediate & cancrinite or disordered cancrinite, P: - Powder

Table 5.6b Phase identification, nature of product formed and lattice parameters for experiments performed at 150 °C for 48 hours, (e.s.d.s. in parentheses).

Polymeric Additives 150 °C				
Polymer	**Phase**	**Form**	**Lattice Parameters Å (Intermediate)**	**Lattice Parameters Å (Cancrinite)**
1	I	P	7.300(2) 2.583(1)	12.646(3) 5.167(4)
1	I	P	7.306(3) 2.583(2)	12.651(4) 5.169(4)
2	I	P	7.303(2) 2.584(2)	12.650(2) 5.160(2)
2	I	P	7.305(2) 2.583(1)	12.650(4) 5.168(9)
3	I	P	7.302(4) 2.583(1)	12.653(3) 5.166(6)
3	I	P	7.303(2) 2.582(1)	12.640(3) 5.160(3)
4	I	P	7.293(3) 2.581(2)	12.648(5) 5.164(4)
4	I	P	7.302(2) 2.584(1)	12.642(2) 5.159(3)
5	I	P	7.310(2) 2.582(1)	12.644(7) 5.159(6)
5	I	P	7.300(1) 2.580(1)	12.645(4) 5.160(5)
6	I	P	7.312(2) 2.581(1)	12.672(6) 5.177(5)
6	I	P	7.309(2) 2.582(2)	12.659(5) 5.165(6)
7	I	P	7.303(2) 2.581(1)	12.661(2) 5.171(3)
7	I	P	7.304(1) 7.2584(2)	12.655(4) 5.169(4)
Blank	I	P	7.303(2) 2.582(1)	12.648(3) 5.166(3)

I: - Intermediate & cancrinite or disordered cancrinite, P: - Powder

Table 5.6c Phase identification, nature of product formed and lattice parameters for experiments performed at 220 °C for 48 hours, (e.s.d.s. in parentheses).

Polymeric Additives 220 °C				
Polymer	**Phase**	**Form**	**Lattice Parameters Å (powder)**	**Lattice Parameters Å (balls)**
1	C	P & B	12.654(4) 5.150(3)	12.658(2) 5.150(2)
1	C	P & **B**	12.656(3) 5.148(2)	12.657(3) 5.149(3)
2	C	**P** & B	12.655(4) 5.144(3)	12.659(3) 5.146(1)
2	C	**B**		12.652(2) 5.155(1)
3	C	**P** & B	12.661(3) 5.162(3)	12.652(3) 5.151(3)
3	C	**P**	12.662(3) 5.152(3)	
4	C	P & **B**	12.660(5) 5.151(4)	12.662(3) 5.163(3)
4	C	P	12.663(2) 5.159(2)	
5	C	P & **B**	12.643(3) 5.160(3))	12.647(2) 5.157(2)
5	C	P & **B**	12.648(4) 5.155(3)	12.650(3) 5.154(3)
6	C	P & **B**	12.651(3) 5.149(3)	12.654(4) 5.149(3)
6	C	**B**		12.653(2) 5.159(2)
7	C	P & B	12.659(2) 5.150(3)	12.650(4) 5.150(3)
7	C	P & **B**	12.658(3) 5.148(4)	12.656(3) 5.151(1)
Blank	C	P	12.668(2) 5.166(2)	

I: - Intermediate & cancrinite or disordered cancrinite, P: - powder, B: - spheres

The aluminosilicate phase formation is consistent with that reported in the literature for systems containing no additives[4]. That is at the lower temperatures (135 and 150 °C) a combination of Intermediate and cancrinite or disordered cancrinite is observed, whilst at 220 °C, the ordered sodium carbonate cancrinite is the only product formed. The calculated lattice parameters are consistent throughout the investigation; no change has occurred as a result of introducing the additives. No alternative or secondary phases were observed in these investigations.

At 220 °C the formation of spheres constructed from cancrinite occurs; this phenomenon has not been observed in any other experiments during the course of this research. The sphere formation is clearly dependent upon temperature; a high temperature of 220 °C is required, however even at this temperature it is impossible to predict when the reaction will result in a sphere product. Addition of all seven polymers results in some spheres being produced though the degree of formation is somewhat inconsistent.

Effect of Reaction Time

Table 5.7 Phase identification and nature of product formed for experiments performed at 220 °C for 6 hours.

Polymeric Additives:- 6 h Reactions						
	135 °C		150 °C		220 °C	
	Phase	Form	Phase	Form	Phase	Form
Polymer 1	I	P	I	P	I	P
Polymer 2	I	P	I	P	I	P
Polymer 3	I	P	I	P	C	P
Polymer 4	I	P	I	P	I	P
Polymer 5	I	P	I	P	C	P
Polymer 6	I	P	I	P	C	P
Polymer 7	I	P	I	P	I	P
Blank	I	P	I	P	I	P

I: - Intermediate & cancrinite or disordered cancrinite

The aluminosilicate phase formation is consistent with that reported in the literature for systems containing no additives[4]. At 220 °C the variation in the phase formed between cancrinite, disordered cancrinite or a mixture of cancrinite and Intermediate may be a result of polymer addition or because the synthesis of phase pure cancrinite at such short reaction times is inconsistent. No sphere formation is observed for reactions performed for 6 h, thus longer reaction times are necessary for this phenomenon to occur.

Effect of Additive Concentration

A series of reactions were performed to investigate the effect of additive concentration on the phase/nature of the phase formed. The polymers were added at the following levels; 0.001, 0.003, 0.005, 0.007, 0.009, 0.011, 0.013, 0.015 and 0.017 g. All the reactions were performed at 220 °C for 48 h; all products yielded were cancrinite; the phase expected under these conditions. The formation of spheres or powder was random; the polymer concentration appeared to have no definitive effect on the nature

of the phase formed, spheres were yielded at low and high polymer concentrations, as were powders.

Effect of Sodium Carbonate Concentration

Table 5.8 Phase identification, nature of product formed and lattice parameters for experiments performed at 220 °C for 48 hours, omitting sodium carbonate.

Polymeric Additives:- no Sodium Carbonate			
Polymer	**Phase**	**Form**	**Lattice Parameters Å**
1	S	**P**	8.887(2)
2	S	**P**	8.895(1)
3	S	**B&P**	8.888(1)
4	S	**P**	8.889(1)
5	S	**B&P**	8.894(1)
6	S	**B&P**	8.889(1)
7	S	**B&P**	8.889(1)
Blank	S	**P**	8.893(1)

S: - sodalite, P: - powder, B: - spheres

The aluminosilicate phase formation is consistent with that reported in the literature for systems containing no additives[4]. That is that in the absence of sodium carbonate, hydroxy sodalite is yielded under these conditions.

Upon the addition of Polymers 3,5,6, and 7 the formation of spheres built from sodalite crystals occurs. The spheres are the same shape and have the same particle size distribution as those constructed from cancrinite. It is possible that sphere formation may occur upon the addition of the other three polymers; it was seen in Table 5.6c that the degree of sphere formation is somewhat inconsistent.

Effect of Sodium Hydroxide Concentration

Table 5.9 Phase identification and nature of product formed for experiments performed at 220 °C for 48 hours with varying sodium hydroxide concentration.

Polymeric Additives:- Sodium Hydroxide Concentration																
NaOH M	**Blank**		**Polymer 1**		**Polymer 2**		**Polymer 3**		**Polymer 4**		**Polymer 5**		**Polymer 6**		**Polymer 7**	
	Phase	**Form**	**Phase**	**Form**	**Phase**	**Form**	**Phase**	**Form**	**Phase**	**Form**	**Phase**	**Form**	**Phase**	**Form**	**Phase**	**Form**
1	**I**	**P**	**C**	**P**	**I**	**P**	**I**	**P**	**I**	**P**	**I**	**P**	**I**	**P**	**I**	**P**
2	**I**	**P**	**C**	**P**	**I**	**P**	**I**	**P**	**C**	**P**	**I**	**P**	**I**	**P**	**I**	**P**
3	**C**	**P**	**C**	**P**	**I**	**P**	**C**	**P**	**C**	**P**	**I**	**P**	**C**	**P**	**C**	**P**
4	**C**	**P**	**C**	**B&P**	**C**	**P**	**C**	**P**	**C**	**P**	**C**	**P**	**C**	**P**	**C**	**B&P**
5	**C**	**P**	**C**	**B&P**	**C**	**P**	**C**	**B&P**	**C**	**B&P**	**C**	**B&P**	**C**	**B&P**	**C**	**B&P**
6	**C**	**P**	**C**	**B&P**	**C**	**B&P**	**C**	**B&P**	**C**	**B&P**	**C**	**B&P**	**C**	**B&P**	**C**	**B&P**
7	**C**	**P**	**C**	**B&P**	**C**	**B&P**	**C**	**B&P**	**C**	**B&P**	**C**	**B&P**	**C**	**B&P**	**C**	**B&P**
8	**C**	**P**	**C**	**B&P**	**C**	**B&P**	**C**	**B&P**	**C**	**B&P**	**C**	**B&P**	**C**	**B&P**	**C**	**B&P**

I: - Intermediate & cancrinite or disordered cancrinite

P: - powder

B: - spheres

The aluminosilicate phase formation is consistent with that reported in the literature for systems containing no additives[4]. At the low NaOH concentrations the variation in the phase formed between cancrinite, disordered cancrinite or a mixture of cancrinite and Intermediate may be a result of polymer addition or because the synthesis of phase pure cancrinite at low concentrations is inconsistent.

The sphere formation is dependent upon sodium hydroxide concentration; a minimum concentration of 4 –5 M is required. As with the effect of temperature however, even under these 'ideal' reaction conditions it is impossible to predict when the reaction will result in a sphere product. Addition of each of the seven polymers results in the formation of some spherical products, though the degree of formation is inconsistent.

Variable Temperature PXD

Variable temperature PXD was performed on two samples; both were sodium carbonate cancrinite formed at 220 °C. The first was a powder sample, the result of a blank experiment, whereas the second was a sphere sample, a result of the addition of Polymer 5. The PXD data were collected over the 2θ range 10 ° to 60 ° for 30 minutes at each temperature, the heat rate between temperatures was 0.5 °C/sec. Figures 5.5 and 5.6 present the PXD patterns attained for the two experiments.

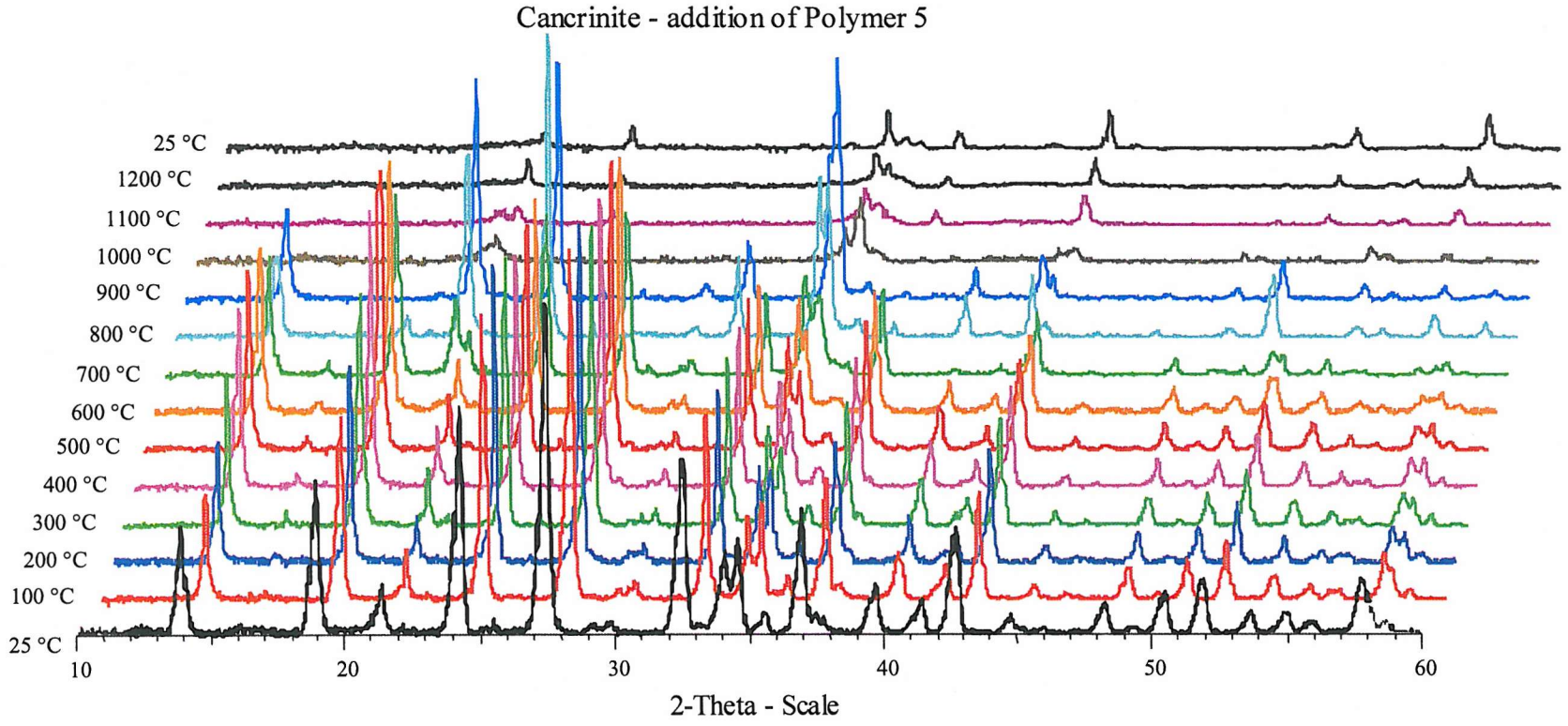

Figure 5.6 Variable temperature PXD patterns for cancrinite formed with the addition of Polymer 5.

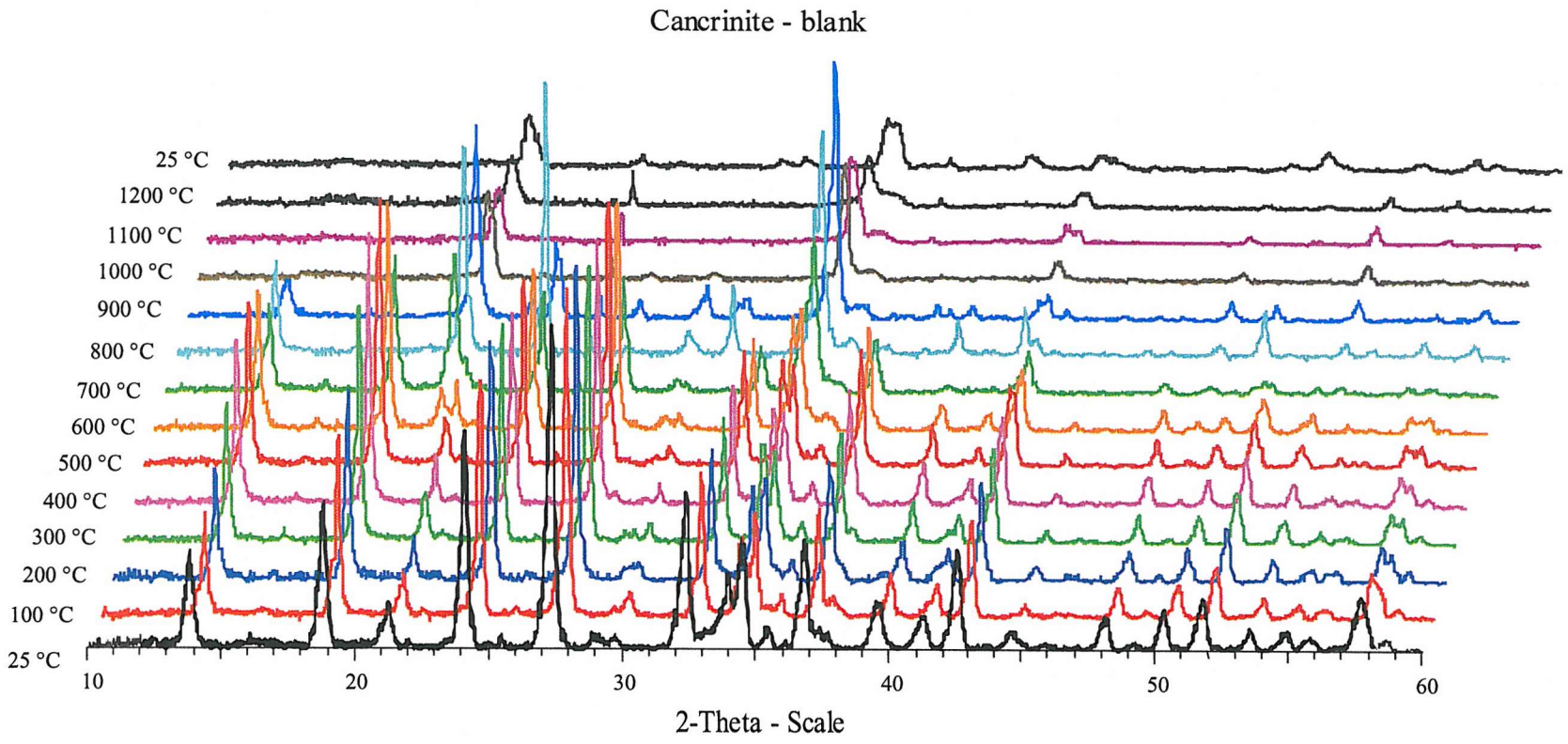

Figure 5.5 Variable temperature PXD patterns for cancrinite formed without the addition of any additive.

The decomposition of the two structures is almost identical; variations in the peaks present in the PXD patterns occur at the same temperatures for both data sets. At 800 °C changes in the patterns are observed. Prior to reaching this temperature very few differences between the patterns are seen; the framework is stable up to this temperature and the loss of water is the only event occurring within the framework. At 800 °C an additional peak at ≈ 31 ° appears in the patterns; this peak is also present in the 900 °C patterns but is not observed in the ones collected at 1000 °C. At this temperature other peaks also disappear and those that do remain become increasingly broader. The cancrinite products are clearly undergoing two phase transitions. The first at 800 °C is associated with the loss of sodium carbonate at ≈ 760 °C and the thermal destruction of the aluminosilicate framework. Examination of the patterns collected at 800 °C revealed the presence of two phases, sodium aluminium silicate (JCPDS 40-0101) and α-carnegieite (JCPDS 76-1733). After the second phase transition at 1000 °C aluminium oxide, silicon oxide, aluminium hydrate, sodium silicate oxide and a nepheline like structure (JCPDS 09-0338) are evident in the patterns. These results are consistent with those reported by Hackbarth *et al*[4]. It can be seen from the PXD patterns recorded at 25 °C after cooling, that the phase transitions are irreversible.

Examination of the lattice parameters calculated for the two phases at each temperature further supports the evidence that there is no difference between the two. The *a* and *c* parameters along with unit cell volume increase with increasing temperature, Figure 5.7. The three parameters all follow the same trend, that there is an initial increase, a slight decrease and then a gradual increase before a sharp increase at 700 °C. The slight decrease is associated with loss of water and the large increase at 700 °C is a result of expansion of the framework before its destruction. The variations of the percentage change of unit cell parameters between the two are again almost identical. These results agree with those reported by Hassan[5], although the natural cancrinite studied in his investigations appears to show thermal stability to a higher temperature (1200 °C).

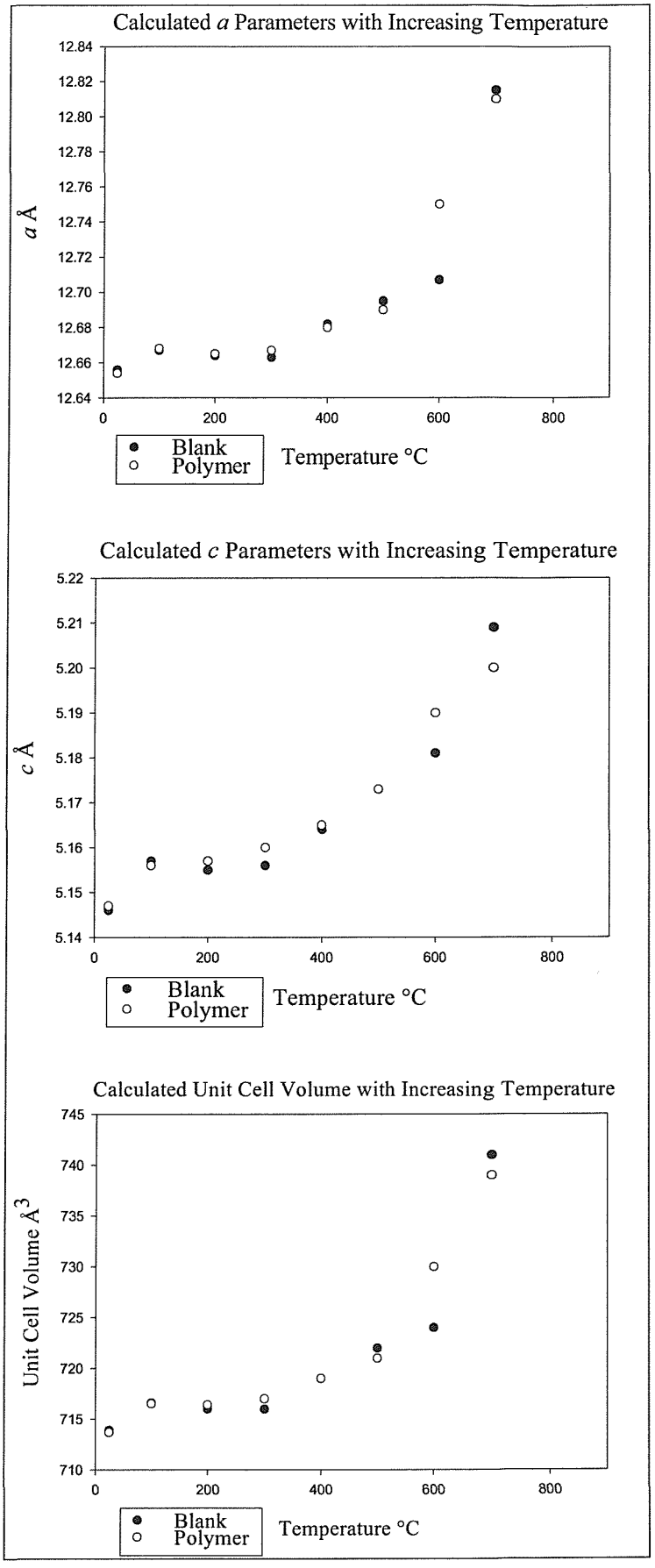

Figure 5.7 Effect of temperature on calculated lattice parameters.

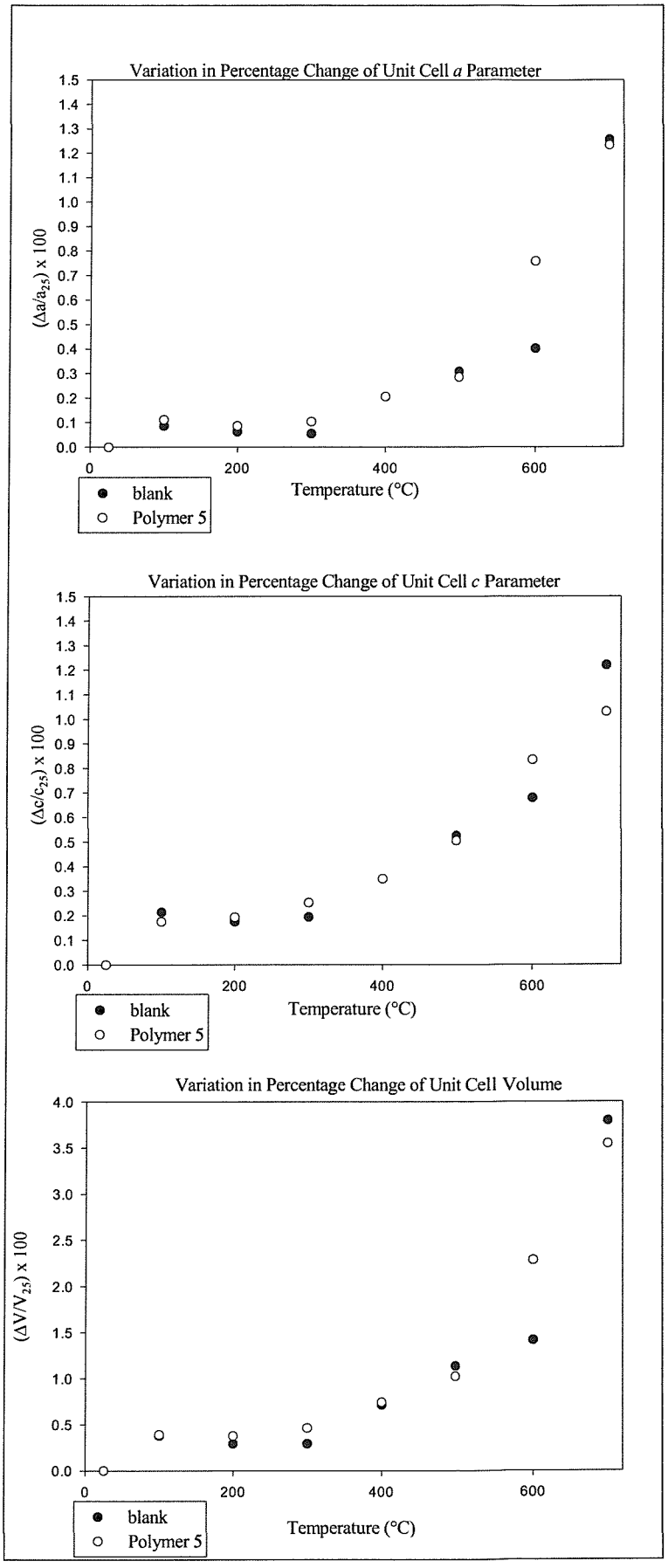

Figure 5.8 The variation of percentage change in unit call parameters with temperature.

5.4.2.2 Electron Microscopy Results

Products from the syntheses, under the various conditions were examined using SEM.

SEM Micrographs

SEM micrographs confirm that the spheres are composed of cancrinite or sodalite (for the experiments performed without sodium carbonate). Regular shaped cancrinite rods 2 - 4 μ are seen to adhere together giving the spheres their rigidity and structure, Figure 5.9. Where sodalite spheres have been formed, sodalite crystals, ≈ 2 μ in diameter, adhere together giving the spheres their structure and rigidity, Figure 5.10.

Examination of the powders yielded in these investigations using SEM revealed that no change in microcrystalline morphology had occurred. The presence of the phases identified using PXD were confirmed by the presence of either regular shaped rods – cancrinite, or irregular shaped plate-like crystallites – Intermediate, in some instances a mixture of the two was observed.

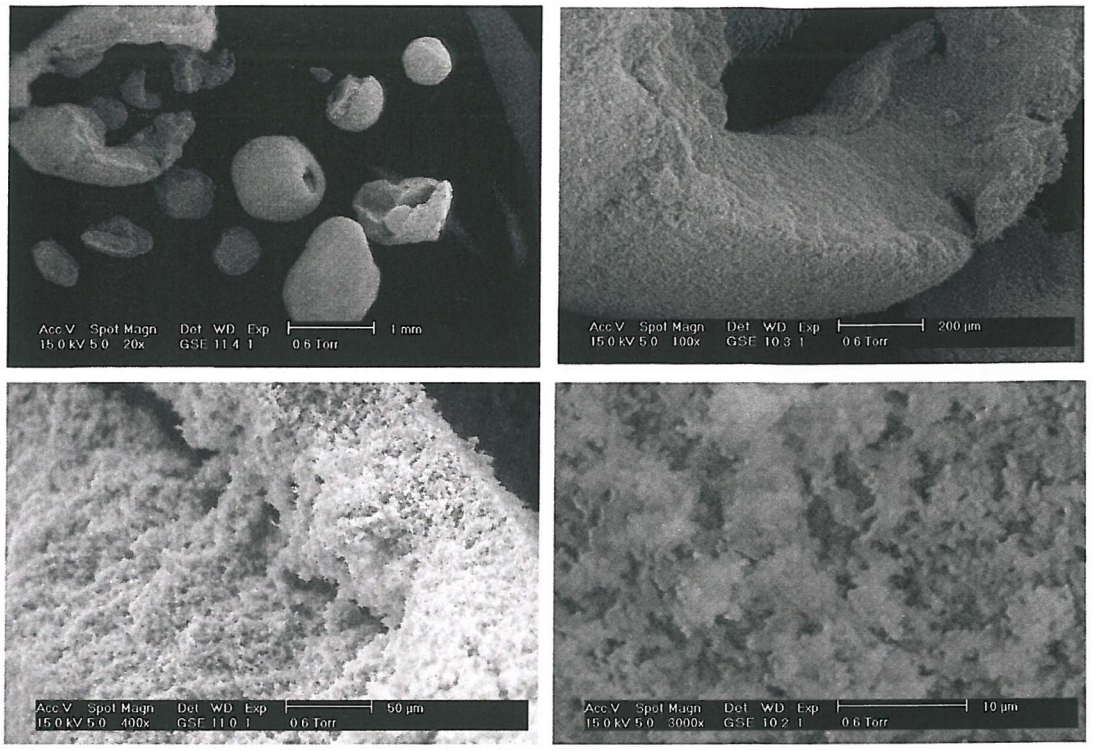

Figure 5.9 SEM micrographs of cancrinite spheres at increasing magnifications.

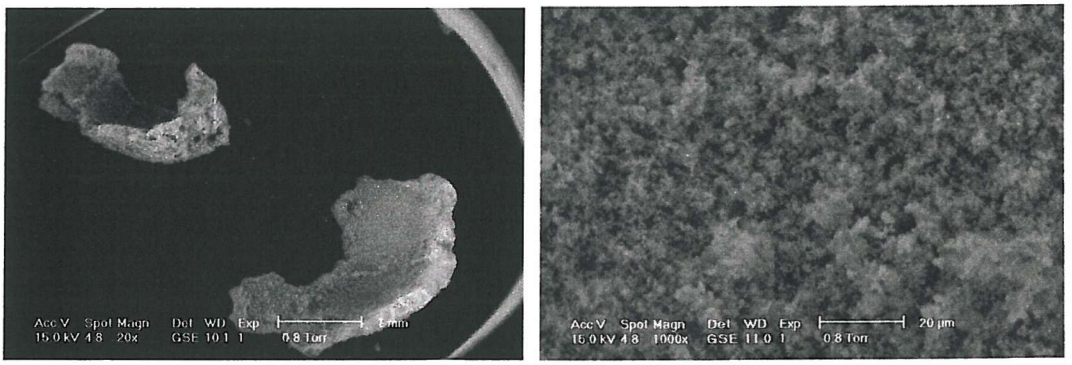

Figure 5.10 SEM micrographs of fragments of sodalite spheres at increasing magnifications.

EDX Analysis

EDX analysis revealed that no sulphur had been incorporated into the structures. In instances where potassium salts had been added, potassium levels were also investigated; none were detected using EDX analysis.

5.4.2.3 FTIR Results

Products from the syntheses, under the various conditions were examined using FTIR. Characteristic cancrinite and Intermediate absorptions confirmed the presence of these phases. Presented below in Figure 5.11 are the FTIR scans measured on the products formed upon the addition of each polymer during the 220 °C, 48 h, 8 M reactions. The scans were not measured quantitatively and so a comparison of intensities cannot be made, however the bands present in each scan are identical and are indicative of carbonate cancrinite.

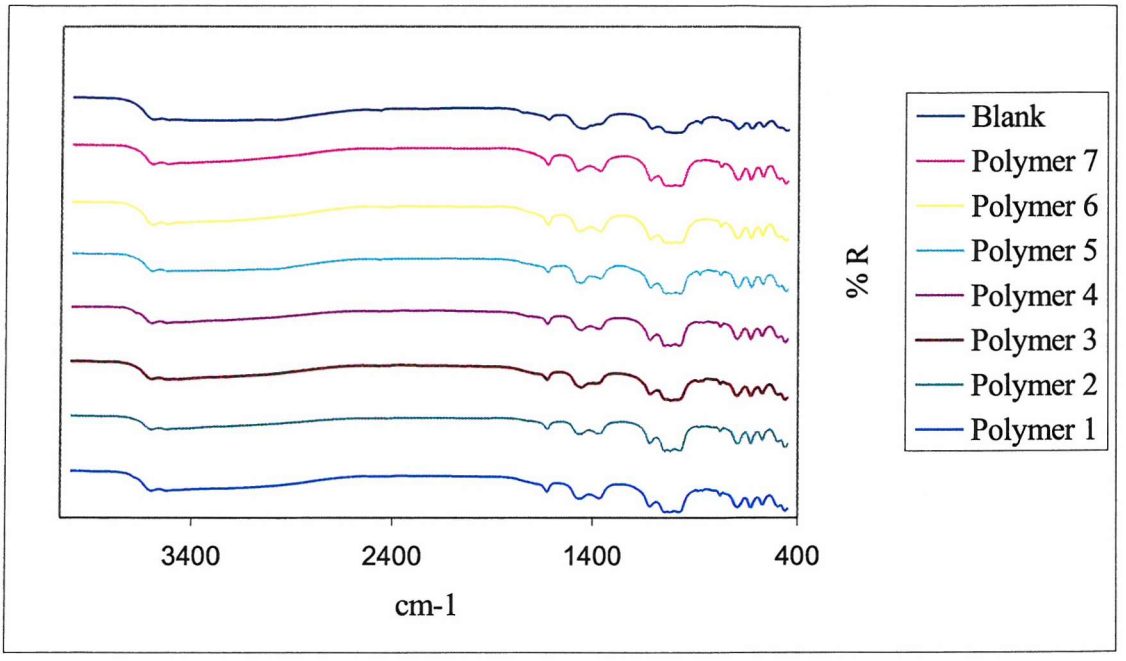

Figure 5.11 IR spectra recorded on the products formed upon the addition of polymeric additives.

5.4.3 Discussion

The formation of cancrinite spheres is seen to occur upon addition of each of the seven different polymeric additives employed in this investigation, though the degree of sphere formation is somewhat inconsistent and difficult to predict. Sphere formation is however clearly dependent upon temperature, reaction time and sodium hydroxide concentration. For optimum sphere growth, a temperature of 220 °C is required along with a reaction time of 48 h and sodium hydroxide concentration of 8 M. In the absence of sodium carbonate, the spheres observed are constructed from sodalite.

In an attempt to understand sphere formation, two mechanisms have been considered. The first is micelle formation; a schematic two-dimensional representation of an ionic spherical micelle is presented below in Figure 5.12. The polymer is orientated in such a way that the hydrophobic part forms the core of the micelle while the polar head groups (sulphate/sulphonate groups) are located at the micelle-water interface.

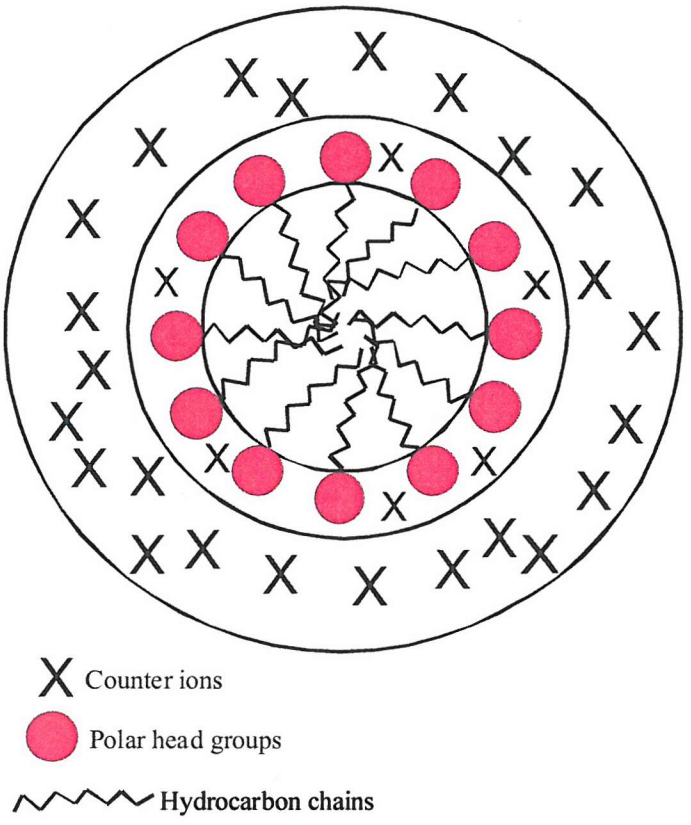

Figure 5.12 A two-dimensional schematic representation of the components of a spherical ionic micelle.

The polar heads or templating groups located at the micelle-water interface may be providing a nucleation site for growth. In theory this approach appears viable however a typical diameter of an ionic micelle ranges between 12 and 30 Å[6], thus the micelle would only support the formation of spheres of a similar size. The spheres observed in this investigation range from 5 x 10^6 to 4 x 10^7 Å in diameter and so are much too large to have been formed by a micelle effect.

The second mechanism, which is perhaps more likely, is that the organic additive decomposes to produce organic droplets that act as sites for nucleation and growth. The formation of balls could be attributed to growth around a droplet, as too could bead formation. Should the droplet adhere to the side of the container whilst the cancrinite grows around it, a hole would be produced, hence bead formation. The organic droplet may be orientated such that the templating groups are providing nucleation sites for cancrinite growth, however unlike the micelle effect, larger bubble sizes could be anticipated.

The factors that effect sphere formation, temperature, reaction time and sodium hydroxide concentration would suggest that the formation proceeds via a side product of the polymer. The high temperature suggests a decomposition product is necessary and high sodium hydroxide concentration suggests that an organic side product is required, the formation of which requires highly basic conditions. The long reaction time required may be a result of either of the other two factors taking action, though it is more likely to due to the length of time for substantial nucleation to occur.

The elements described above that affect sphere formation also affect the nature of the cancrinite product that is yielded. Reactions carried out at 220 °C, for 48 h employing an 8 M sodium hydroxide solution would result in the formation of a very pure crystalline product. It is possible that such a product is needed in order for the crystals to adhere together and give the spheres their rigid structures. Thus under conditions where the product is less pure and contains some Intermediate, which as can be seen from SEM micrographs is composed of large plate-like crystallites, such adhesion is less likely to be achieved.

5.5 Conclusions

Investigations using organic sulphate/sulphonate additives as potential scale modifiers/reducers resulted in only the formation of the regular powdered aluminosilicate phases. That is at 100 °C Intermediate formation is observed and at 220 °C, cancrinite is the phase yielded.

The formation of cancrinite spheres is seen to occur upon addition of each of the seven different polymeric additives employed in this investigation. It has been shown that although the degree of sphere formation is somewhat inconsistent and difficult to predict it is clearly dependent upon temperature, reaction time and sodium hydroxide concentration. For optimum sphere growth, a temperature of 220 °C is required along with a reaction time of 48 h and sodium hydroxide concentration of 8 M. In the absence of sodium carbonate, the spheres observed are constructed from sodalite.

Two mechanisms for sphere formation have been proposed; the formation of the aluminosilicate phase on either the surface of a micelle or an organic droplet. A micelle would typically support the formation of spheres, however those observed in this investigation are probably too large to be the result of a micelle effect and so the second mechanism has to be considered the more likely. Should the organic additive decompose to produce organic droplets, these could then act as sites for nucleation and growth. The formation of balls could be attributed to growth around a droplet, as too could bead formation. Should the droplet adhere to the side of the container whilst the cancrinite grows around it, a hole would be produced, hence bead formation. The organic droplet may be orientated such that the templating groups are providing nucleation sites for cancrinite growth, however unlike the micelle effect, larger droplet sizes could be anticipated.

As a result of these synthetic investigations it was proposed that cancrinite spheres would be a more favourable scale product than the closely packed cancrinite crystallites that currently adhere to the ball of the heat exchangers. Should spheres form under Bayer plant conditions they may not stick to the heat exchanger walls and thus not lower their efficiency and, with the addition of a sieve to the system, the spheres could be captured and removed. Alternatively the spheres could be used to act as a fluidised

bed; should a form of holding tank be added at some point in the system before the heat exchangers, spheres could be synthesised and held there in order to act as nucleation sites for other silicate scale contaminants. However it is unlikely that sphere formation would occur in a Bayer plant as the reaction conditions required would be impossible to achieve (e.g. reaction time of 48 h), unless a holding/reaction tank could be incorporated. Sphere formation may also be affected by the flowed nature of the Bayer plant; it may prevent formation or the agitation may break up the spheres should they form. Investigation into sphere formation under more representative Bayer conditions is reported in Chapter 7.

5.6 References

1 Cytec Technology Group, International Patent Application, International Application No. PCT/US97/06914, (1997).

2 Cytec Technology Group, International Patent Application, International Application No. PCT/US97/06886, (1997).

3 J. Addai-Mensah, A.R. Gerson, R. Jones, M. Zbik, *Light Metals,* 13, (2001).

4 J. Buhl, M. Fechtelkord, Th.M. Gesing, K. Hackbarth, *Microporous and Mesoporous Materials,* **30**, 347, (1999).

5 I. Hassan, *Mineralogical Magazine*, **60**, 949, (1996).

6 J.H. Fendler, E.J. Fendler, Catalysis in Micellar and Macromolecular Systems, Academic Press, London, (1975).

Chapter 6

Potassium Hydroxide

6.1 Introduction

Barrer *et al*[1,2,3] have performed in depth studies into the effect of reacting different alkali-metal hydroxides with kaolinite in order to synthesise alkali-metal aluminosilicates. The formation of sodalite and cancrinite, the scale products formed in the Bayer process are only observed when the alkali-metal hydroxide, sodium hydroxide, is used. Reactions of kaolinite with caesium, rubidium, potassium and lithium all result in the formation of alternative alkali-metal aluminosilicates. Table 6.1 presents some of the phases observed when potassium hydroxide alone was used.

Table 6.1 Phases formed as a result of hydrothermal synthesis using potassium hydroxide.

Ref. letter	Mineral/Class	Ref. letter	Mineral/Class
K-A	Sanidine	K-G	K-Zeolite (φ-chabazite)
K-B	α-Quartz	K-H	Bayerite
K-C	Leucite	K-I	Boehmite
K-D	Kaliophilite	K-M	K-Zeolite (φ-phillipsite)
K-E	K-Analcite	K-N	Kalsilite
K-F	K-Zeolite		

Since cancrinite and sodalite are only observed when sodium hydroxide is used in the reactions reported by Barrer it is possible that the replacement of sodium hydroxide with an alternative alkali-metal hydroxide in Bayer liquor may inhibit the precipitation of these phases on the surfaces of the heat exchangers. More recent studies by Colella et al[4,5] report cancrinite formation upon addition of lithium, caesium and rubidium thus replacement of sodium hydroxide with the hydroxide of one of these alkali-earth metals may still result in cancrinite formation. Thus with the exception of francium, potassium is the only alkali-earth metal for which cancrinite formation has not been observed.

Studies into the formation of potassium aluminosilicates with respect to alumina production were reported by Aveeda and Novolodskaya[6]. These investigations were however, concerned with the desilication of sodium and potassium aluminate solutions similar in composition to the industrial aluminate liquors obtained in the production of

alumina from nepheline by the sintering method and not by the Bayer process. The potassium hydroaluminosilicate observed is described as being K-zeolite and it is reported that under the same conditions it crystallises more slowly than sodium hydroaluminosilicate.

The bauxite used in China consists mainly of diaspore, which requires high temperatures for digestion (> 230 °C). At these temperatures, illite ($(K,H_3O)(Al,Mg,Fe)_2(Si,Al)_4O_{10}[(OH)_2,H_2O]$), the main potassium mineral present in the ore can also be reacted completely and so potassium hydroxide may accumulate in the aluminate solution. This observation instigated research by Guihua *et al*[7] into the formation and solubility of potassium aluminosilicate. An amorphous potassium aluminosilicate was synthesised from saturated aluminate solutions, its solubility was dependent upon temperature and sodium hydroxide concentration; solubility increasing with an increase in both parameters.

6.2 Aims

As sodalite and cancrinite do not form when kaolinite is reacted with potassium hydroxide, it is proposed that it may be used as an alternative to sodium hydroxide in the Bayer process. The aim of this investigation was monitor the effect of replacing different levels of sodium hydroxide with potassium hydroxide over a range of temperatures and concentrations. The observed phases were characterised and a comparison made with existing scale products.

6.3 Effect of Potassium Hydroxide Concentration and Reaction Temperature

6.3.1 Experimental

Syntheses were carried out under hydrothermal conditions at temperatures of 135, 150, 175 and 220 °C and autogenous pressure in Parr 23 ml Teflon-lined steel autoclaves under static conditions. Kaolin (0.2520 g) and sodium carbonate (0.3996 g) were used in all the experimental preparations. 4.7 M and 8 M solutions composed of sodium hydroxide and potassium hydroxide were prepared. In one series of experiments the 4.7 M solution (14 ml) was added to each autoclave, in the other series the 8 M solution (14 ml) was used. The exact ratios used to formulate the solutions are presented below in Table 6.2. The reactions were executed for 48 hrs. The resulting white powders were washed with 150 ml of distilled water and dried for 24 h at 80 °C.

Table 6.2 Ratios of sodium hydroxide to potassium hydroxide used; 4.7 M or 8 M.

NaOH (conc) %	100	90	80	70	60	50	40	30	20	10	0
KOH (conc) %	0	10	20	30	40	50	60	70	80	90	100

6.3.2 Results

The resulting white microcrystalline powders were characterised using PXD, SEM and FTIR.

6.3.2.1 PXD Results

Initial phase identification was achieved by the analysis of PXD data collected over the 2θ range 10 ° to 60 ° for 30 minutes. Table 6.3 below present the results of this analysis, detailing the reaction conditions and phase obtained. Over the series of experiments four phases were identified, cancrinite, the Intermediate, potassium aluminium silicate hydrate ($KAlSiO_4.1.5H_2O$, K-F) and potassium aluminium silicate ($KAlSiO_4$). Where more than one phase was identified in the product, the phase in bold is present in the higher quantity.

Lattice parameters were calculated and in instances where a mixture of cancrinite and Intermediate were observed the lattice parameters were calculated for both the ordered cancrinite unit cell and the Intermediate disordered unit cell. Table 6.3 is followed by a series of graphs showing the effect of potassium concentration on the unit cell volume (Figures 6.1-6.4). Where appropriate graphs for both cancrinite and the Intermediate have been plotted. A line of best fit has been calculated and included on each plot, this is only intended as a guide towards the observed trend and not as a means of predicting unit cell volume. Standard deviations are included on the plots and for the reactions performed at 135, 150 and 175 °C, these errors are smaller for the unit cell volumes calculated using the Intermediate disordered unit cell than the ordered cancrinite unit cell indicating the Intermediate is the more likely phase.

Table 6.3 Phase identification for experiments performed at 135, 150, 175 and 220 °C using 4.7 M and 8M solutions for 48 h.

	Phase Identification for the Products Formed for 48 h Reaction.							
	135 °		**150 °**		**175 °**		**220 °**	
NaOH/KOH %	**4.7 M**	**8 M**	**4.7 M**	**8 M**	**4.7 M**	**8 M**	**4.7 M**	**8 M**
100/0	I C	I C	I C	I C	I C	I C	C	C
90/10	I C	I C	I C	I C	I C	I C	C	C
80/20	I C	I C	I C	I C	I C	I C	C	C
70/30	I C	I C	I C	I C	I C	I C	C	C
60/40	I C	I C	I C	I C	I C	I C	C	C
50/50	I C	I C	I C	I C	I C	I C	C	C
40/60	I C	I C	I C	I C	I C	I C	K	K
30/70	I C	I C	I C	I C	I C	K	K	K
20/80	K-F I C	K	I C	K	K	K	K	K
10/90	K-F	K	K	K	K	K	K	K
0/100	K-F	K	K	K	K	K	K	K

I: - Intermediate, C: - Carbonate Cancrinite

K-F: - potassium aluminium silicate hydrate (JCPDS number 38-0216)

K: - potassium aluminium silicate (JCPDS number 76-0635)

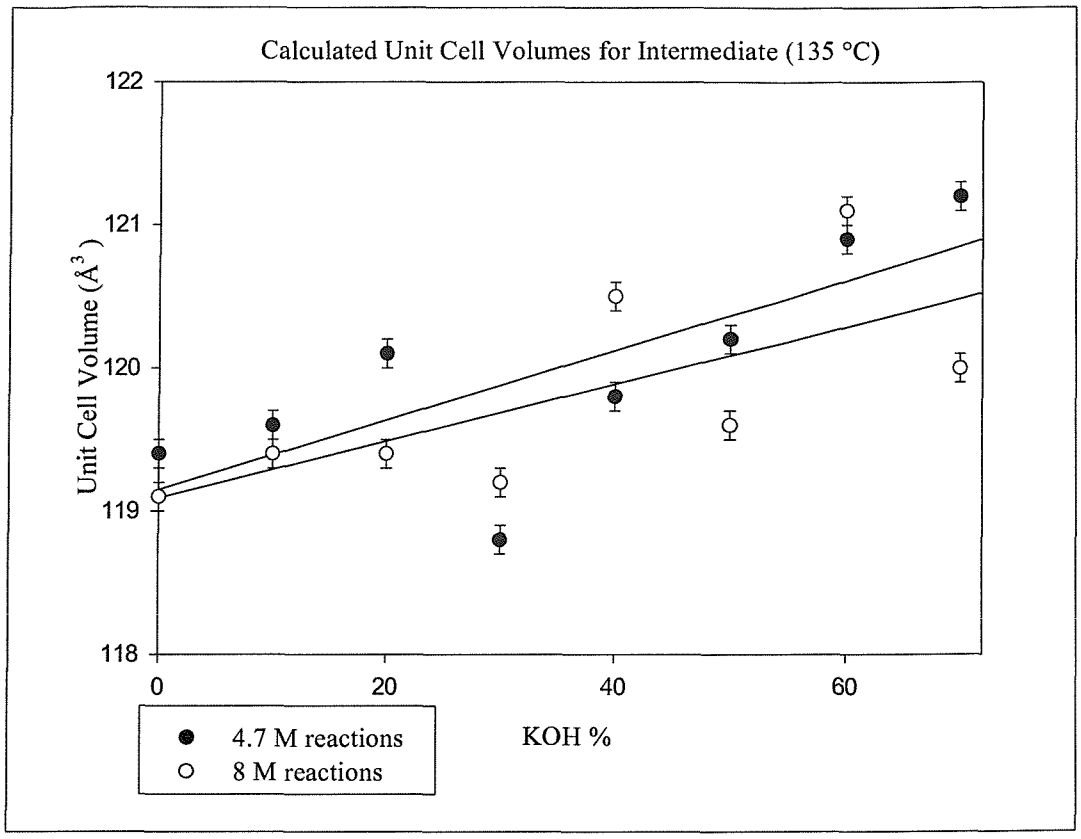

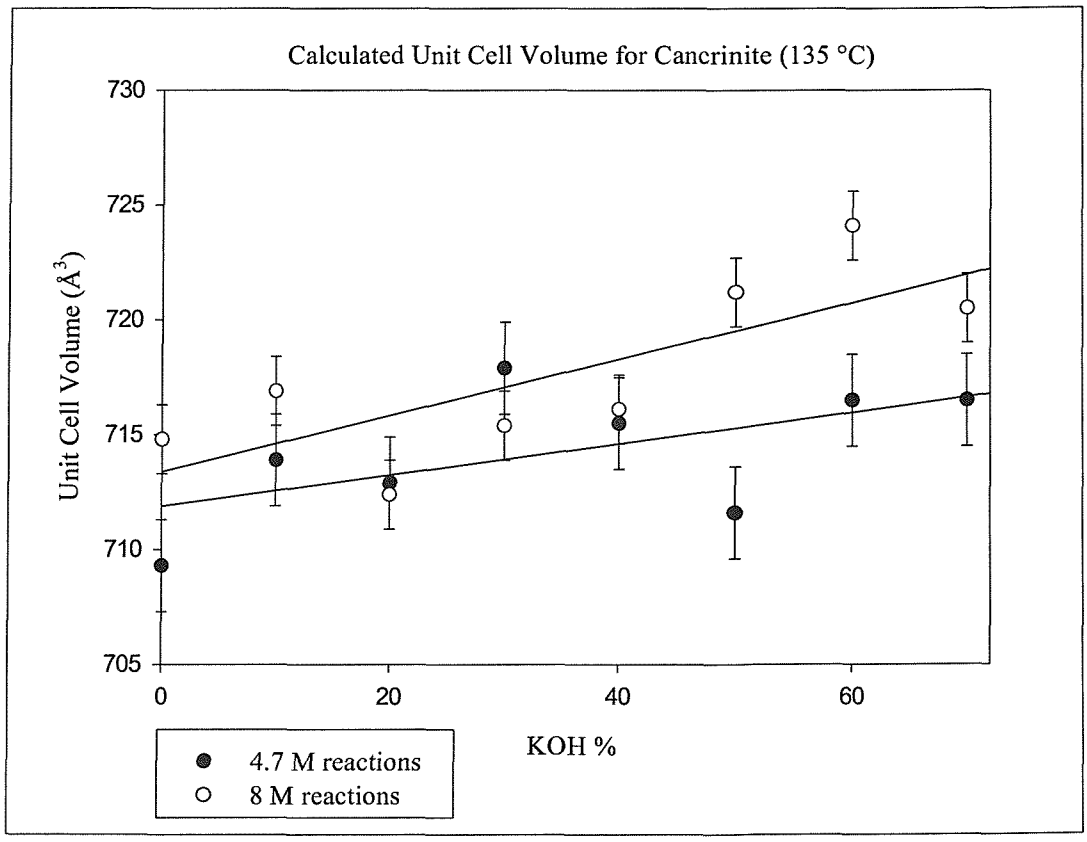

Figure 6. 1 The effect of increasing KOH concentration on unit cell volume (135 °C).

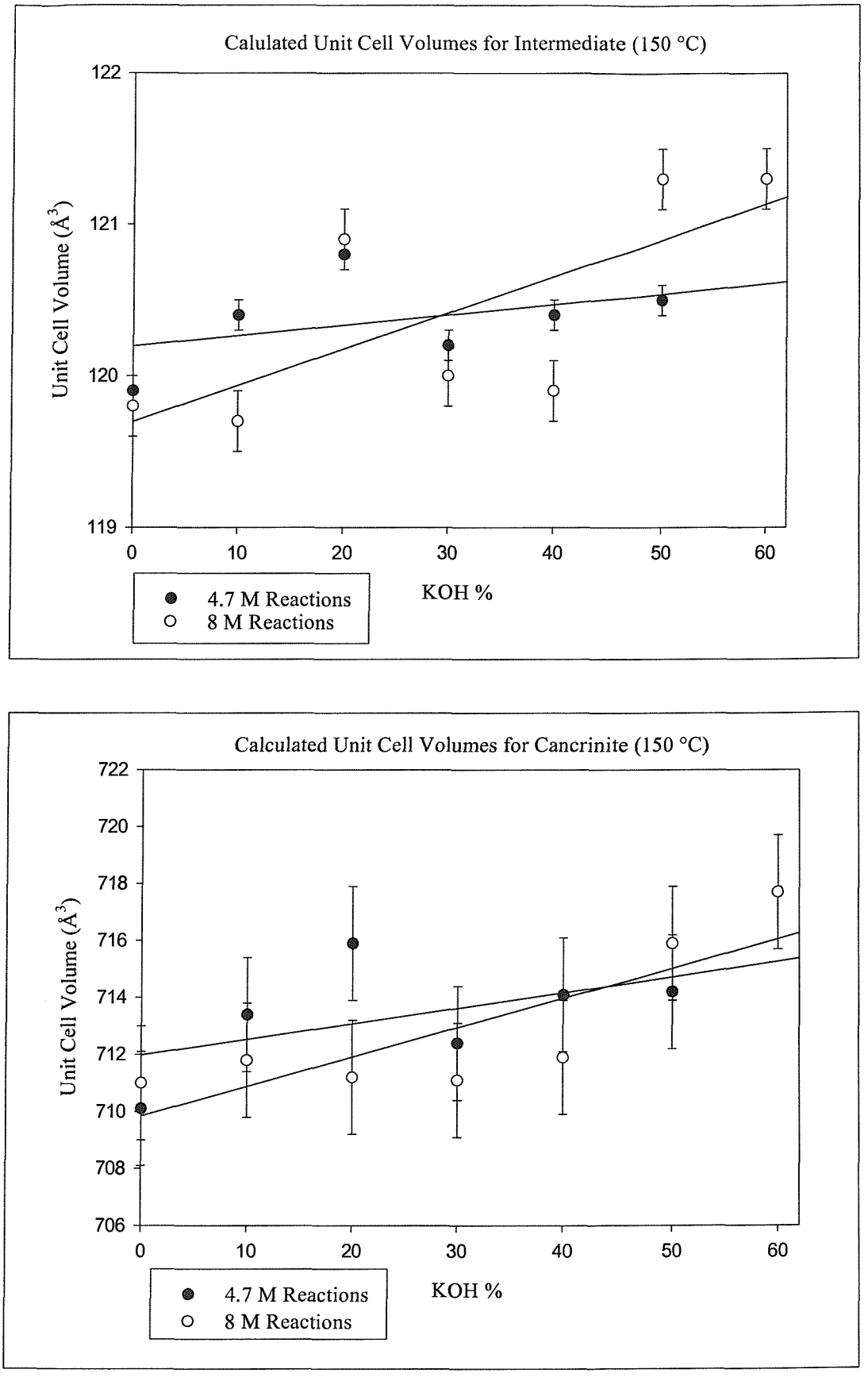

Figure 6.2 The effect of increasing KOH concentration on unit cell volume (150 °C).

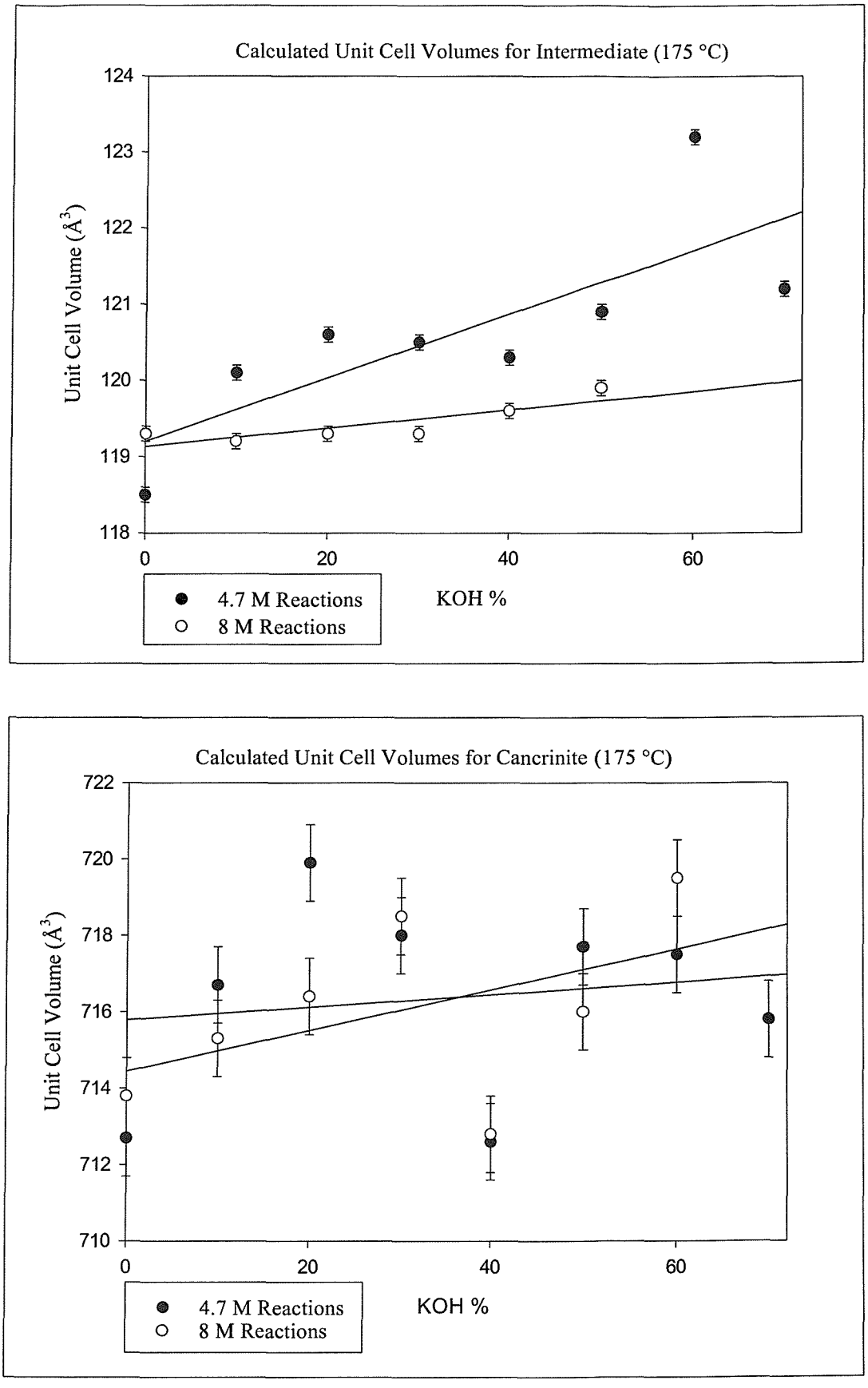

Figure 6.3 The effect of increasing KOH concentration on unit cell volume (175 °C).

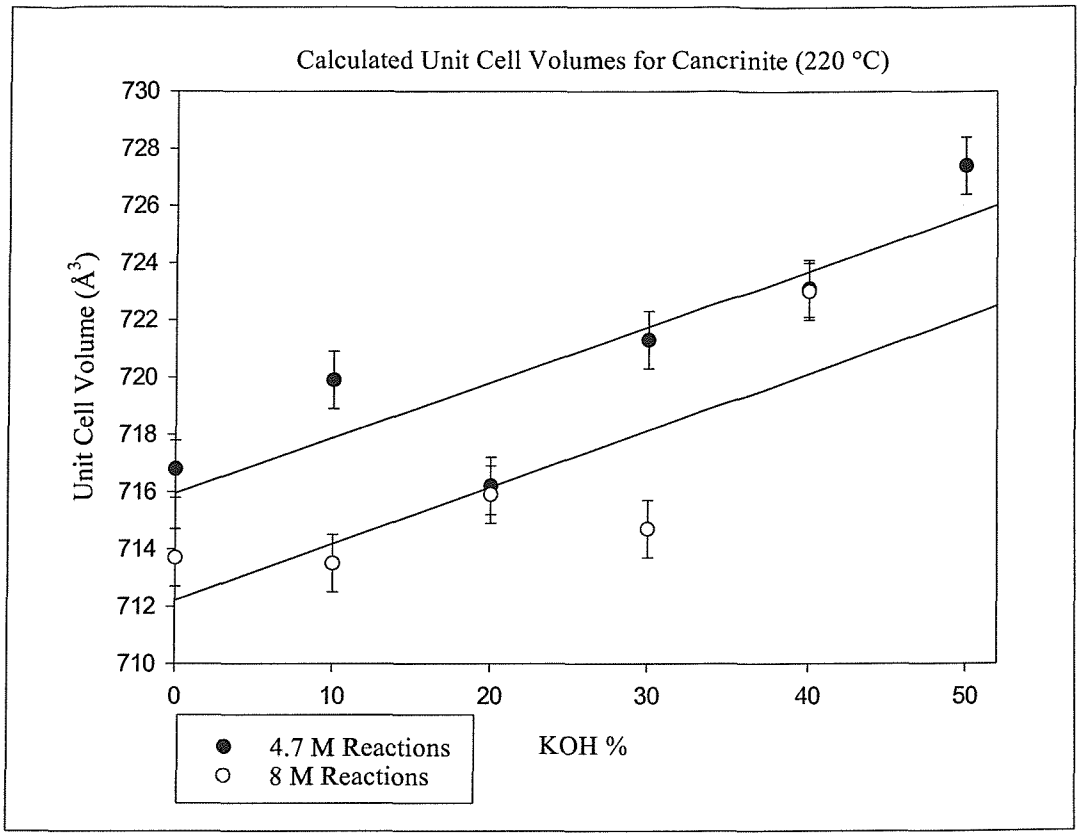

Figure 6.4 The effect of increasing KOH concentration on unit cell volume (220 °C).

The phases formed in these experiments are broadly in line with literature reported for systems containing no potassium[8]. That is at 135 and 150°C the main phase observed is Intermediate while at the higher temperatures, 175 and 220°C, the ordered cancrinite structure is the product formed.

Determination of the lattice parameters and unit cell volumes of the cancrinite/Intermediate phases formed at all temperatures was carried out. The unit cell volumes are summarised in Figures 6.1 - 6.4. As potassium levels in the reaction medium increase, so too does unit cell volume. Replacement of sodium by potassium in other zeolite structures shows similar results, e.g. for Zeolite A sodium form, cell volume = 1851.80 $Å^3$ and potassium form, cell volume = 1864.96 $Å^3$ [9]. This increase in unit cell volume is to be expected as potassium has a larger ionic radius (1.38 Å) than sodium (1.02 Å). Hence replacement of some sodium with potassium in the reaction mixture leads to its incorporation into the cancrinite structure though from the analysis of the powder X-ray data collected the exact composition is impossible to define. In the case of cancrinite it is likely to lie between $Na_{7.5}K_{0.5}[AlSiO_4]_6.(CO_3)_1.nH_2O$ and

$Na_6K_2[AlSiO_4]_6.(CO_3)_{1.5}.nH_2O$. This is supported by the chemical analysis carried out using EDX in the SEM, detailed in section 6.3.2.2.

The formation of K-F zeolite/potassium aluminium silicate hydrate ($KAlSiO_4.1.5H_2O$) is observed at high potassium concentrations at 135 °C using 4.7 M solutions. The formation of this phase under these conditions is consistent with results obtained by Barrer *et al*[1,3], who crystallised this material at temperatures up to and including 160 °C. At temperature of 150 °C and above Barrer *et al* only report the formation of K-F for KOH concentrations below 2 M. In the same studies by Barrer this phase was seen to form at higher KOH concentrations, but only at temperatures below 120 °C which is again consistent with the findings of this investigation, i.e. this phase is not observed for reactions performed at 135 °C using 8 M solutions. The lattice parameters for this phase were calculated using the tetragonal system described by Kosorukov and Nadel[10].

At all other temperatures investigated, the formation of potassium aluminium silicate ($KAlSiO_4$) occurs at high potassium levels. The extent to which $KAlSiO_4$ forms is dependent upon the concentration of KOH in the system and temperature. When the reaction is carried out at 220 °C the $KAlSiO_4$ phase forms at lower KOH levels than at 150 °C. The sharp change over between cancrinite/Intermediate to the $KAlSiO_4$ phase is somewhat unusual suggesting that in the presence of sodium, the formation of $KAlSiO_4$ proceeds via the dissolution of the cancrinite/Intermediate phase.

The $KAlSiO_4$ structure consists of alternating chains of $[SiO_4]^{4-}$ and $[AlO_4]^{5-}$ tetrahedra. Between each layer of chains are charge balancing K ions. The structure is presented overleaf in Figure 6.5.[11]

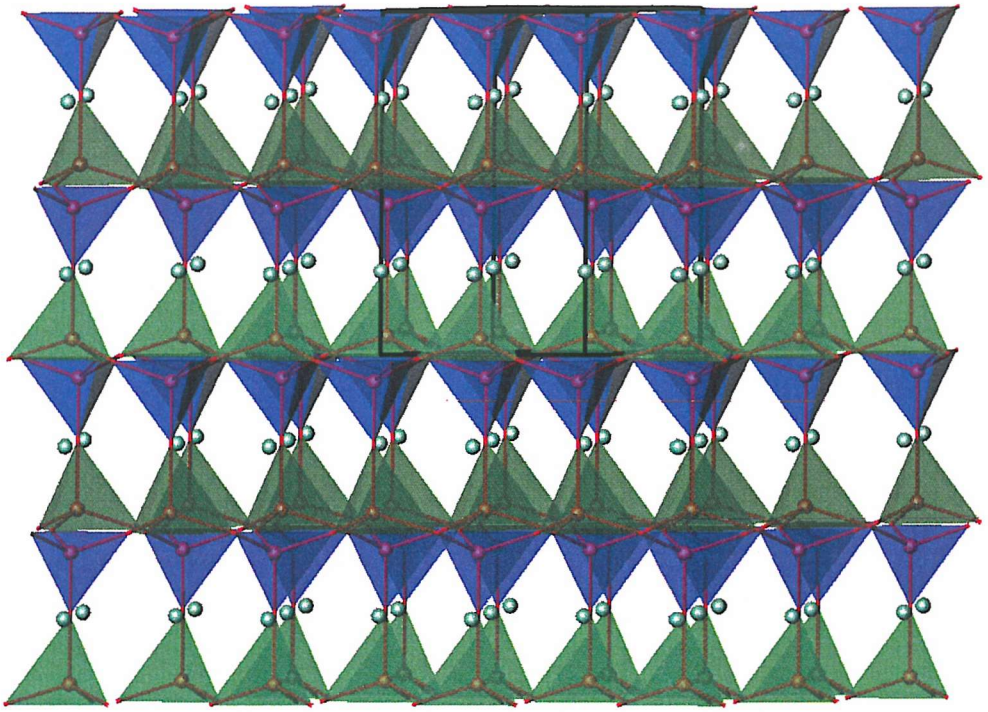

Figure 6.5 The $KAlSiO_4$ structure. Blue polyhera represent the $[SiO_4]^{4-}$ tetrahedra, green polyhedra the $[AlO_4]^{5-}$ tetrahedra and light blue spheres the charge balancing K^+ ions.

6.3.2.2 Electron Microscopy Results

SEM micrographs were recorded for selected samples in order to investigate crystal morphology. The presence of potassium and general composition of a range of samples was investigated using EDX analysis.

SEM Micrographs

SEM micrographs reveal that the two potassium phases formed have distinctly different morphologies from the cancrinite and the Intermediate phases. The low temperature phase $KAlSiO_4.1.5H_2O$ consists of amorphous agglomerates, Figure 6.6. The phase observed at all other temperatures at high potassium concentration, $KAlSiO_4$, forms regular shaped hexagons, 20 – 60 μ in diameter with a thickness of ~ 5 μ, Figure 6.7.

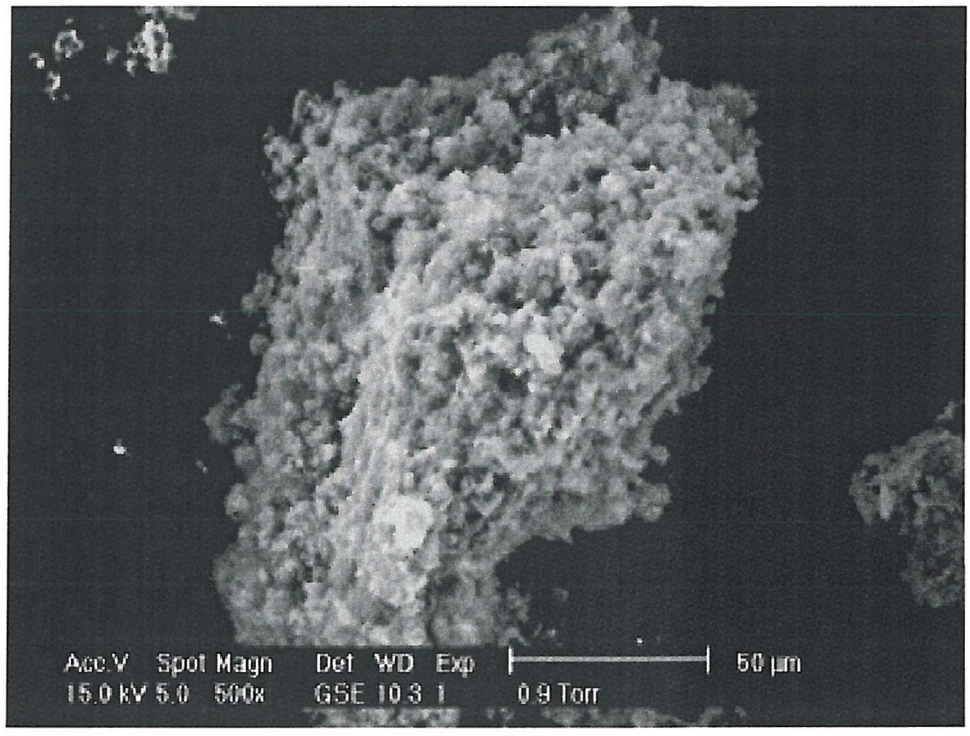

Figure 6.6 SEM micrograph of $KAlSiO_4.1.5H_2O$.

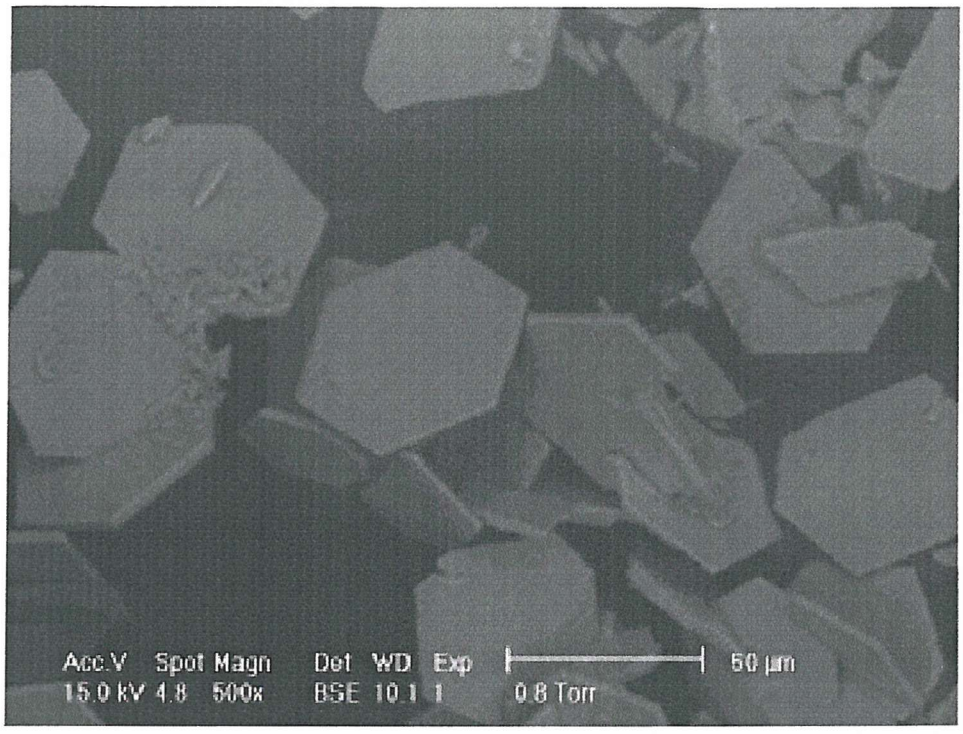

Figure 6.7 SEM micrograph of $KAlSiO_4$.

EDX Analysis

Analysis of the composition of the materials formed at the four temperatures was undertaken using EDX analysis and is presented overleaf in Tables 6.4 and 6.5. For each temperature and concentration measurements have been performed on products yielded from low, medium and high potassium to sodium ratios.

At 135, 150, 175 and 220 °C the low K:Na cancrinite /Intermediate products are seen to contain very little potassium, giving compounds with stoichiometries near $Na_{7.5}K_{0.5}[AlSiO_4]_6(CO_3).nH_2O$. Where the K:Na is ≈1 the level of potassium incorporated into the cancrinite/Intermediate products increases, giving compounds with stoichiometries near $Na_{6.8}K_{1.2}[AlSiO_4]_6(CO_3).nH_2O$. These levels of potassium incorporation are consistent with those reported by Wiggen[12] for potassium ion exchange reactions with pure sodium carbonate cancrinite.

Table 6.4 Sodium to potassium ratios in $KAlSiO_4.1.5H_2O$, $KAlSiO_4$ and cancrinite or the Intermediate phase determined by EDX, 4.7 M solutions.

Temperature, Solution Concentration, (% NaOH/KOH), Product	**Na:K Atomic percentage ratio determined composition of aluminosilicate phase.**
135 °C, 4.7 M, (90/10), C/I	0.07, $Na_{7.4}K_{0.6}[AlSiO_4]_6(CO_3).nH_2O$
135 °C, 4.7 M, (60/40), C/I	0.22, $Na_{6.3}K_{1.7}[AlSiO_4]_6(CO_3).nH_2O$
150 °C, 4.7 (90/10), C/I	0.07, $Na_{7.6}K_{0.4}[AlSiO_4]_6(CO_3).nH_2O$
150 °C, 4.7 M, (30/70), C/I	0.25, $Na_6K_2[AlSiO_4]_6(CO_3).nH_2O$
175 °C, 4.7 M, (90/10), C/I	0.08, $Na_{7.4}K_{0.6}[AlSiO_4]_6(CO_3).nH_2O$
175 °C, 4.7 M, (30/70), C/I	0.24, $Na_{6.1}K_{1.9}[AlSiO_4]_6(CO_3).nH_2O$
220 °C, 4.7 M, (90/10), C,	0.03, $Na_{7.8}K_{0.2}[AlSiO_4]_6(CO_3).nH_2O$
220 °C, 4.7 M, (60/40), C/I	0.25, $Na_6K_2[AlSiO_4]_6(CO_3).nH_2O$

C: - carbonate cancrinite

I: - Intermediate

Table 6.5 Sodium to potassium ratios in $KAlSiO_4.1.5H_2O$, $KAlSiO_4$ and cancrinite or the Intermediate phase determined by EDX, 8 M solutions.

Temperature, Solution Concentration, (% NaOH/KOH), Product	**Na:K Atomic percentage ratio determined composition of aluminosilicate phase**
135 °C, 8 M, (90/10), C/I	0.04, $Na_{7.7}K_{0.3}[AlSiO_4]_6(CO_3).nH_2O$
135 °C, 8 M, (30/70), C/I	0.24, $Na_{6.1}K_{1.9}[AlSiO_4]_6(CO_3).nH_2O$
150 °C, 8 M, (90/10), C/I	0.06, $Na_{7.5}K_{0.5}[AlSiO_4]_6(CO_3).nH_2O$
150 °C, 8 M, (60/40), C/I	0.21, $Na_{6.3}K_{1.7}[AlSiO_4]_6(CO_3).nH_2O$
175 °C, 8 M, (90/10), C/I	0.04, $Na_{7.7}K_{0.3}[AlSiO_4]_6(CO_3).nH_2O$
175 °C, 8 M, (60/40), C/I	0.15, $Na_{6.8}K_{1.2}[AlSiO_4]_6(CO_3).nH_2O$
220 °C, 8 M, (90/10), C	0.03, $Na_{7.8}K_{0.2}[AlSiO_4]_6(CO_3).nH_2O$
220 °C, 8 M, (60/40), C	0.15, $Na_{6.8}K_{1.2}[AlSiO_4]_6(CO_3).nH_2O$

C: - carbonate cancrinite

I: - Intermediate

6.3.2.3 FTIR Results

Products from the syntheses, under the various conditions were examined using FTIR. Characteristic cancrinite and Intermediate absorptions confirmed the presence of these phases.

The absorptions observed for $KAlSiO_4.1.5H_2O$ and $KAlSiO_4$ are shown below in Table 6.6. Absorptions at 3370 and 1650 cm^{-1} are present in both phases though are much stronger in $KAlSiO_4.1.5H_2O$; these peaks are indicative of water. The presence of these bands in the $KAlSiO_4$ sample is assigned to moisture present in either the sample or the KBr used to run the experiments.

Table 6.6 Observed FTIR absorptions for $KAlSiO_4.1.5H_2O$ and $KAlSiO_4$.

Assignment of Absorption	IR Absorption for Phase (cm^{-1})	
	$KAlSiO_4$	$KAlSiO_4.1.5H_2O$
T-O stretch (asymmetric) ←OT→←O	1105 1003	995
T-O stretch (symmetric) ←OTO→	690 605	830 738 669 618
T-O (bending)	477 432	477 432

6.3.3 Discussion

Replacement of some or all of the NaOH with KOH in the reaction mixture results in a change of product from that that would usually be observed under normal conditions. When the syntheses are carried out using a high or 100 % level of KOH the formation of alternative phases is seen. At 135 °C employing a high level of 4.7M KOH solution, the $KAlSiO_4.1.5H_2O$ phase is yielded. At all other temperatures high KOH levels, $KAlSiO_4$ is obtained; the extent to which this phase forms is dependent upon both KOH concentration and temperature. At high temperatures $KAlSiO_4$ forms at lower KOH levels.

At lower potassium levels where cancrinite or Intermediate are the products yielded an increase in unit cell volume is observed, this indicates that there is a degree of potassium incorporation in the structure. Through analysis of the PXD data collected the exact level of incorporation is impossible to define, though EDX analysis shows that the potassium levels are likely to lie between 0.2 and 2. The level of potassium incorporation is never seen to exceed 2 even when the amount of KOH in the reaction mixture is much greater than the amount of NaOH employed. This indicates that there is a limit to the degree of potassium incorporation. The method of potassium incorporation and the site occupied by potassium may be the limiting factors; this is discussed further in section 6.4.3.

6.4 Effect of Reaction Time

The change over of product formation from cancrinite/Intermediate to $KAlSiO_4$ is very sharp, for example at 220 °C using 8 M solutions, for a NaOH/KOH % of 60/40 the resulting material is cancrinite whereas for 50/50 it is $KAlSiO_4$. In an attempt to develop the understanding of these systems, reaction time was investigated. The systems studied were 220 °C, 8M solutions NaOH/KOH % 40/60 (**system 1**) and 220 °C, 8M solutions NaOH/KOH % 0/100 (**system 2**). Both systems yielded $KAlSiO_4$ as a single phase in section 6.3, however the formulation for **system 1** contains NaOH but for **system 2** it consists purely of KOH. Both systems were chosen to ascertain if the formation of KAlSiO4 proceeds directly or by the dissolution of an another phase. If formation does proceed via the dissolution of another phase, an alternative phase may be seen for **system 2** where in the absence of sodium, cancrinite cannot form.

6.4.1 Experimental

Syntheses were carried out under hydrothermal conditions at 220 °C and autogenous pressure in Parr 23 ml Teflon-lined steel autoclaves under static conditions. Kaolin (0.2520 g) and sodium carbonate (0.3996 g) were used in all the experimental preparations. An 8 M solution composed of sodium hydroxide (40 %) and potassium hydroxide (60 %) was prepared and 14 ml added to each autoclave for **system 1**. An 8 M solution of 100 % potassium hydroxide was prepared and 14 ml added to each autoclave for **system 2**. The reactions were executed for 1, 2, 3, 4, 5, 6, 24 and 48 hrs. The resulting white powders were washed with 150 ml of distilled water and dried for 24 h at 80 °C.

6.4.2 Results

The resulting white microcrystalline powders were characterised using PXD.

6.4.2.1 PXD Results

Initial phase identification was achieved by the analysis of PXD data collected over the 2θ range 10 ° to 60 ° for 30 minutes. Table 6.7 and 6.8 overleaf present the results of this analysis, detailing the reaction conditions, phase obtained and the calculated lattice parameters.

Table 6.7 The effect of reaction time on the formation of $KAlSiO_4$ (**system 1**).

Experiments Performed at 220 °C, 40 % NaOH & 60 % KOH (8 M)		
Reaction Time	**Phase(s) Present**	**Lattice Parameters (Å)**
1 h	cancrinite	insufficient peaks for refinement
2 h	cancrinite	12.815(7) 5.230(5)
3 h	cancrinite	12.81(2) 5.23(1)
4 h	cancrinite	12.81(1) 5.24(1)
5 h	cancrinite	12.81(1) 5.23(1)
6 h	cancrinite	12.85(2) 5.23(1)
24 h	**potassium aluminium silicate** & cancrinite	5.20(1) 8.74(1)
48 h	potassium aluminium silicate	5.19(1) 8.73(1)

Table 6.8 The effect of reaction time on the formation of $KAlSiO_4$ (**system 2**).

Experiments Performed at 220 °C, 100 % KOH (8 M)		
Reaction Time	**Phase(s) Present**	**Lattice Parameters (Å)**
1 h	potassium aluminium silicate	5.16(4) 8.60(2)
2 h	potassium aluminium silicate	5.17 (5) 8.57(6)
3 h	potassium aluminium silicate	5.16(4) 8.59(2)
4 h	potassium aluminium silicate	5.16(3) 8.59(5)
5 h	potassium aluminium silicate	5.17(4) 8.56(2)
6 h	potassium aluminium silicate	5.17(4) 8.57(2)
24 h	potassium aluminium silicate	5.170(2) 8.721(3)
48 h	potassium aluminium silicate	5.165(1) 8.709(1)

In the presence of NaOH, cancrinite is formed at short reaction times (1-6 h), after 24 h $KAlSiO_4$ is also observed. In a pure KOH synthesis, at all reaction times $KAlSiO_4$ is the only phase yielded.

The lattice parameters refined for the carbonate cancrinite products formed in this investigation are larger than those formed in a purely NaOH system, as seen in the section 6.3. This is characteristic of a degree of potassium incorporation into the structure.

6.4.2.2 Electron Microscopy Results

EDX Analysis

Analysis of the potassium and sodium levels of the cancrinite crystallites formed in the 220 °C, 8M solutions NaOH/KOH % 40/60 (**system 1**) experiments was undertaken using EDX analysis and is presented below in Table 6.9, two measurements were recorded for each sample. Figure 6.8 plots the potassium levels observed in this analysis.

Table 6.9 Sodium and potassium levels observed for cancrinite products of **system 1**.

Reaction Time	**Experiment No.**	**Sodium & Potassium Level**	
		Analysis 1	Analysis 2
1 h	1	6.8 & 1.2	6.9 & 1.1
2 h	2	7.3 & 0.7	7.3 & 0.7
3 h	3	6.6 & 1.4	7.1 & 0.9
4 h	4	6.8 & 1.2	7 & 1
5 h	5	7.1 &0.9	6.8 & 1.2
6 h	6	6 & 2	6.9 & 1.1
24 h	7	6.6 & 1.4	6.6 & 1.4

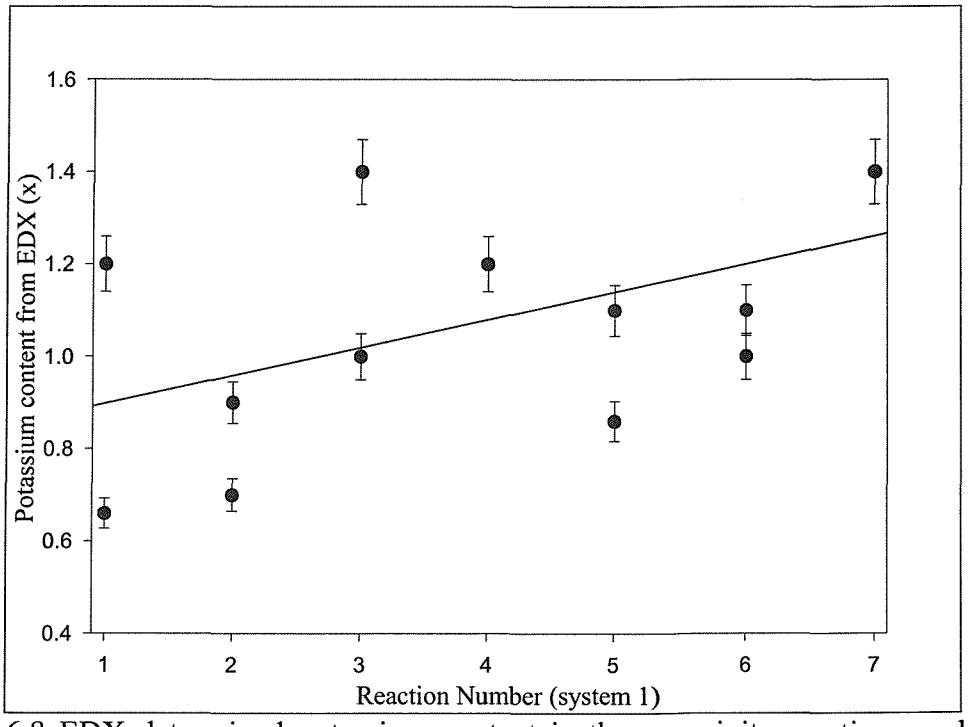

Figure 6.8 EDX determined potassium content in the cancrinite reaction products of **system 1** formed at 220°C, assuming a composition $Na_{8-x}K_x[AlSiO_4]_6.(CO_3)_{(1+x)/2}.nH_2O$.

6.4.3 Discussion

The results obtained for these experiments show that in mixed Na/K solutions, the formation $KAlSiO_4$ is also dependent upon reaction time. The formation of this phase is only observed after 24 h, prior to this cancrinite is obtained as a single phase. This shows that the rate formation of cancrinite is faster than the formation of $KAlSiO_4$ and confirms that in the presence of mixed Na/K solutions, where potassium is present at a concentration high enough for $KAlSiO_4$ formation, it proceeds via the dissolution of cancrinite. In a pure KOH synthesis, at all reaction times $KAlSiO_4$ is the only phase yielded. Increased lattice parameters for the cancrinite products are indicative of potassium incorporation into the structure.

The EDX analysis shows that the level of potassium incorporated within the cancrinite structure gradually increases over time until it reaches the limit of 2, at the same time the level of sodium within the structure decreases. There are three possible site combinations that the potassium may occupy, the 11-hedral $\in$-cages, the 12-ring channels or both the cages and the channels. Whilst the precise location has not been refined in this work it is proposed that the latter of the three possibilities is true.

Colella *et al*[4,5] discovered that dual-cation occupancy within the cancrinite structure can result in two options, in the case of lithium and caesium the caesium is seen only to occupy sites within the cancrinite cages and cannot be ion-exchanged, the lithium ions are located within the channels. However when the smaller thallium ion is employed along with lithium, the thallium is observed in both the cages and channels though only the latter can ion-exchange.

It is proposed that potassium behaves in a similar way to thallium (due to their similar ionic radii[13], (K^+=1.38 Å, Tl^+=1.50 Å)) and to some degree occupies both sites, perhaps only cages upon formation and then ion exchanges with some of the sodium located in the channels. The potassium ion has a larger radius than the sodium ion (K^+=1.38 Å, Na^+=1.02 Å), thus making ion exchange through the cage apertures created by a 4 membered ring of 1.6 Å unfavourable.

It is not clear why 2 is the limit of potassium occupancy, though clearly the size is likely to contribute to this. Further structural studies may allow the understanding of this system to be developed.

6.5 Conclusions

The replacement of some or all of the NaOH with KOH in synthetic systems that would typically yield carbonate cancrinite or Intermediate results in the formation of modified or alternative phases. The crystallisation of $KAlSiO_4.1.5H_2O$ (K-F) occurs at high/100 % KOH levels at 135 °C using 4.7 M solutions. At all other temperatures and high KOH levels, $KAlSiO_4$ is obtained; the extent to which this phase forms is dependent upon both KOH concentration and temperature. At high temperatures $KAlSiO_4$ forms at lower KOH levels. The crystal morphology of $KAlSiO_4$ is different to both cancrinite and Intermediate, the crystallites are regular shaped hexagons, 20 – 60 μ in diameter with a thickness of ~ 5 μ. At low KOH levels the incorporation of potassium into the cancrinite and Intermediate structure is observed.

When the reactions are undertaken using a mixture of NaOH and KOH the formation of $KAlSiO_4$ is also dependent upon reaction time. A reaction time of 24 h is required to synthesise $KAlSiO_4$; prior to this cancrinite is observed as a single phase. This shows that the rate formation of cancrinite is faster than the formation of $KAlSiO_4$ and confirms that in the presence of mixed Na/K solutions, where potassium is present at a concentration high enough for $KAlSiO_4$ formation, it proceeds via the dissolution of cancrinite. In a pure KOH synthesis, at all reaction times, $KAlSiO_4$ is the only phase yielded.

As a result of these investigations it was proposed that the difference in size and morphology of the $KAlSiO_4$ phase could make it a more favourable scale product; the size and shape being less likely to form such tight packing layers as cancrinite and Intermediate. In order to synthesise this phase either high KOH levels and long reaction times (48 h) are needed, or a 100 % KOH solution is required. A reaction time of 48 h would be impossible to achieve in the heat exchangers of a Bayer plant, therefore the use of high KOH level solutions would not result in the formation $KAlSiO_4$. The replacement of NaOH solution with KOH is in theory viable, however much more detailed investigations would have to be undertaken in order to ascertain the consequences for the remainder of the plant. Areas that may be affected by this change are the solubility of the bauxite, scaling in other regions of the plant and corrosion rates throughout the plant. The incorporation of potassium into the structures of both

cancrinite and Intermediate may permit easier removal of these phases; further investigations into how the sodium-potassium form of these phases differs to the pure sodium forms are required; one possible difference is the acid dissolution rate.

6.6 References

1 R.M. Barrer, J.W.Baynham, *Journal of the Chemical Society,* 2882, (1956).

2 R.M. Barrer, J.F. Cole, H. Sticher, *Journal of the Chemical Society,* **A**, 2475, (1968).

3 R.M. Barrer, D.E. Mainwaring, *Journal of the Chemical Society,* 1254, (1972).

4 C. Colella, M. de'Gennaro, in Zeolite Synthesis, edited by M.L. Occelli, H.E. Robson, American Chemical Society Symposium Series, Washington DC, **398**, 196, (1989).

5 P. Norby, I.G.K. Anderson, E.K. Anderson, C. Collela, M. de'Gennaro, *Zeolites,* **11**, 248, (1991).

6 T.I. Avdeeva, A.A. Novolodskaya, *Zhurnal Prikladnoi Khimii,* **39**, 298, (1966).

7 L. Guihua, L. Xiaobin, Z. Chuanfu, P. Zhihong, *Trans. Nonferrous Met. Soc. China,* **8,** 120, (1998).

8 J. Buhl, M. Fechtelkord, Th.M. Gesing, K. Hackbarth, *Microporous and Mesoporous Materials,* **30**, 347, (1999).

9 P.C.W. Leung, K.B. Kunz, K. Seff, I.E. Maxwell, *The Journal of Physical Chemistry,* **79**, 2157, (1975).

10 A.A. Kosorukov, L.G. Nadel, *Russian Journal of Inorganic Chemistry,* **30**, 961, (1985).

11 A.J. Perotta, S.M. Smith, J.V. Smith, *Mineralogical Magazine,* **35**, 588, (1965).

12 S. Wiggin, 3rd Year M.Chem. Report, Southampton University, (2000).

13 R.D. Shannon, *Acta Crystallographica*, **A32**, 751, (1976).

Chapter 7

Flow Loop

7.1 Introduction

The experiments described in chapters 3, 4, 5, and 6 have been carried out under hydrothermal static laboratory conditions. The investigations reported in this chapter describe the use of a large-scale cyclic flowing system; a flow loop.

The flow loop simulates conditions in the heat exchanger section of a Bayer plant, the area of the plant where the most severe aluminosilicate scaling and corrosion occurs. The corrosion of steel surfaces is another problem that occurs within the heat exchangers and the problem is amplified by the acid cleaning performed to remove the aluminosilicate scale. The objectives for the use of the flow loop are to examine a number of parameters, including the effects of flow rate, temperature and liquor composition on scaling and corrosion rates of different materials.

The rig uses between 25 L and 45 L of plant Bayer liquor (NaOH based), or synthetic liquor. The liquor is introduced to the rig via a hopper (Figure 7.1) before being circulated round using a controllable, variable speed, positive displacement pump (flow rates ~0.2 to ~1.8 m^3h^{-1}). The rig uses steam to heat the liquor through the heat exchanger walls and can achieve temperatures up to 170°C, controllable by regulation of the steam pressure or individual selection of the 4 passes to be heated. Each heat exchanger is followed by a test section that has the capacity to permit the appropriate measurements to be taken, an image of the test sections is presented Figure 7.1.

The effect of different parameters on the degree of scaling is investigated by examining removable pieces of pipe or coupons that are located in the corrosion test sections. The weight of the pipe is measured before and after an experiment so the mass of scale deposited on the surface can be determined. The coupons are held directly in the flow of the liquor by Teflon inserts in 'Swagelok' fittings; after removal the surfaces can be examined to monitor the composition and level of scale.

In order to maintain silica levels, a constant flow of 150 g/l SiO_2 solution is added to the liquor. Addition is carried out via a peristaltic pump (on which the speed can be set) through a check valve and into an in-line mixer, which works by inducing turbulence between the liquor and the silica solution. This addition takes place directly before the

inlet to the hopper so the stream is greatly diluted in the bulk of the liquor in the hopper, hopefully eliminating any regions of high silica concentration.

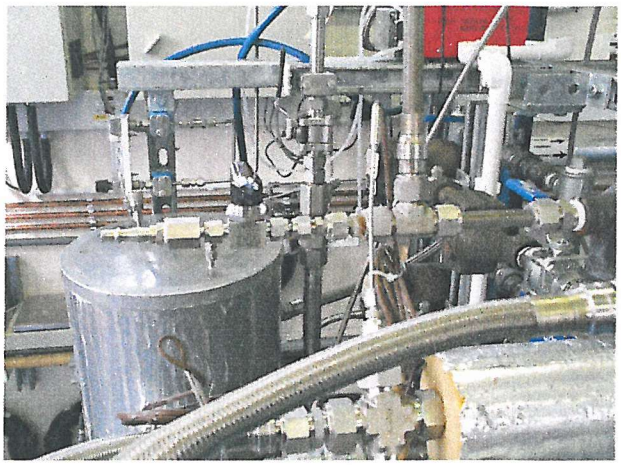

The hopper, the point of liquor addition.

The four consecutive test sections.

The silica pump and solution supply.

Figure 7.1 Photographs showing some of the different areas of the flow loop.

The flow loop offers much more flexibility than a plant in terms of experimental tests. Only 25 L of liquor is required for each test and the tests can be set up an run in a couple of days rather than a number of weeks which would be needed for a plant test. The use of plants for such tests is also undesirable due to the immense costs associated with a plant shut down and the loss of production.

7.2 Aims

This chapter describes the use of a large-scale cyclic system. The aim of the investigation was to ascertain how three systems from laboratory investigations as potential scale inhibitors/modifiers perform under more representative plant conditions. Four tests were carried out, a standard, one with the addition of $Ca(OH)_2$, one with the addition of a polymeric additive and one with KOH replacing NaOH.

7.3 Flow Loop Investigations

7.3.1 Experimental

Before commencing with the experiments synthetic liquor was prepared and the test sections were assembled to allow analysis. During the tests the conditions in the flow loop were monitored.

7.3.1.1 Liquor Synthesis

Standard

Synthetic liquor was prepared in a 25 L stirred glass vessel. Sodium hydroxide (2.4 kg) and sodium carbonate (0.75 kg) were dissolved in water (10 L), this solution was added to the reaction vessel along with sodium aluminate solution (274 g/L Al_2O_3, 6.6 L) and further water (7.4 L). The solution was stirred until homogenous and then stirred rapidly achieving a deep vortex. Sodium metasilicate (0.05 kg) dissolved in water (1 L) was slowly added down the vortex. After stirring for 1 h the solution was transferred to a 30 L plastic container where it was stored until required on the flow loop, at which time it was added to the hopper.

Calcium Hydroxide Addition

Previous investigations into the addition of $Ca(OH)_2$ to systems that normally yield cancrinite or Intermediate show that a change in the nature of phase formed can be achieved using 6.56 g/L $Ca(OH)_2$. That is at this level the formation of $NaCaHSiO_3OH$ is observed along with calcium containing cancrinite and Intermediate. At this level the presence of unreacted $Ca(OH)_2$ is less marked than at higher levels. Owing to the fact that that $Ca(OH)_2$ has limited solubility in liquor it was added in portions over the course of the experiment to prevent lumps forming and clogging up the system.

Synthetic liquor was prepared according to the method described above. At the point at which the liquor was added to the hopper, calcium hydroxide (0.08 kg) was also added. Calcium hydroxide additions (0.014 kg) were made to the hopper at 1 h intervals until 1h prior to completion of the experiment.

Polymer Addition

In previous investigations the formation of hollow spheres composed of cancrinite has been observed following the addition of polymeric additives to systems that normally yield powders of this phase. Additions of the polymers were made at levels of approximately 1 g/L. In order to ensure that the polymer was thoroughly dispersed within the flow loop liquor, two additions were made, a quantity was added to the bulk liquor and a quantity was supplied with the SiO_2 solution. In order to determine which polymer to employ in this investigation, solubility tests in SiO_2 solution were performed, Table 7.1a. The SiO_2 solutions in which the polymers had dissolved were used to carry out laboratory synthesis of cancrinite, Table 7.1b. Each reaction was performed four times, Polymer 1 addition resulted in the highest level of sphere formation, a further 6 tests were carried out to confirm this Table 7.1c. Tables 7.1a,b & c are presented overleaf.

Table 7.1a The solubility of the seven polymeric additives in SiO_2 solution.

Polymer Solubility in 150 g/L SiO_2 Solution	
Polymer	**Soluble**
1 Poly(2-acrylamido-2-methyl-1-propanesulfonicacid)	Yes
2 Poly(anetholesulfonic acid, sodium salt)	No
3 Poly(sodium 4-styrenesulfonate)	Yes
4 Poly(styrenesulfonic acid-*co*-maleic acid), sodium salt	Yes
5 Poly(ethyleneglycol)4-nonylphenyl 3-sulfopropyl ether, potassium salt	No
6 Poly(1,4-phenylene ether-ether sulfone) powder	No
7 Poly(1,4-butanediol) divinyl ether	Yes

Table 7.1b Degree of sphere formation using SiO_2 solutions with soluble polymers.

	Sample 1	**Sample 2**	**Sample 3**	**Sample 4**
Polymer 1	S & P	P	P & S	P & S
Polymer 2	P & S	P & S	P & S	P
Polymer 3	P	P	P	P
Polymer 4	P & S	P	P	P

P: - Powder, S: - Spheres

Table 7.1c Sphere formation using Polymer 1 in SiO_2 solution.

Polymer 1	**Sample 1**	**Sample 2**	**Sample 3**	**Sample 4**	**Sample 5**	**Sample 6**
Result	P & S	P	P & S	P & S	P & S	P & S

P: - Powder, S: - Spheres

Synthetic liquor was prepared according to the method described for the standard liquor. Before transferring the liquor to the plastic vessel poly(2-acrylamido-2-methyl-1-propanesulphonic acid), Polymer 1 (0.02 kg) was added to the solution, it was then stirred for a further 0.5 h. The liquor was transferred to the hopper, as described previously. Additional polymer (0.01 kg) was added to the silica supply (see section 7.3.2.3) and fed into the reaction mixture at a constant rate over the course of the reaction.

KOH Addition

The addition of 2.4 kg of NaOH to the standard liquor gives a concentration of 2.4 M, however when the total amount of Na added to the solution is expressed as NaOH this concentration increases to 4.7 M. Previous investigations into the addition of KOH to systems that normally yield sodium cancrinite or Intermediate show that a change in the nature of phase formed can be achieved using NaOH/KOH % of 40/60. That is at this level the formation of $KAlSiO_4$ is observed along with potassium containing cancrinite and Intermediate. KOH was added such that this ratio was achieved for a 4.7 M solution when the total Na in the system is expressed as NaOH.

Synthetic liquor was prepared according to the method described for the standard liquor omitting the sodium hydroxide and replacing it with potassium hydroxide (3.8 kg). The liquor was transferred to the hopper, as previously described.

7.3.1.2 Test Section Preparation

The four test sections were prepared according to the diagram in Figure 7.2. The test sections were numbered 1 - 4 and the temperature increased from position 1 through to position 4, the average temperature achieved in each section was recorded every time an experiment was performed, section 7.3.2.3.

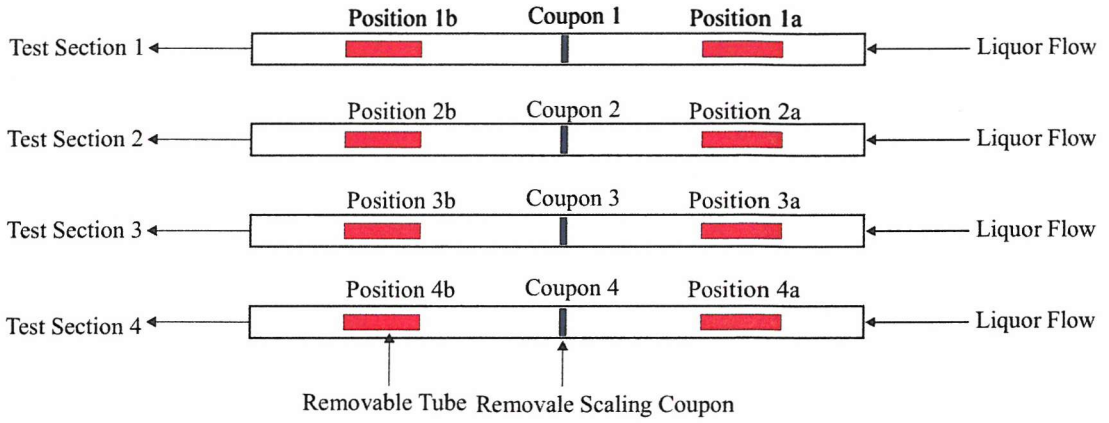

Figure 7.2 The arrangement of the four test sections; temperature increasing from section 1 to 4.

Each test section was fitted with two removable stainless steel tubes, in positions termed a and b. These tubes were weighed prior to the start of an experiment and removed and reweighed at the end of the experiment so that the mass of scale deposited on the surface could be calculated. A stainless steel coupon was also positioned directly in the liquor flow between the two tubes in each test section. The scale deposited on the surface of the coupons was analysed using PXD and SEM.

7.3.1.3 Flow Loop Conditions

Each reaction was performed for seven hours. The liquor was heated whilst being pumped through the flow loop and allowed to pass through the four test sections. The temperature of the test sections fluctuated somewhat through the experiments, approximately ±3 °C from the average temperature. The average temperatures of each section were calculated and are presented below in Table 7.2 and Figure 7.3. For the most part the temperature increases passing from the first to the last test section.

Table 7.2 Average temperature achieved in the test section for the four experiments.

	Temperature of Experiment (°C)			
Test Section	**Standard**	**Calcium**	**Polymer**	**Potassium**
1	147.5	150.0	155.0	152.0
2	158.0	160.0	162.5	167.0
3	163.0	166.5	167.5	167.0
4	161.0	169.0	170.5	170.0

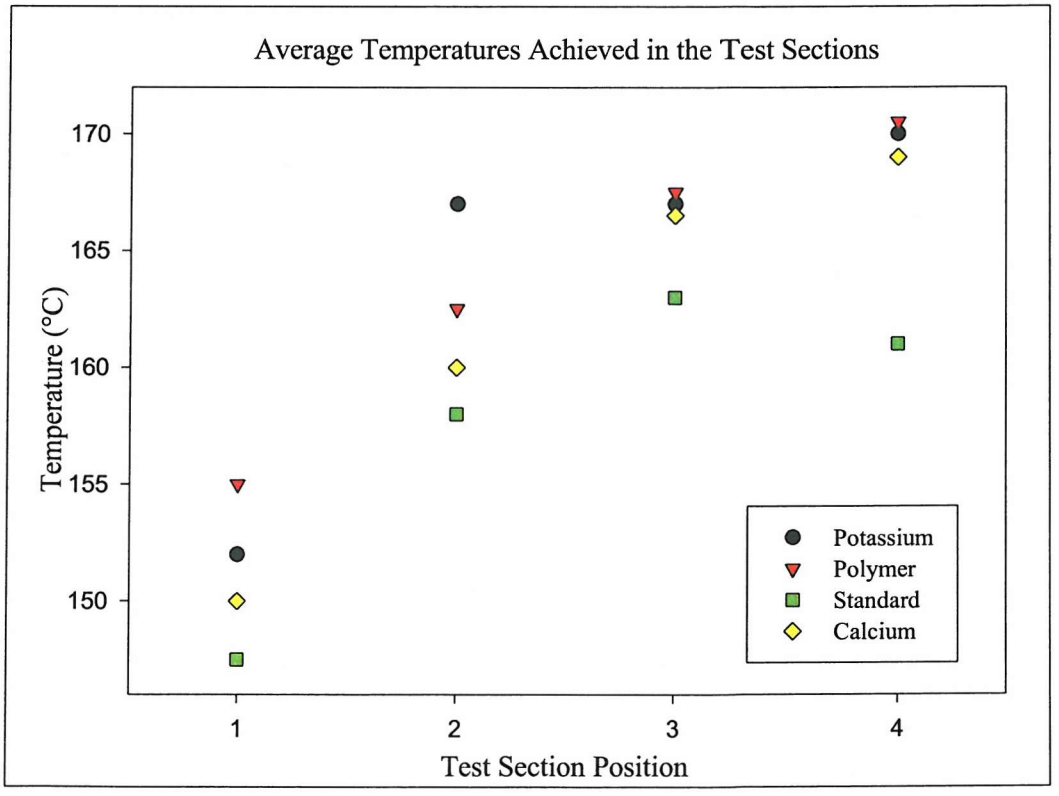

Figure 7.2 A comparison of the average temperature achieved in each test section in each experiment.

150 g/l SiO_2 solution was pumped into the liquor stream at a constant rate. The amount of SiO_2 solution added over the course of the reactions achieved SiO_2 concentrations of approximately 10 g/L. Table 7.3 below records the mass of solution added during each of the four experiments.

Table 7.3 Mass of SiO_2 solution pumped through reaction mixture.

	Standard	**Calcium**	**Polymer**	**Potassium**
SiO_2 solution added (g)	1743.3	1667.6	1655.0	1642.5

7.3.1.4 Acid Cleaning

Sulphuric acid was used to clean the flow loop and all removable parts before commencing with each experiment; this is the standard cleaning method employed for cleaning the heat exchangers in the Bayer plant.

7.3.2 Results

The scale coupons and sections of pipe removed from the flow loop were characterised using PXD and SEM. Heat transfer rates were also calculated for each experiment.

Observations

The scale coupons retrieved from the standard, calcium and potassium tests appeared to be unchanged, however under closer inspection with an electron microscope it was discovered that they are in fact covered by a layer of scale.

The coupons recovered from the polymer experiment were very different in appearance to those from the other three experiments. The coupons appeared to be both corroded and coated with a metallic orange surface (this was later confirmed as copper through EDX analysis).

7.3.2.1 Heat Transfer Analysis

During the course of the four experiments heat transfer measurements for the surfaces of the test sections were performed by engineers at Alcan International. A graph collating these measurements is presented below in Figure 7.3.

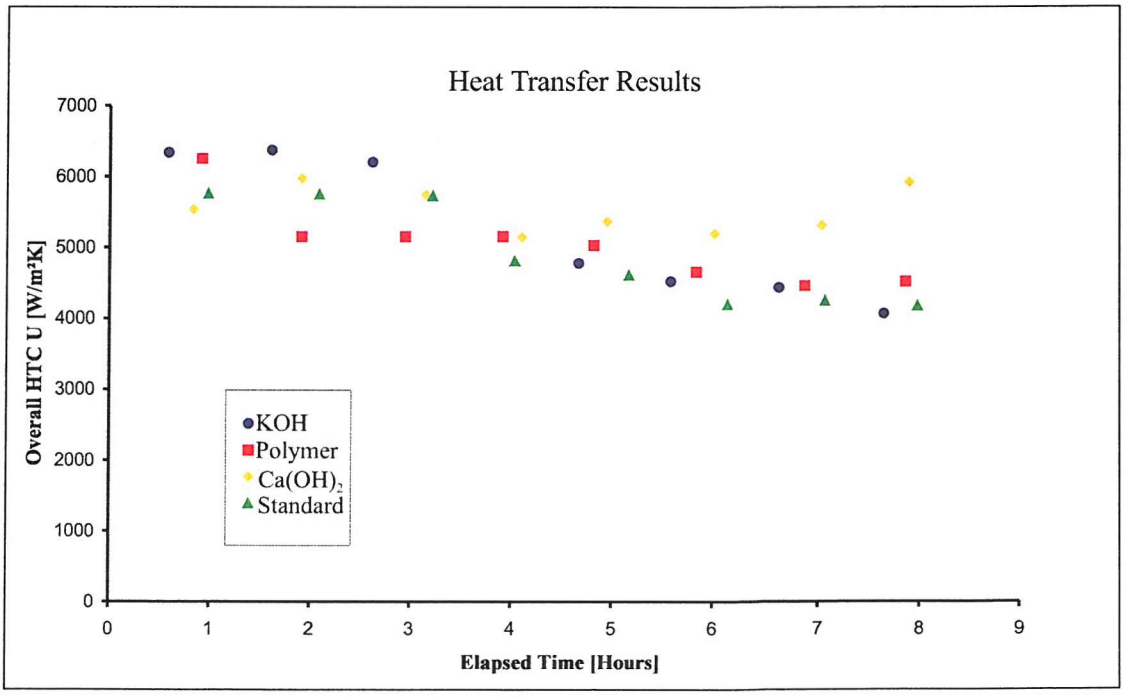

Figure 7.3 Heat transfer measurements calculated for the four experiments.

Analysis of these heat transfer results provided the first indication that the flow loop experiments had been successful in simulating Bayer plant conditions to produce scale. It can be seen that in general, as the reactions proceed the amount of heat transfer reduces. This is consistent with the formation of scale on the inner surfaces of the tubes; this scale acts as an insulator, which then reduces heat transfer.

After 8 hours, when the experiments were terminated the calcium investigation is the one seen to have the least reduction in heat transfer, this suggests that the least amount of scale was precipitated in this experiment. This result is confirmed by the analysis of the weight gained in the removable tubular sections, section 7.3.2.2.

7.3.2.2 Weight Analysis

The removable tubular pieces of each test section were weighed before and after each experiment and the mass of scale deposit on each occasion calculated, Table 7.4.

Table 7.4 Mass of scale deposit collected in removable tubular sections.

Mass of Scale Deposit Calculated for Each Experiment (g)				
Tube Position	**Standard**	**Calcium**	**Polymer**	**Potassium**
1a	0.1291	0.0368	-9.0×10^{-3}	0.1342
1b	0.1352	0.0411	-7.6×10^{-3}	0.1369
2a	0.1680	0.0582	-0.0183	0.1687
2b	0.1791	0.0537	-0.0181	0.3042
3a	0.2204	0.0711	-0.0114	0.2054
3b	0.2138	0.0632	1.0×10^{-4}	0.2355
4a	0.2519	0.0679	-8.7×10^{-3}	0.2231
4b	0.2470	0.0670	-9.0×10^{-3}	0.2407

Figure 7.4, overleaf presents a graph comparing the level of scaling for each test.

Figure 7.4 Comparison of the scaling levels in each of the four experiments.

The overall general trend observed in this comparison is that the mass of scale deposited on the tubes increases as a progression down the four test sections is made. This result is obtained due to the increase in temperature from test section 1 to test section 4; hot surfaces promote the precipitation of scale.

The results obtained for the polymer experiment are not representative of scaling levels. As described in section 7.3.3 (observations) other reactions occurred within the system that damaged the scale coupons, a loss of mass is observed for the tubular sections and so it can be concluded that similar corrosion has also occurred within the tubes.

The results obtained for the standard and potassium test are very similar (apart from the mass calculated for 2b of the potassium experiment). EDX analysis shows that some degree of potassium is present in the aluminosilicate deposited on the surface however this appears not to have had any affect on the mass of scale deposited.

The results obtained for the calcium experiment show the most significant reduction in the amount of scale deposited on the surface of the tubes. Comparison of the level of scale between the calcium and standard test reactions show an overall reduction of 30 % upon the employment of $Ca(OH)_2$, Table 7.5.

Table 7.5 Percentage reduction of scaling between standard and calcium experiments.

Tube Position	Standard	Calcium	Reduction %
1a	0.1291	0.0368	28.5
1b	0.1352	0.0411	30.4
2a	0.1680	0.0582	34.6
2b	0.1791	0.0537	30.0
3a	0.2204	0.0711	32.2
3b	0.2138	0.0632	29.6
4a	0.2519	0.0679	27.0
4b	0.2470	0.0670	27.1
		Average	29.9

7.3.2.3 PXD Results

Attempts to collect PXD data on the scale coupons removed from the flow loop using a glancing angle technique proved unsuccessful due to the depth of the deposit being only microns thick.

7.3.2.4 Electron Microscopy Results

The scale coupons removed from the four test sections were for each experiment were examined using SEM.

SEM Micrographs

Blank Scale Coupon

In order to confirm scale deposits on the surface of the stainless steel coupons, SEM analysis was performed on a coupon that had not been exposed to any liquor. The image is presented below in Figure 7.5.

Figure 7.5 SEM image of a scale coupon that has not been exposed to any synthesis liquor or experimental conditions.

The surface is seen to be generally smooth aside from lines created whilst cutting the coupon. There is no evidence of a crystalline deposit on the surface.

Experiment 1 – Standard

SEM micrographs of the scale coupons removed from two of test sections were taken. Two images are presented below, Figures 7.6a and b; the first is from test section 1 and the second from test section 3. Deposits can be seen on both surfaces however they differ in morphology. A poorly crystalline deposit covers the surface of the coupon from test section 1; this is consistent of Intermediate that forms a combination of amorphous agglomerates and plate-like crystallite. The deposit on the coupon from section 3 consists of rod-like crystallites, consistent with cancrinite formation. EDX analysis performed on coupon 3 confirms the presence of an aluminosilicate phase, details in Table 7.6.

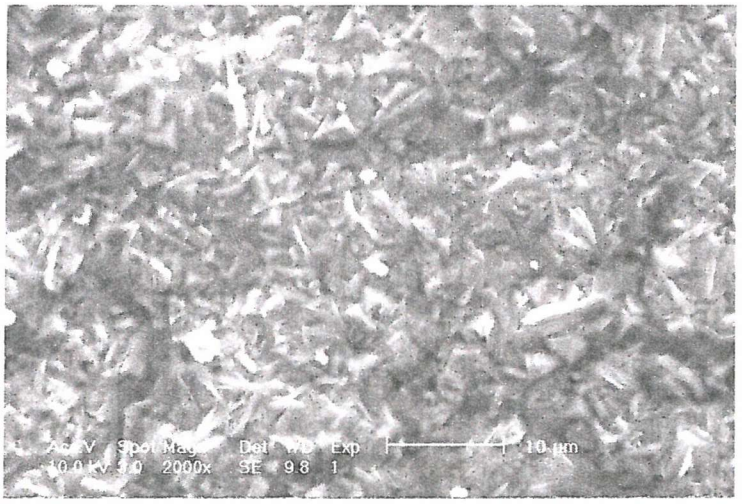

Figure 7.6a SEM image of the surface of a scale coupon retrieved from test section 1 of the standard experiment.

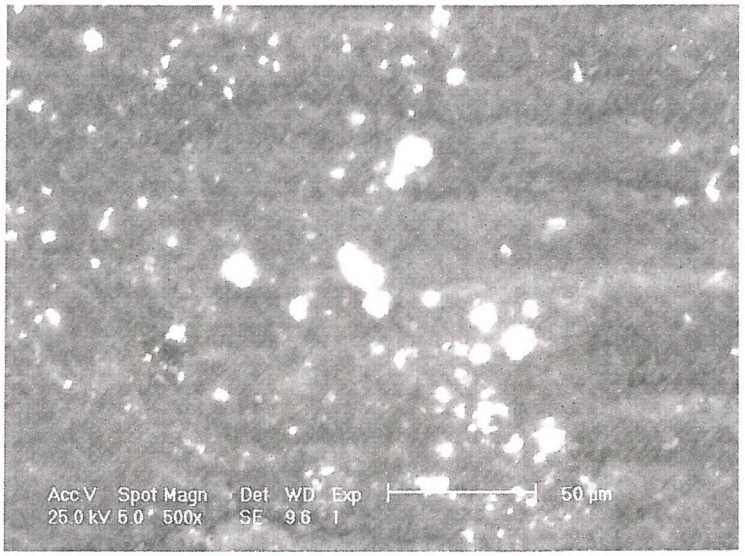

Figure 7.6b SEM image of the surface of the scale coupon retrieved from test section 3 of the standard experiment.

Experiment 2 – Calcium

SEM micrographs of the scale coupons removed from two test sections were taken. The image taken of the surface of the coupon from test section 2, Figure 7.7a showed a plate-like crystalline deposit very similar in appearance to that obtained for the standard experiment, though this deposit appears to contain some rods. An image from test section 4 is also presented below, Figure 7.7b. The deposit covering the coupon consists of rod-like crystallites, consistent with cancrinite formation. Whilst the morphology of the crystallites forming the deposit are identical to those seen in the standard experiment, the distribution is somewhat more uneven. EDX analysis performed on coupon 4 confirms the presence of an aluminosilicate phase containing a small amount of calcium, details in Table 7.6.

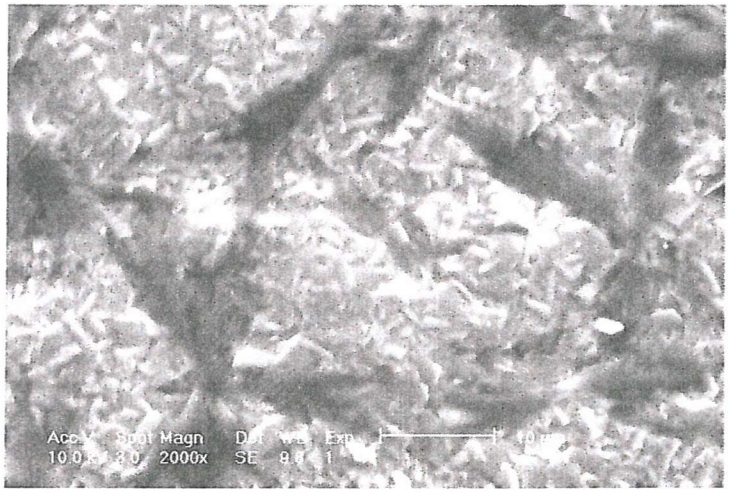

Figure 7.7a SEM image of the surface of the scale coupon retrieved from test section 2 of the calcium experiment.

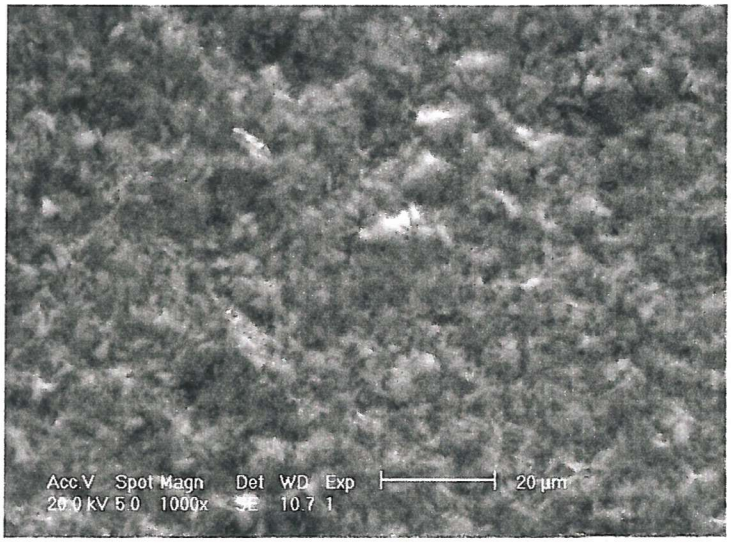

Figure 7.7b SEM image of the surface of the scale coupon retrieved from test section 4 of the calcium experiment.

Experiment 3 – Polymer

The scale coupons retrieved from the polymer experiment were very different in appearance from those retrieved for the other three experiments, as described in section 7.3.3 (observations). The micrograph below presents the surface of the coupon from test section 4 in an area where a flaky copper coating was evident.

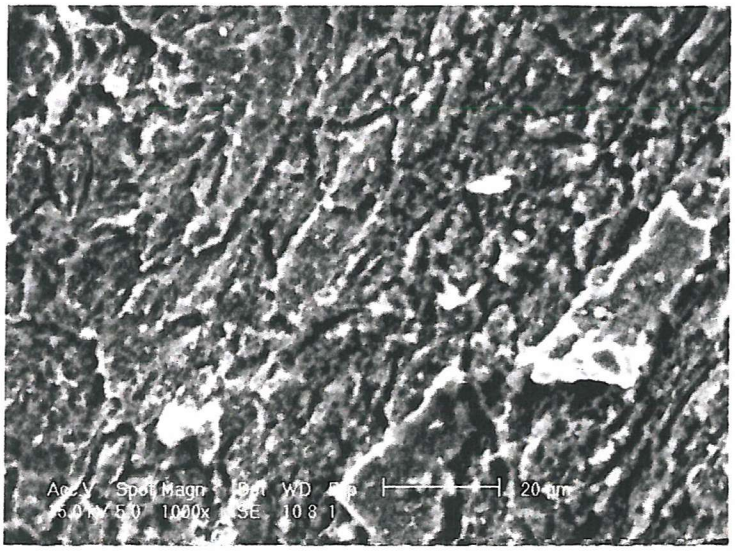

Figure 7.8 SEM image of the surface of the scale coupon retrieved from position 4 of the polymer experiment.

In comparison to the blank scale coupon the surface has clearly been exposed to some form of coating, however it is not a layer of scale deposit as seen in the other experiments.

An electron probe map of the surface of this coupon was generated at Alcan's Banbury laboratories to allow further analysis. The coupon examined was generally the orange metallic copper colour with a central region that was a yellowish colour; the scan performed on this coupon focused on the yellow region. The electron probe map shows that the area consists of mainly iron with areas of iron oxide, isolated regions of copper and some copper oxide, Figure 7.9 overleaf. Background signals of aluminium and silicon were detected showing that any scale present was at a negligible level.

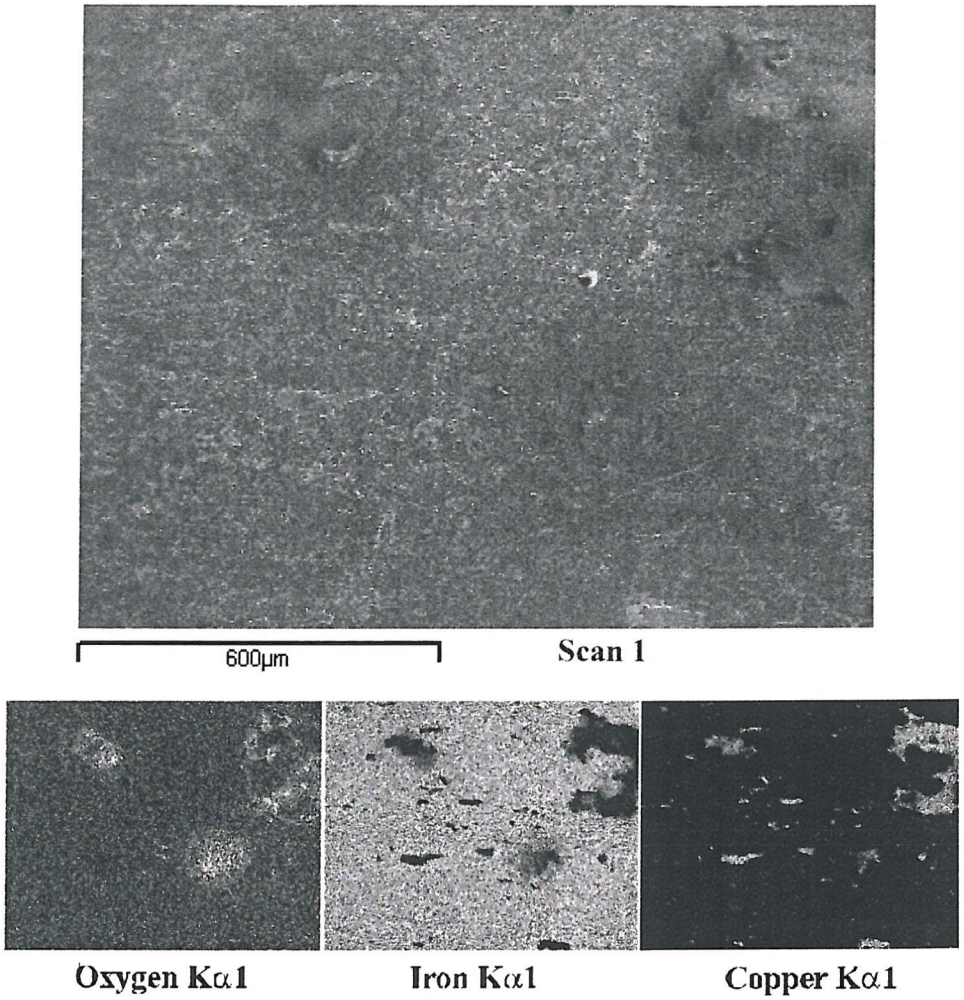

Figure 7.9 Electron probe map of an area of surface of scale coupon removed from the polymer experiment. The large picture (top), shows an overall image whereas the three small images (bottom) highlight the presence of specific elements. Where the elements are present the image is light.

Experiment 4 – Potassium

SEM micrographs of the scale coupons removed from two test sections were taken. The image taken of the surface of the coupon from test section 12, Figure 7.9a shows an amorphous deposit covering the surface, somewhat different to that seen on other scale coupons. An image from test section 4 is also presented below, Figure 7.9b. The deposit covering the coupon consists of rod-like crystallites, consistent with cancrinite formation. EDX analysis performed on coupon 4 confirms the presence of an aluminosilicate phase containing potassium details in Table 7.6.

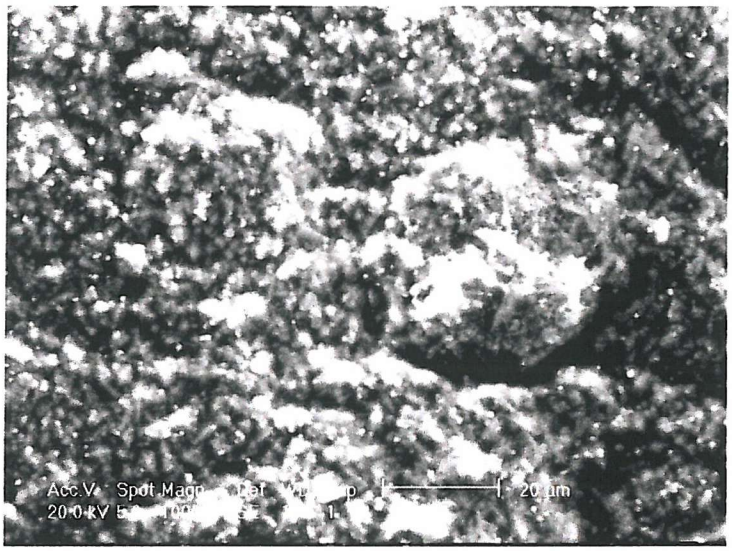

Figure 7.9a SEM image of scale coupon retrieved from position 1 of the potassium experiment.

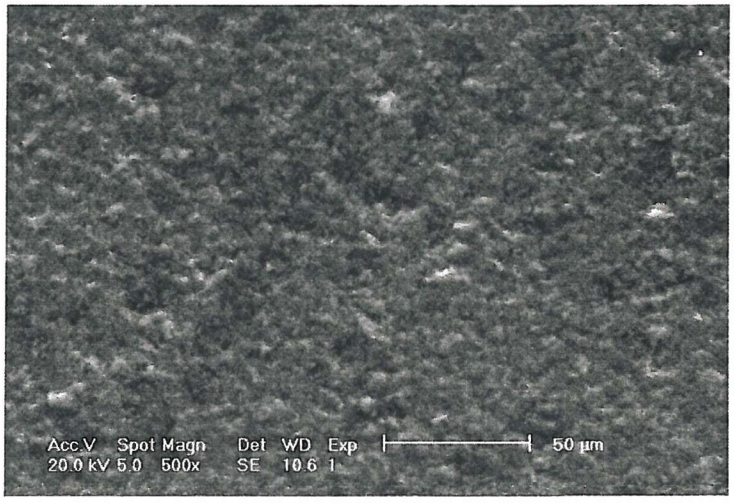

Figure 7.9b SEM image of scale coupon retrieved from position 4 of the potassium experiment.

EDX Analysis

Analysis of the composition of the scale coatings formed on the coupons in the four experiments was undertaken using EDX analysis and is presented below in Table 7.6.

Table 7.6 EDX analysis of the scale coupons removed from test section 3 of each of the four experiments.

Elemental Analysis (Atomic %)					
Element	**Clear Coupon**	**Standard Coupon**	**Calcium Coupon**	**Polymer Coupon**	**Potassium Coupon**
C	17.1	12.1	10.1		6.5
O	6.9	51.2	50.2		51.2
Fe	76.0	0.17	0.34	10.5	0.13
Na		13.8	14.1		10.5
Al		12.4	12.5		13.6
Si		11.4	12.7		13.2
Ca			0.8	-	
K					4.9
Cu				89.5	0

EDX analysis performed on a blank scale coupon showed the presence of only carbon, oxygen and iron. EDX analysis performed on each of the other four coupons confirmed the presence of a surface coating.

The elements detected for the standard experiment confirm the presence of a sodium aluminosilicate phase, the Al:Si ratio of almost 1:1 is consistent with the elemental analysis observed for cancrinite. Similar elemental ratios are detected for the calcium experiment; however, in this instance a trace amount of calcium was also discovered. It is possible that some calcium may have been incorporated into the aluminosilicate structure or it may residual calcium hydroxide that has been deposited on the surface. An aluminosilicate coating is also observed in the potassium experiment however the elemental percentage of sodium detected is somewhat less and a significant level of potassium is present. The level of potassium is higher than that observed in laboratory experiments, this would suggest that as well as some potassium being incorporated into

the cancrinite structure the formation of a further potassium aluminosilicate phase may have occurred. The EDX analysis carried out on the Polymer coupon confirms that the surface has indeed been coated with a layer of copper.

7.3.3 Discussion

Scale build-up was observed on the surfaces of the removable scale coupons in three instances; the blank, calcium and potassium experiments. In the fourth reaction carried out, the addition of Polymer 1, no scaling was observed, instead a layer of copper was deposited on the surface of the scale coupons.

Focusing only on the blank, calcium and potassium experiments, after eight hours, upon termination of the experiment, the calcium experiment is seen to have the least reduction in heat transfer and the lowest gain in weight, therefore also the lowest amount of scale. The blank and potassium experiments demonstrate very similar heat transfer and weight analysis results. Analysis of the surfaces using SEM shows what appear to be cancrinite rods at the high temperature and the Intermediate at the lower temperatures in all three cases. However, these coatings in the calcium experiment look to have a more uneven distribution. EDX analysis on the surfaces of the scale coupons shows the presence of aluminosilicate phases in all three instances. A degree of potassium is detected by EDX in the potassium experiment though this does not appear to have had any affect on scale reduction. Only a very small amount of calcium was detected by EDX on the surface of the coupon, however clearly the presence of calcium in the reaction mixture has led to significant scale reduction. Further investigation into the effect of calcium addition on scale reduction under such representative plant conditions is required.

Upon the addition of Polymer 1 no scale formation was observed, scaling was detected using SEM or weight measurement analysis. The surface of the scale coupon is coated with a layer of copper, confirmed as such by EDX. The addition of the Polymer appears to have caused leaching of copper from somewhere within the flow loop, though exactly which part has not been determined. Attempts to induce copper leaching from a copper source in the laboratory, using Polymer 1 were ineffective. The purpose of the polymer experiment was to try and create cancrinite spheres; it should be considered that if the formation of such spheres had occurred it is unlikely that they would stick to the surfaces within the flow loop. It is more likely that they would remain in the liquor and thus the idea of polymer addition/sphere formation should not be discarded.

Attempts to collect PXD data on the surface coatings proved unsuccessful thus making it impossible to confirm the presence of cancrinite/Intermediate. To overcome this problem in future flow loop experiments, longer reaction times should be employed thus permitting a thicker layer of scale to grow on the surface of the scale coupons. This may allow direct PXD analysis of the surface or even generate enough scale to scrape off and use for a PXD experiment.

7.4 Conclusions

Four reactions have been performed under representative Bayer plant conditions with the successful employment of a flow loop. Scale build-up was observed during three of these experiments; the blank, the addition of calcium and the replacement of some sodium with potassium.

Of the three reactions where scaling occurred, the blank and potassium showed very similar results; that is that the replacement of some sodium with potassium appeared to have no impact on scale reduction. The addition of calcium however shows a significant reduction in the level of scale produced. It shows the least variation over the course of the experiment in the heat transfer on the heat exchanger surfaces and an average scaling weight reduction of 30 % in comparison to the blank experiment. These results show that the addition of $Ca(OH)_2$ to the heat exchangers of the Bayer process should reduce aluminosilicate scaling.

Upon addition of Polymer 1, a very different result was observed. The removable scale coupons were coated with a layer of copper, how and where this copper was leached from has not been determined. What is interesting however, is that very little, if indeed any aluminosilicate scaling has been deposited on the surface of the copper coating; thus copper plating of the heat exchanger surfaces may result in reduced scaling. The concept of polymer addition/sphere formation should not be discarded at this stage, as had sphere formation occurred it is unlikely that they would stick to the surfaces within the flow loop, it is more likely that they would remain in the liquor. Thus not reducing the efficiency of the heat exchanger walls, and with the addition of a sieve to the system, the spheres could be captured and removed.

Chapter 8

Conclusions

8.1 Introduction

Aluminosilicate scale formation within the heat exchangers of the Bayer process generates immense costs for aluminium producers such as Alcan International Limited who provided the funding for this work. The aim of this research was to further the understanding of the chemistry behind scale formation and to investigate methods of reducing, modifying or eliminating it.

8.2 Synthesis and Characterisation of Synthetic Aluminosilicate Scale

Synthetic aluminosilicate scales were prepared using hydrothermal routes and characterised using PXD, FTIR SEM and PND. Having established reliable synthetic reaction methods for the formation of cancrinite and Intermediate, which have been identified as the two major aluminosilicate scales, and characterisation techniques that allow the two phases to be distinguished, the effect of additives and reaction conditions on scale formation could be measured.

The structural study of cancrinite using PND and variable temperature PND undertaken proved successful in locating previously uncharacterised imbibed water molecules and sodium ions, allowing the determination of accurate atomic positions. The structure of the Intermediate phase could not be determined.

8.3 Effect of Additives on Synthetic Scale

A series of additives were introduced into the synthetic scale formulation to assess their impact on scale formation.

8.3.1 Calcium Hydroxide Addition

The first additive considered was $Ca(OH)_2$; $Ca(OH)_2$ is used already in Bayer plants to alleviate other problems making it widely accessible. The addition of $Ca(OH)_2$ to the synthetic systems that yield carbonate cancrinite or Intermediate resulted in the formation of these two aluminosilicate phases and also $NaCaHSiO_3OH$. Since $NaCaHSiO_3OH$ is different in size and morphology to cancrinite and Intermediate it could be a more favourable scale product; the size and shape being less likely to form such tight packing crystallites as cancrinite and Intermediate. Despite the reaction

conditions that are required to form this phase as a single product being impossible to achieve in the heat exchangers of a Bayer plant, when $Ca(OH)_2$ was added to the synthetic liquor used in the large scale reactions using the flow loop a 30 % reduction in scaling was observed.

Accurate hydrogen positions for the structure of $NaCaHSiO_3OH$ were determined by refinement of neutron data.

8.3.2 Chemical Additives

The incorporation of low molecular weight organic sulphate and sulphonate sodium salts and high molecular weight organic polymers possessing similar/related functional groups were investigated. It was anticipated that the ionic end of the additive would template the structure, leaving the organic molecule protruding out and the presence of the organic molecule thus inhibiting or preventing further growth in that direction.

The addition of organic sulphate/sulphonate additives resulted in only the formation of the regular powdered aluminosilicate phases.

Addition of each of the seven different polymeric additives employed in this investigation resulted in the formation of cancrinite spheres. It was proposed that cancrinite spheres would be a more favourable scale product than the closely packed cancrinite crystallites that currently adhere to the ball of the heat exchangers. Addition of Polymer 1 to the synthetic liquor in the large scale experiment utilising the flow loop did not result in the formation of cancrinite spheres. However another interesting result was obtained; the removable scale coupons were coated with a layer of copper (leached from within the flow loop) and where coated with copper, very little, if indeed any aluminosilicate scaling has been deposited on the surface. Thus copper plating of the heat exchanger surfaces may result in reduced scaling.

8.3.3 Potassium Hydroxide

With the exception of francium, potassium is the only alkali-earth metal for which cancrinite formation is not reported in the literature; it was proposed that replacement of NaOH with KOH in Bayer liquor would inhibit the precipitation of cancrinite.

The replacement of some or all of the NaOH with KOH in synthetic systems that would typically yield carbonate cancrinite or Intermediate resulted in the formation of modified or alternative phases; $KAlSiO_4.1.5H_2O$ (K-F) and $KAlSiO_4$, the latter to greater extent. The crystal morphology of $KAlSiO_4$ is different to both cancrinite and Intermediate; it was proposed that this difference may make $KAlSiO_4$ a more favourable scale product; the size and shape being less likely to form such tight packing layers as cancrinite and Intermediate. However replacement of NaOH with KOH in the synthetic liquor in the large scale experiment utilising the flow loop appeared to have no impact on scale reduction.

8.4 Summary

The addition of $Ca(OH)_2$ to the synthetic Bayer systems showed the greatest potential benefit with regards to scale reduction. Further research into the scale reducing properties of $Ca(OH)_2$ under flowed conditions on a large scale would be recommended, focusing on the acid dissolution properties of the scale that is precipitated and also assessing how the $Ca(OH)_2$ can be added into the system in a practical fashion.

The observation that scale did not adhere to the surface of the copper leached scale coupons during the addition of Polymer 1 to the flowed system suggests that research into copper/other coatings for the inside of the heat exchanger pipes might result in less scale precipitation. It would also be interesting to investigate the other Polymers under the same conditions, in conjunction with development of a sieving technique for the recovery of spheres to see if indeed they do form under such conditions. On a laboratory scale further research into the mechanism of sphere formation may be fruitful, as may the utilisation of computer modelling to design a scale inhibitor now that the understanding of the cancrinite structure has been developed.

Future experiments utilising the flow loop might benefit from longer reaction times; to permit the growth of a thicker layer of scale on the removable coupons, allowing PXD analysis. Also modification of the flow loop to achieve higher temperatures; the maximum temperature currently achievable using the flow loop is somewhat below that of the temperatures reached in Bayer plants.